Master Thesis, Department of Geosciences

Reservoir quality of Jurassic sandstones in SW Barents Sea

A mineralogical, petrographical and petrophysical approach

Farakh Mahmood

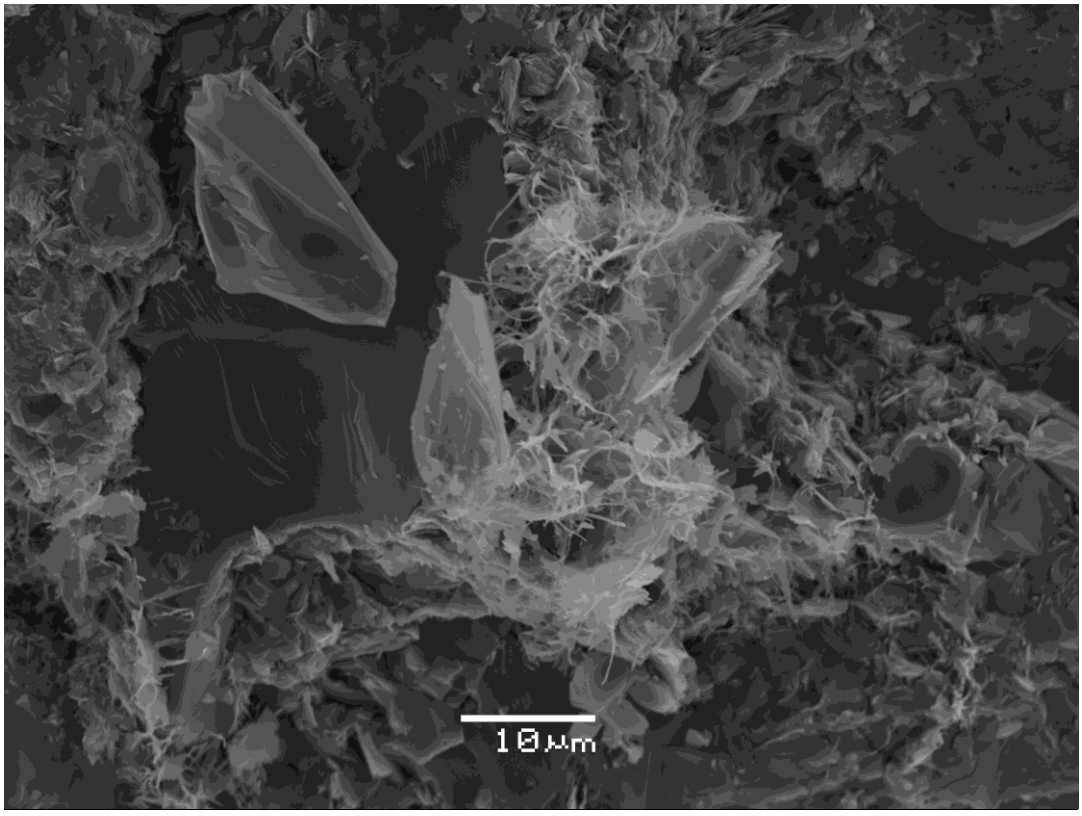

UNIVERSITY OF OSLO

FACULTY OF MATHEMATICS AND NATURAL SCIENCES

Reservoir quality of Jurassic sandstones in SW Barents Sea

A mineralogical, petrographical and petrophysical approach

Farakh Mahmood

Master Thesis in Geosciences

Discipline: PEGG

Department of Geosciences

Faculty of Mathematics and Natural Sciences

University of Oslo

03.06.2013

Tutor(s): **Jens Jahren (Uio), Md Nazmul Haque Mondol (Uio) and Jan Inge Faleide (Uio).**

This work is published digitally through DUO – Digitale Utgivelser ved UiO

http://www.duo.uio.no

It is also catalogued in BIBSYS (http://www.bibsys.no/english)

Preface

This thesis is part of the BarRock project and is submitted to the Department of Geosciences, University of Oslo (UiO), in Candidacy of the M.Sc. Degree.

This research has been performed at the Department of Geosciences, University of Oslo, during the period of January 2013 – May 2013 under the supervision of Jens Jahren, Md Nazmul Haque Mondol and Jan Inge Faleide Associate Professors, Department of Geosciences, University of Oslo, Norway.

ACKNOWLEDGEMENTS

I would like to acknowledge the enthusiastic supervision of Jens Jahren and my Co-supervisors Md Nazmul Haque Mondal and Jan Inge Faleide throughout my thesis. Apart from the efforts by me, the success of this research was dependent largely upon all the people working on BarRock project.

I wish to express my special gratitude to Berit Løken Berg and Maarten Aerts for always being supportive and helpful during SEM & XRD studies.

Special thanks to all my friends and class fellows for their guidance throughout the thesis.

At the last many thanks to all my entire family for their support and love during my stay in Oslo.

Farakh Mahmood

ABSTRACT

The Stø and Nordmela Formations of Early to Middle Jurassic age are represented in wells 7119/12-1, 7120/7-1and 7120/7-3 located in the Tromsø/Hammerfest transition zone area and in wells 7120/8-1, 7120/9-1, 7121/4-1, 7121/5-1 and 7120/6-1in the Hammerfest Basin area in the SW Barents Sea. The study deals with the petrographic understanding, diagenetic development and their influence on reservoir quality. Several techniques like microscopic analysis, scanning electron microscopy, x-ray diffraction analysis and petrophysical analysis have been applied during the study.

The sandstones of Stø Formation are mineralogically and texturally mature, while the Nordmela Formation is mineralogically mature like Stø but texturally less than this. The quartz content in the Stø Formation and overall formation thickness is high in the SW side of the study area. The area has been subjected to an average of 800m uplift suggested by the amount of quartz cement. The reservoir quality is influenced by this process. The degree of quartz cementation is higher in the deepest well (7119/12-1) as compared to shallowest well (7121/4-1) which reflects that the magnitude of uplift is higher towards the shallower well (NE) and results in decrease in temperature. Dissolution of detrital grains at stylolites is the main source of silica cementation. The quartz cementation in the study area is controlled by the grain size and the spacing of stylolites.

Cementation is the major reason of porosity loss in the Stø Formation, where both mechanical compaction and cementation are the major porosity reducing factors in the Nordmela Formation. The reservoir quality of Stø Formation is fair with the porosity ranges from 10.5% to 18.1% and some samples from sandy portion of the Nordmela Formation show a reasonable porosity but reservoir quality in the study area may not be good due to hetrolithic nature of the formation.

Table of Contents

Chapter 1: Introduction

1.1 Background and motivation

1.2 Research objectives

1.3 Study area

1.4 Database and methodology

1.5 Chapter descriptions

Chapter 1: Introduction

1.1 Background and motivation

The Norwegian Barents Sea has an area of 230000 km^2 which is 1,5times greater than the Norwegian portion of the North Sea (Dore 1995). For the petroleum exploration point of view, the Norwegian Continental Shelf is distributed into three main provinces; North Sea, Mid-Norwegian continental margin and Western Barents Sea. These provinces were the part of a large epicontinental sea before continental break-up which was lying between the continental masses of Fennoscandia, Svalbard and Greenland (Faleide et al. 2010). The Barents Sea is bounded by the Norwegian Sea and the Svalbard (Norway) in the west and northwest respectively, the islands of Franz Josef Land and Novaya Zemlya in the northeast and east and in the south Norway and Russia (Fig. 1).

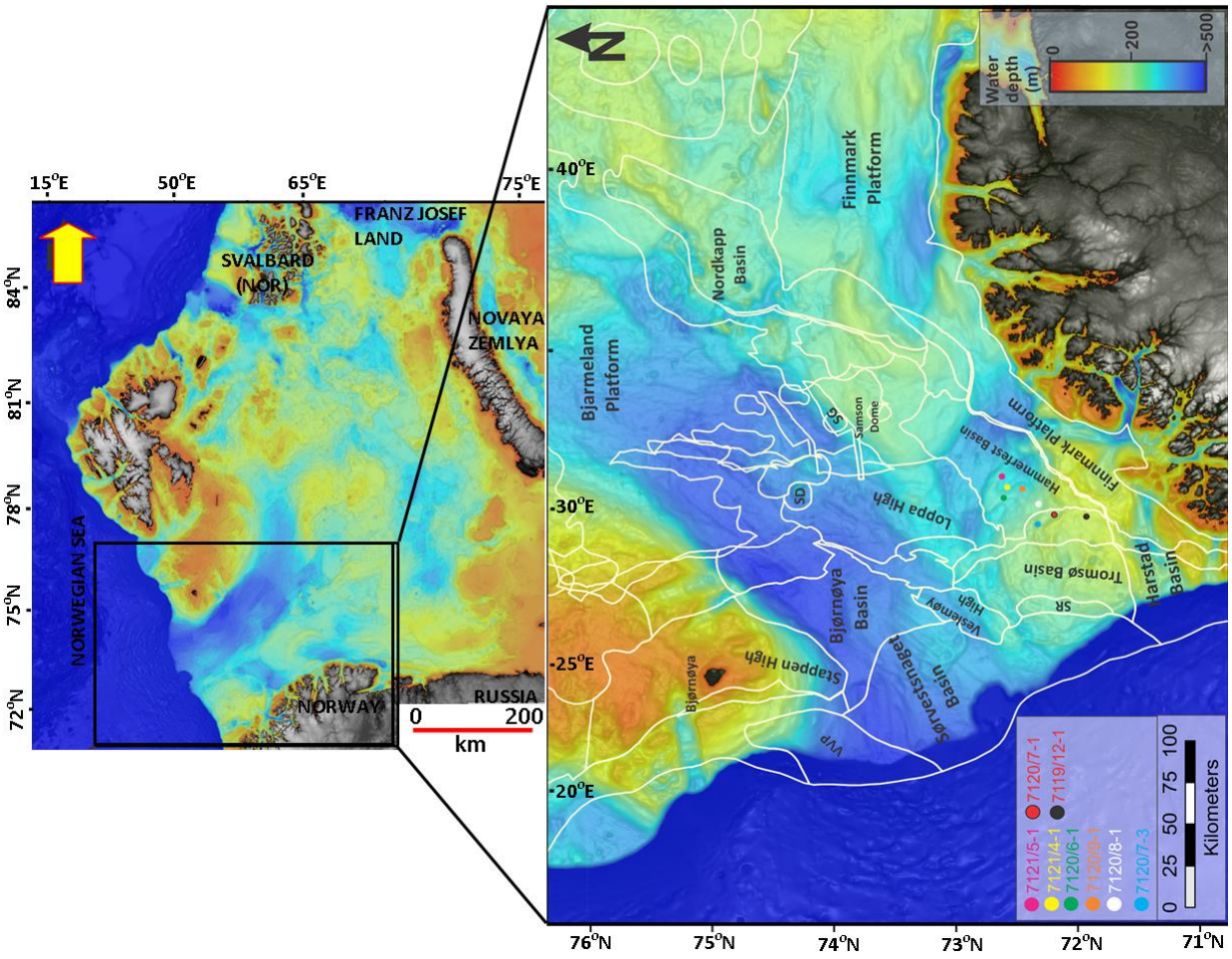

Figure 1.1: Location of the Barents Sea along with zoom view of the study area (raw data from Jackobssen et al. 2012).

In 1980, the licensing opened in the Norwegian Barents Sea. Upto now roughly 96 exploration wells have been drilled. Though, nearly 25 discoveries have been achieved and most of them are in the Hammerfest Basin (Fig. 2). The success rate is high as compared to the Norwegian North Sea. The cause behind this achievement is the presence of a number of petroleum systems (Ohm et al. 2008; Faleide et al. 2010). The multiplicity traps (fault and salt structures, stratigraphic pinch-out) and seals, different source rocks ranged from the Carboniferous to the Cretaceous in age and good quality reservoir rocks from Permian to Paleocene age are present in the area. Mainly, there are gas discoveries (eg. Snøhvit, Askeladd etc.) as well as few small oil discoveries (eg. Goliat, Nucula). Recently, two oil discoveries (Skrugard and Havis) developed the interest of many companies for the further drilling.

Figure 1.2: Locations of hydrocarbon in the Norwegian Barents Sea (Ohm et al. 2008).

The Barents Sea has been faced different phases of uplift and erosion made it difficult to find the viable petroleum accumulation. The northwest part toward the Stappen High is the more uplifted part e.g. 300m (Dore and Jensen 1996) while in the Hammerfest and Tromsø Basins its range is 0 to 500m (Nyland et al. 1992).

The updated technology and ideas are essential to extract the petroleum in the uplifted area like the Barents Sea. By the careful estimate of the uplift it will be easy to interpret source rock maturation and reservoir quality forecast which are essential for the exploration success.

As we know the Barents Sea has been faced several stages of subsidence, uplift and erosion which effected the reservoir properties i.e. porosity, permeability. According to Worden and Morad (2009), the reservoir quality of sandstones at any depth is mainly controlled by the initial depositional porosity and permeability, extent of mechanical and chemical compaction and quantity and type of pore-filling cement. The porosity reduction due to the mechanical compaction ceased when the chemical compaction starts. Quartz cementation is the main factor of the porosity loss at the depth greater than 2.5 km (Paxton et al. 2002). The cementation is mainly controlled by the temperature and kinetics. The chlorite coating and micro-quartz coating are the factors which prevent or delay the quartz cementation in deeply buried sandstones (Bjorlykke and Jahren 2010).

1.2 Research objectives

The main objective of my thesis research is to analyze the reservoir quality of Jurassic sandstones in SW Barents Sea from the cored reservoir interval in given eight wells. During this analysis thin section samples made from cores are analyzed under microscope. Additionally, SEM analysis is also employed on both gold coated stub mounted samples as well as carbon coated thin section slides. XRD analysis has been done on selected both bulk and clay separation samples to confirm the mineralogy. Above study will be helpful in the interpretation of the depositional environment which depends on the lithology, distribution of grain size and sorting. This study also consists of the analysis of diagenetic clay coating, micro-quartz coating and its distribution in sandstones, and evaluates their influence on reservoir quality.

1.3 Study area

The study area is comprised of the central part of Hammerfest Basin and eastern part of Tromsø basin (TROMS I) (Fig. 1.3). The area is highly faulted due to several stages of uplift and erosion (Fig. 1.3). The wells 7119/12-1, 7120/7-1 and 7120/7-3 are situated in the transition zone Tromsø/Hammerfest Basin, while the other five wells are in the Hammerfest Basin (Table 1.1). The main reservoir rocks are Lower and Middle Jurassic sandstones of Stø and Nordmela Formations which contain gas, condensate and oil (NPD 2013). The study area is bounded between the Troms-Finmark fault complex (TFFC) and Loppa High towards south

and north respectively, where its eastern and western parts are bordered by Bjarmeland Platform and Tromsø/Hammerfest Basins transition zone

The dominant source of sediments was the east but also some supply came from north and south (Olaussen et al. 1984).

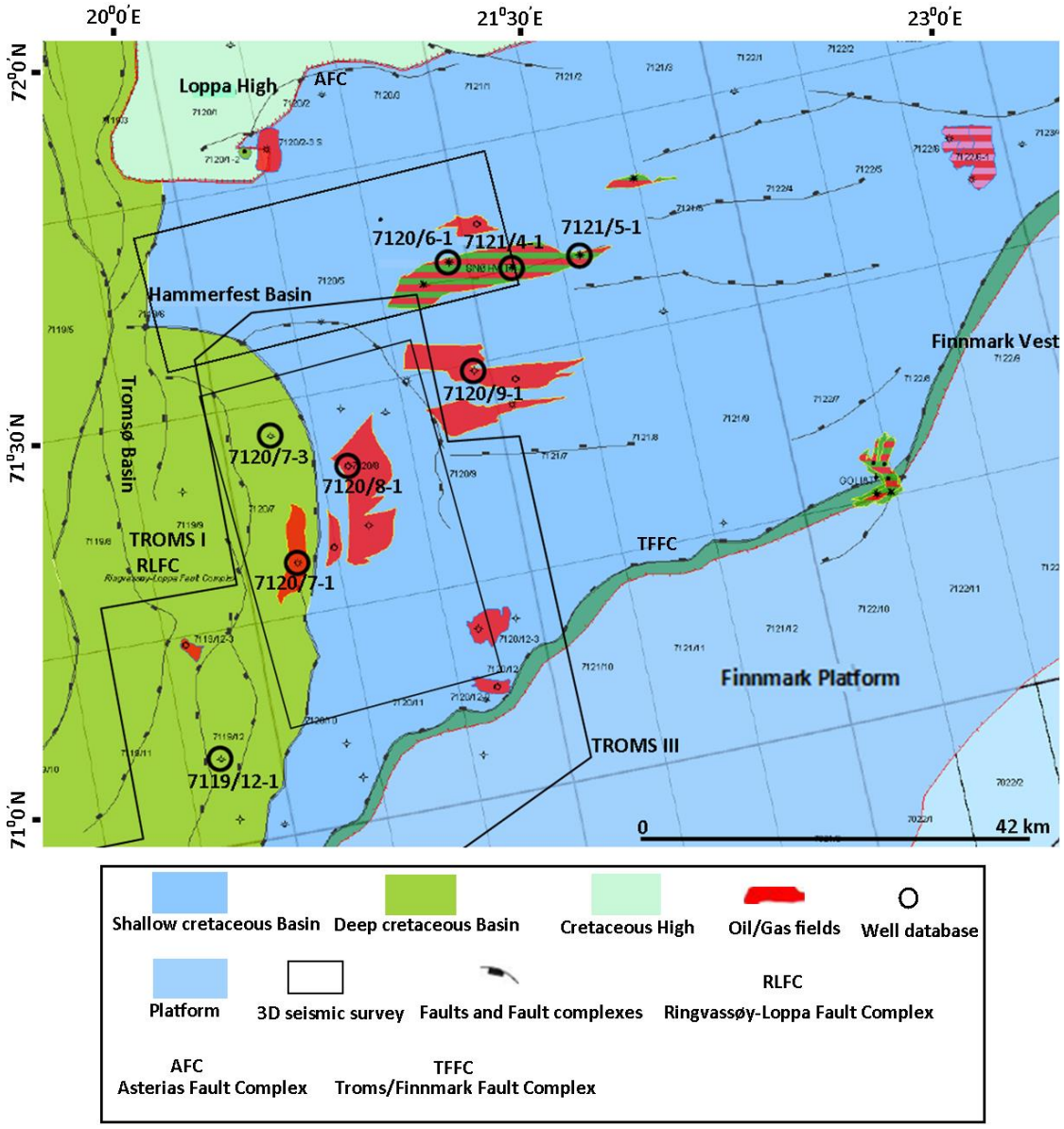

Figure 1.3: Location of the study area along with structural elements. (NPD 2013)

1.4 Database and methodology

A total of 20 thin section samples from 8 exploration wells have been used in this study. Most of the wells are wildcat (W) and two are appraisal. The wells 7119/12-1, 7120/6-1, 7120/7-3 and 7121/5-1 are dry and the rest of others contain the hydrocarbon (mostly gas). All the wells used in this research have been given in the table 1.1.

Table 1.1: All the wells used in the study with their purpose (NPD 2013).

Wells	Total depth (MD)	Entry date	Completion date	Temp. gradient (^{0}C/km)	BHT (^{0}C)	Purpose	Content
7119/12-1	3088	14.06.1980	10.10.1980	29.8	96	W	Oil
7120/6-1	2820	02.02.1985	02.05.1985	35.46	104	A	Oil/Gas
7120/7-1	2839	31.07.1982	08.10.1982	34.52	102	W	Gas
7120/7-3	3062	18.03.1984	09.06.1984	30.38	97	W	Shows
7120/8-1	2610	28.06.1981	10.09.1981	34.86	95	W	Gas/Condensate
7120/9-1	2300	25.07.1982	26.09.1982	30	73	W	Gas
7121/4-1	2609	06.08.1984	27.10.1984	32.2	88	W	Oil/Gas
7121/5-1	3200	07.06.1985	28.09.1985	34.72	115	A	Oil/Gas

The reservoir properties from core cuttings, thin sections and both gold coated stub mounted samples were investigated by these methods:

1. Mineralogical and petrographic analysis

1.1. Optical microscopy

1.2. Scanning electron microscopy (SEM)

1.3. X-Ray diffraction (XRD) analysis

1.5 Chapter descriptions

The master thesis is divided into seven chapters along with their titles.

The introduction with background and motivation, research objectives and methodology is included in the chapter 1.

Chapter 2 describes the regional geology including with Hammerfest and Tromsø Basins along with their stratigraphy with emphases on reservoir rocks.

The theoretical background about mechanical compaction and diagenesis is discussed in chapter 3.

Chapter 4 covers all the methods and materials used in this study for the analysis of the reservoir properties.

Petrophysical analysis which includes well correlation, porosity prediction and different crossplots is discussed briefly in chapter 5.

In Chapter 6, all the observation and results from thin section analysis, SEM analysis and XRD analysis are displayed from both Stø and Nordmela Formations.

The whole discussion of the study is in the chapter 7.

Chapter 2: Geology of SW Barents Sea

2.1 Regional tectonics and geological evolution

2.2 Hammerfest Basin

2.3 Tromsø Basin

2.4 Stratigraphy

Chapter 2: Geology of SW Barents Sea

As compared to the North Sea the geological history of Barents Sea is more complex because of the different stages of tectonic uplift. The reservoir quality in this area is affected by these uplift stages. So, there is a need to understand the geology of this area to estimate the reservoir properties.

2.1 Regional tectonics and geological evolution

The Barents Sea is divided into two main geological provinces due to different tectonic history i.e. eastern province and western province. The western province is affected by the Mesozoic and Cenozoic tectonic activity where the eastern province was influenced by late-Paleozoic tectonism and deformation has occurred in the Post Jurassic time (Gabrielsen et al. 1990). During the Early Palaeozoic time the geological evolution started in the Barents Sea and its surrounding area which divided into four stages (Fig. 2.1).

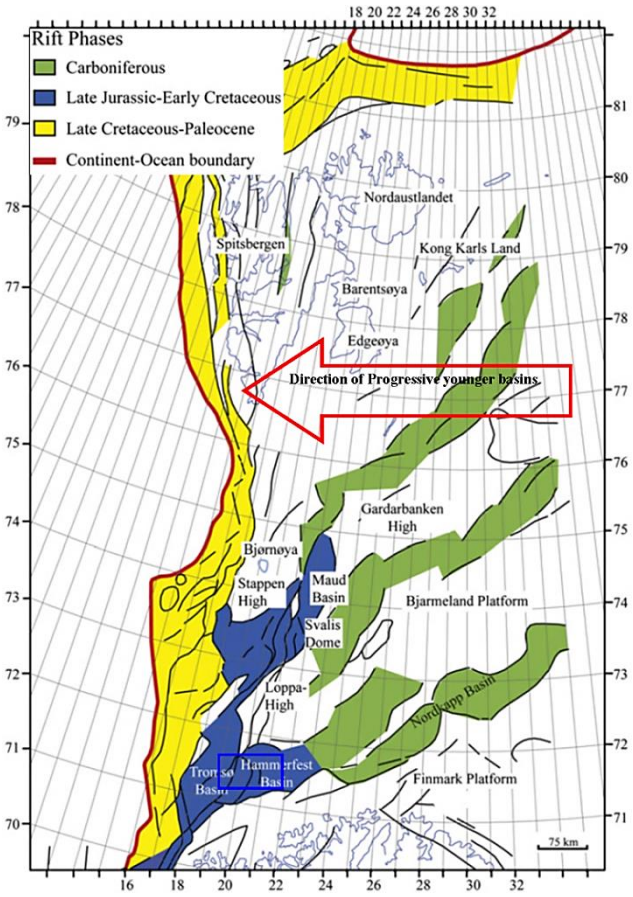

Figure 2.1: Main structural elements in the Barents Sea (Gabrielsen et al. 1990; Faleide et al. 2008). Different colors are showing the focus of tectonic activity through time. Study area is shown by blue rectangle (Modified from Glorstad-Clark et al. 2010).

The oldest tectonic activity which can be regionally mapped in the western part of Barents Sea happened in Late Devonian-Early Carboniferous (Fig. 2.2). The creations of this activity are half-grabens and intervening highs which controlled the depositional environment of source, reservoir and cap rocks (Dengo and Rossland 1992; Gabrielsen et al. 1990; Breivik et al. 1995). The Caledonian basement was formed during late Silurian to early Devonian which was uplifted, eroded and deposited as red molasses sediments into the intramontane basins of Ireland, Scotland, western Norway and Eastern Greenland (Faleide et al. 1984). The extentional fault's directions were NE-SW and WNW-ESE to NW-SE during the late Devonian-Early carboniferous time (Berglund et al. 1986; Rahman 2012).

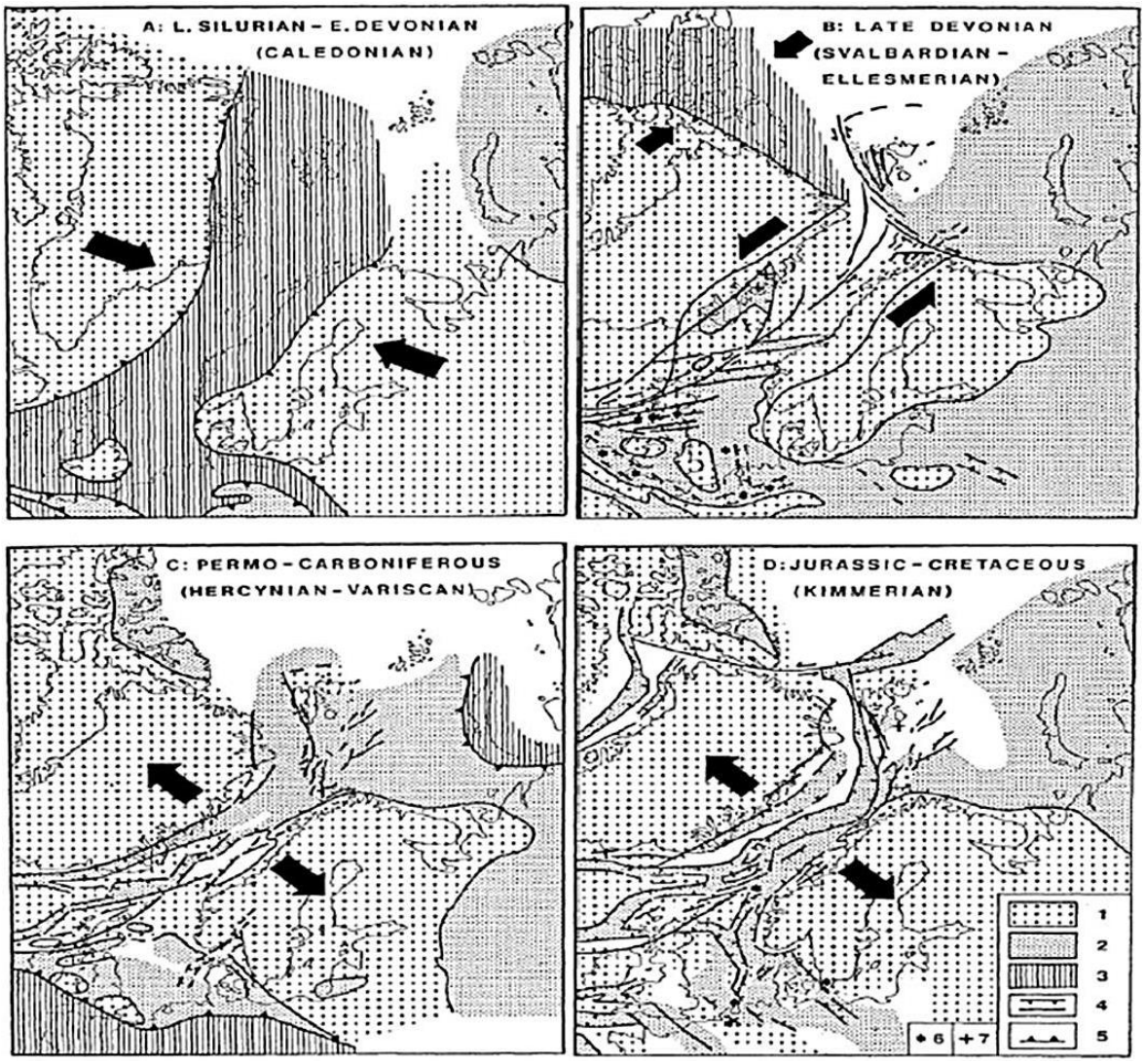

Figure 2.2: Evolution stages in the western Barents Sea and surrounding area. (Modified from Faleide et al. 1984). 1, stable elements – continental cratons and intrabasinal highs; 2, sedimentary basins; 3, active foldbelts; 4, normal and wrench fautls; 5, deformation front of active foldbelts; 6, intrusions; 7, volcanics.

The Pechora Basin in the eastern part of the Barents Sea was similar to the Upper Devonian Basin which was possibly filled with the clastic sediments, carbonates and evaporates. The lower Carboneferous depicts a widespread clastic sequence with coal seams in the west and north while the carbonate sediments were dominated to the east (Nalivkin 1973; Faleide et al. 1984).

In the Nordkapp Basin and Tromsø Basin evaporates were deposited during the quite tectonic period of the middle Carboniferous-Lower Permian. During the Permian times the depocetres for the marine sediments were in the NE and SW direction of the present Hammerfest Basin (Berglund et al. 1986). The low impedance marine sediments like shale, siltstone and sandstone were deposited in the Early to middle Triassic time which marked the Permo-Triassic boundary and the subsidence was pronounced towards the east (Faleide et al. 1984). After the uplift in the east a regional unconformity was created and deposition started toward west (Mark et al. 1982; Faleide et al. 1984). At the end of the Triassic the sea level fall and interbedded high and low energy sediments were deposited. A slightly higher rate of subsidence then deposition reflects a transgressional phase during the whole Jurassic period (Faleide et al. 1984).

The Barents Sea region was relatively stable during the Early Kimmerian tectonics at the Triassic-Jurassic transition but during Mid Kimmerian phase in the Middle Jurassic time significant rifting was started. Kimmerian tectonics started in the Barents Sea with shallow depth normal faults. The discrete pulses in Mid Kimmerian affected the rift system during the Middle and Late Jurassic and during syn-rift stage, Late Jurassic transgressive sediments were deposited in rift basin (Faleide et al. 1984). The relative sea-level rise in Middle Jurassic time managed to deposit the Stø Formation which is generally a good reservoir in the SW Barents Sea (Berglund et al. 1986). The organic rich clays which are good for hydrocarbon generation were deposited and Mid Kimmerian tectonics ended during Upper Jurassic. The Jurassic-Cretaceous transition time was the start of Late Kimmerian tectonic regime and a number of deep penetrated normal faults were formed along the weak zone of the Caledonian basement. Due to this movement the tilted fault blocks in the hinge zone in the SW Barents Sea were created (Faleide et al. 1984).

In the Aptian-Albian time, the whole regional basin subsidence relative to the uplifted and eroded Svalbard Platform created the main structural elements. The Loppa High was reversed

between the subsidence of Bjørnøya and Hammerfest Basins and the rate of subsidence towards the west was higher as compared to the eastern part of the Loppa High fault complex.

2.2 Hammerfest Basin

The Hammerfest Basin lies in the greater Barents Sea and is the most promising basin for hydrocarbon exploration. The Hammerfest Basin is a complex basin (150 km long and 70 km wide) which was developed during the second rift phase (Mesozoic) in Barents Shelf (Berglund et al. 1986). The Hammerfest Basin separated from the Finnmark Platform during Late Carboniferous. The Tromsø and Hammerfest Basins were inter-related parts of a broader epiorogenic depositional system in Triassic to Early Jurassic (Berglund et al. 1986, as cited in Gabrielsen et al. 1990). The Basin is bordered by the Loppa High in the north, the Tromsø Basin in the west, Troms-Finnmark platform to the south and the structural relief gradually dies out towards the eastward (Fig. 2.3).

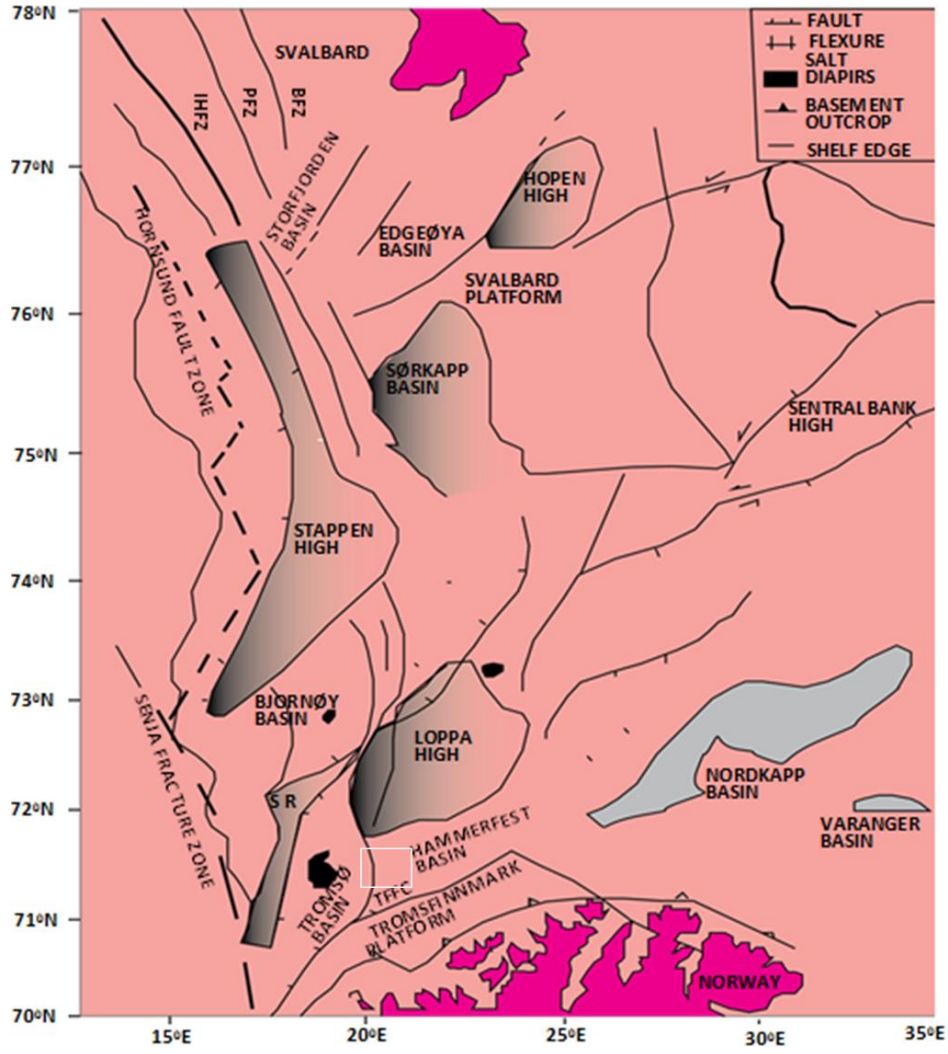

Figure 2.3: Regional level structural map of western Barents Sea. Study area is shown by white triangle (modified after Faleide et al. 1984).

According to Berglund et al. 1986, five types of faults have been recognized in the Hammerfest Basin (Fig. 2.4). Tromso-Finnmark Fault Complex (TFFC) is a listric fault and is controlled by one or two major listric faults, Ringvassøy-Loppa Fault Complex (RLFC) has a number of normal faults which has been reenergized many times and Southern Loppa High Fault Complex (SLHFC) is considered by two southward dipping normal faults jointed with the complex pattern of small south and northward dipping faults. Under the transtensional strike slip regime E-W oriented normal faults formed which latterly reenergized in early cretaceous time due to tensional stress, the shallow faults which may be the growth faults do not breach the lower Triassic succession (Berglund et al. 1986).

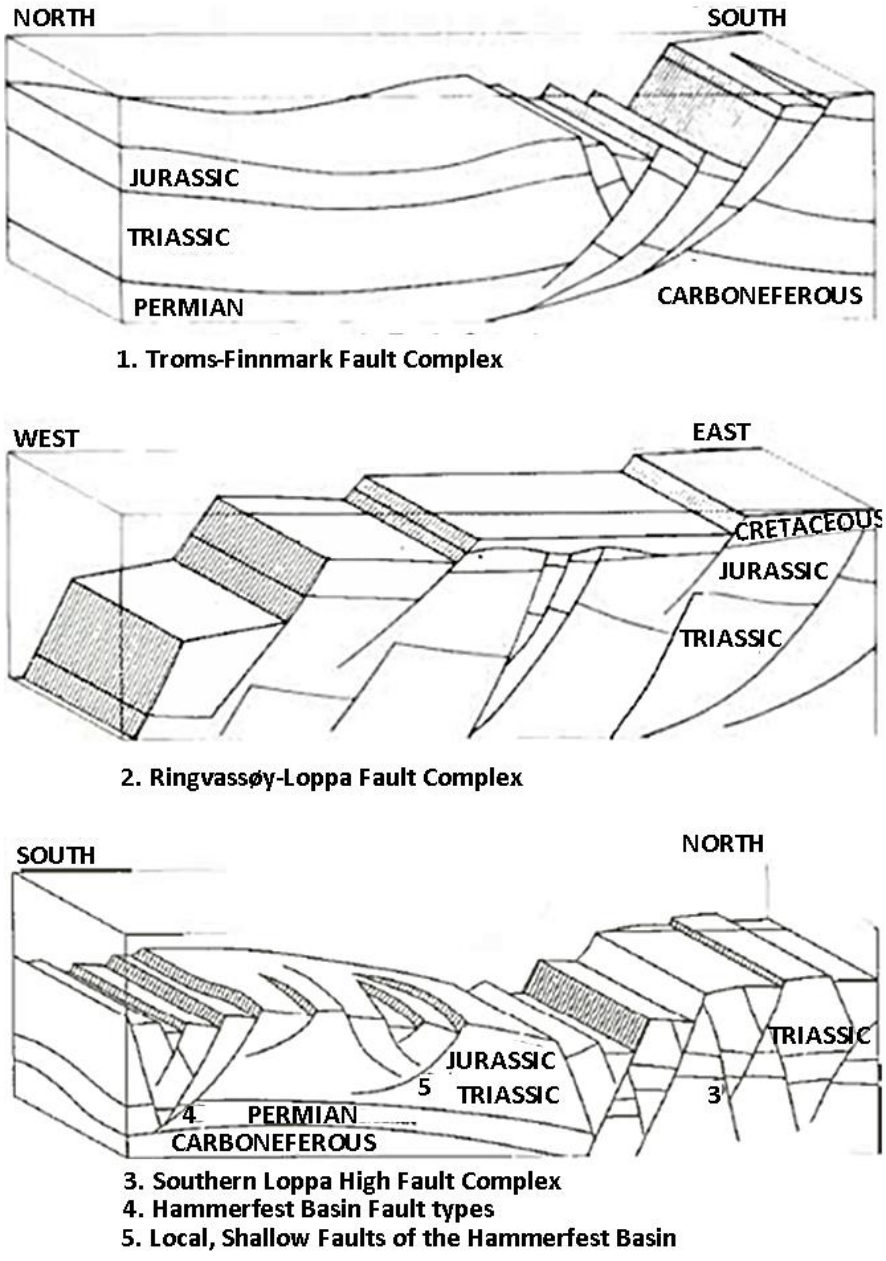

Figure 2.4: Fault types in Hammerfest Basin (modified after Berglund et al. 1986).

2.3 Tromsø Basin

The Tromsø Basin is located at north of the town of Tromsø, from 710-720 15'N and 170 30'-190N 50'E (Fig. 2.3). Ringvassøy-Loppa Fault Complex lies towards the east and its western limit is marked by the Senja Ridge. It is terminated against Troms-Finnmark Fault Complex towards the southeast, where the southwestern margin is still less understood. The Veslemøy High separated the Tromsø Basin from Bjørnøya Basin in the north. The Tromsø Basin contains a series of salt diapirs which are linked together with a smooth flexure and related with a system of detached faults in the central part of the southern area (Gabrielsen et al. 1990). Based upon gravity data, the basement depth has been estimated to 10-13 km (Roufosse 1987, as cited in Gabrielsen et al. 1990).

In the Late Palaeozoic, evaporates deposited in the Tromso Basin. Currently large salt domes penetrate through the thick Mesozoic, Tertiary beds and some of which extend through the sea-bottom (Berglund et al. 1986). Halokinesis has played a major role in the development of structure in Tromsø Basin and subsidence that occurred during the cretaceous time has been described as an effect of salt (Øvrebø & Talleraas 1976, 1977, as cited in Gabrielsen et al. 1990).

2.4 Stratigraphy

Due to the purpose of this thesis project, the focus will be on Kapp Toscana Group. The Kapp Toscana Group is rich in sandstones of different origins which is Triassic and Jurassic in age. The Lower to Middle Jurassic sandstones are present in study area which extended throughout the whole Hammerfest and Tromsø Basins (Fig. 2.5).

- **Snadd Formation**

It consists of basically prodeltaic shales, interbeded siltstones and sandstones and locally developed thin coaly lenses (Dalland et al. 1988).

- **Fruhomen Formation**

It comprises of grey to dark grey shales and upper part has interbedded sandstones, shales and coals (Dalland et al. 1988). The open marine shale was deposited during the Rhaetian transgression when the whole area was covered by water.

- **Tubåen Formation**

The Tubåen Formation is dominated by sandstones, subordinate shale and minor coals. The southeast basinal margins are rich in coals which die out towards the northwest (Dalland et al. 1988).

- **Nordmela Formation**

It consists of interbedded siltstone, sandstone, claystones, shales and minor coal. Towards the top sandstones becomes more dominant (Dalland et al. 1988).

- **Stø Formation**

It is mainly dominated by mature and moderate to well sorted sandstones and the minor shale and siltstone are also present in this Formation. Its thickness is high in the southwest part as compared to the eastward in Hammerfest Basin (Dalland et al. 1988).

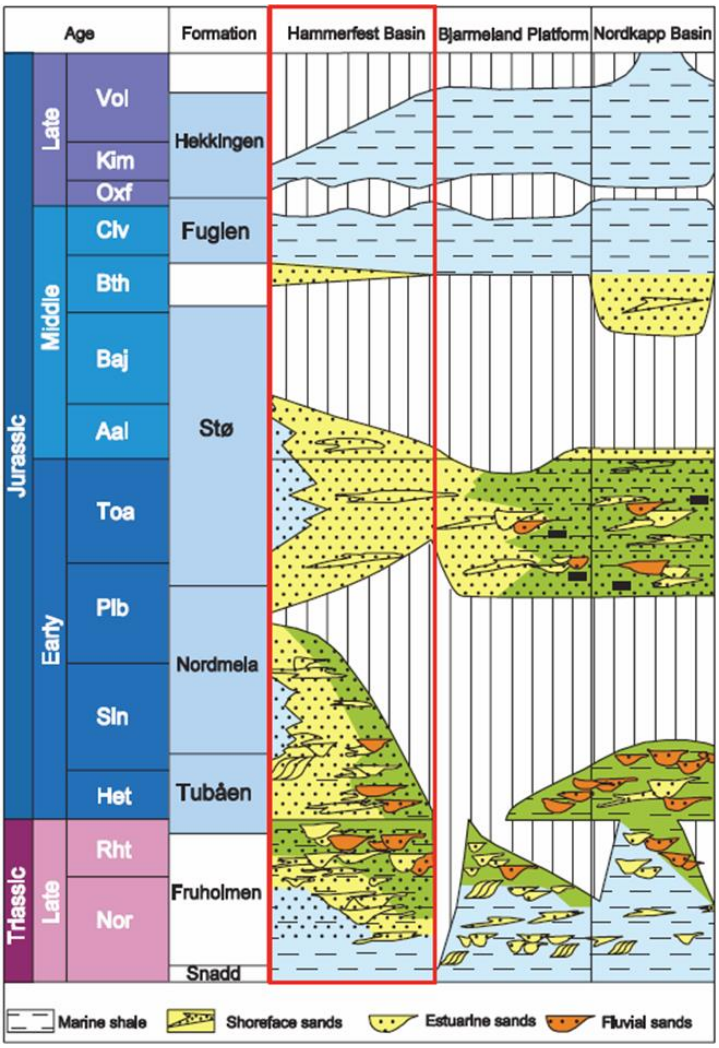

Figure 2.5: Triassic-Jurassic stratigraphy of Hammerfest basin (Wennberg et al. 2008).

The Stø Formation is of shallow marine environment (esturine, lagoonal, beach) while Nordmela and Tubåen Formations are of lower coastal plane and upper coastal plain environments respectively (Fig. 2.6) (Wennberg et al. 2008). The Lower-Middle Jurassic Stø Formation is a clean sandstone which is a main reservoir in this area while the Nordmela and Tubåen Formations also have the good reservoir potential too (Berglund et al. 1986).

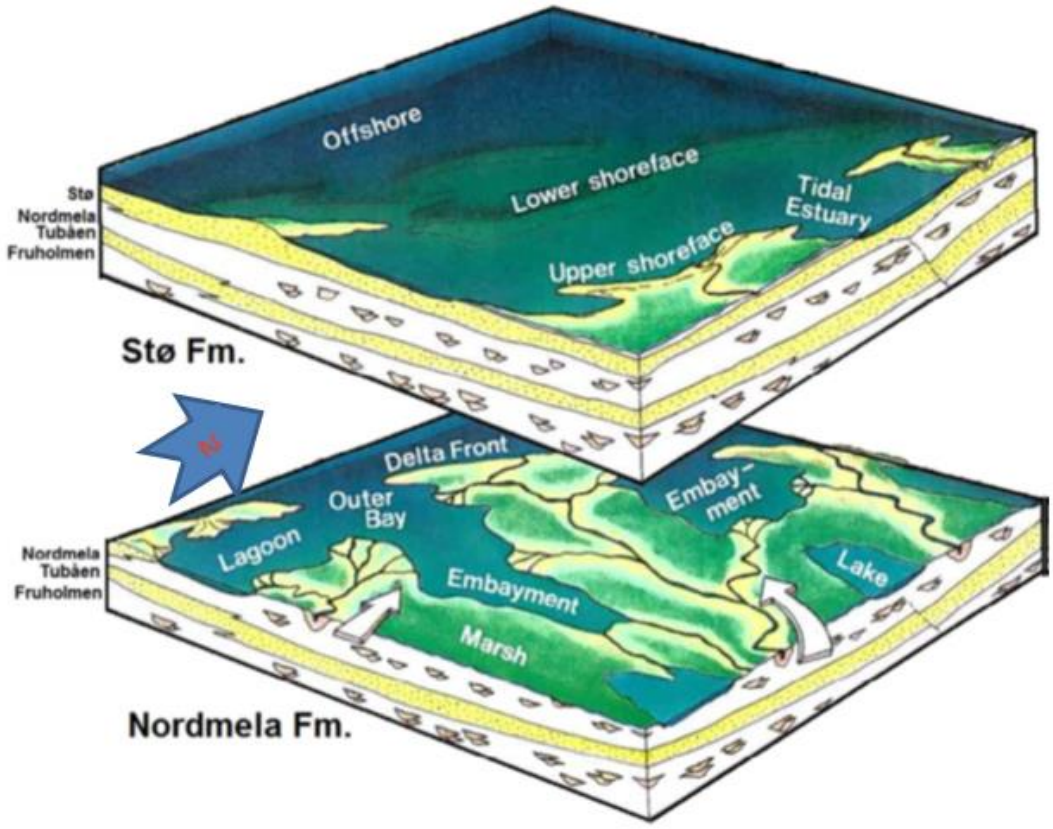

Figure 2.6: Paleogeographic and depositional model for Nordmela and Stø formations (modified after Berglund et al. 1986).

Chapter 3: Theoretical background

Chapter 3: Theoretical background

3.1 Introduction:

The properties of sandstones are continuously changing from the time of deposition, through burial at greater depth and during uplift while these properties depend on its composition at shallow depth, temperature and stress history during burial. The initial composition of sandstones depends upon its provenance, depositional environment and transport. Several different diagenetic processes which act continuously on the sandstones just after their deposition to the present are reported. The initial or primary clastic composition and the depositional environment are the two most important factors to predict reservoir quality at depth (Fig. 3.1) (Bjørlykke and Jahren 2010).

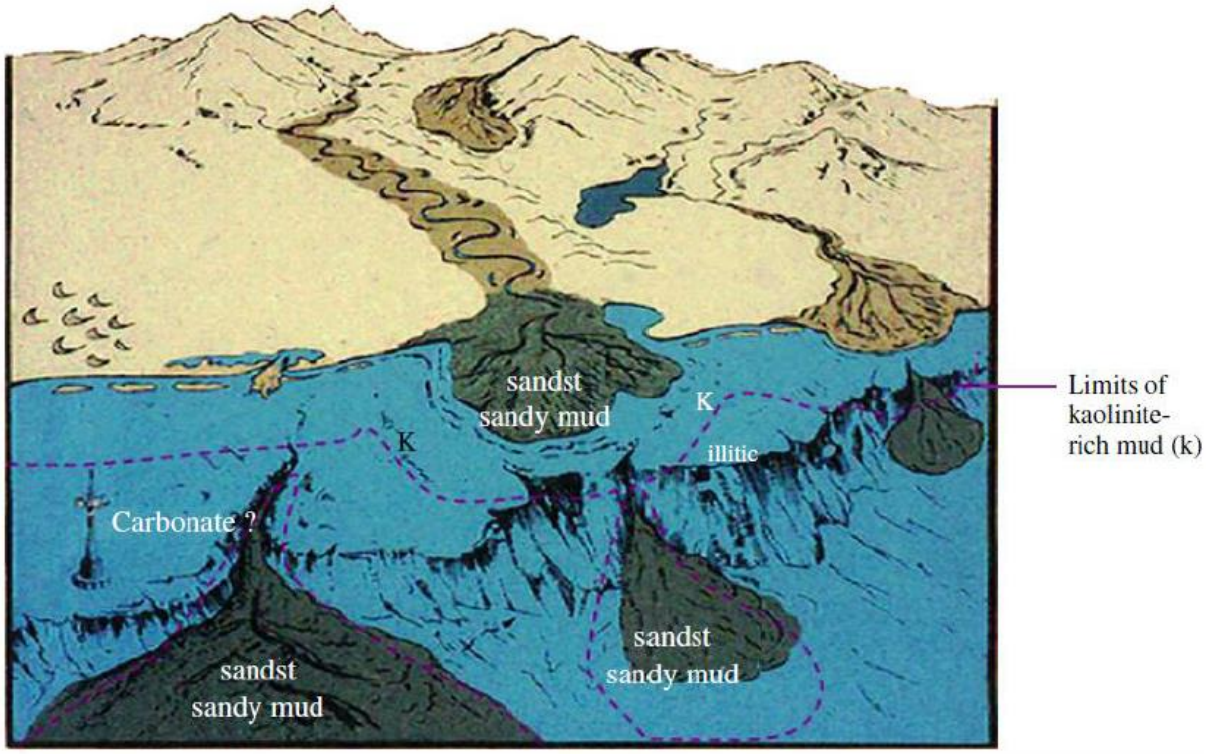

Figure 3.1: Schematic illustration of a sedimentary basin on a continental margin (Bjørlykke, 2010)

3.2 Compaction

The main diagenetic processes are mechanical and chemical compaction where mechanical is stress dependent and chemical depends upon time and temperature (Bjørlykke and Jahren 2010). The main porosity reduction method at shallow depth is mechanical while at deep

burial, porosity is lost by the precipitation of quartz cement. The potential for change in bulk composition of sediments at shallow depth (less than 10 m) is larger compared to at greater burial depth because the sediments react with air or water both by fluid flow and diffusion (Bjørlykke & Jahren 2010). In desert environments the coating of iron-oxides and clays on desert sands avoid the quartz overgrowth at greater depth and preserve porosity.

3.2.1 Mechanical Compaction

Mechanical compaction is controlled by effective stress (difference between lithostatic pressure and pore pressure) and its magnitude depends upon the strength of grains and their framework (Fig. 3.2). Mechanical compaction can reduce the porosity in sandstones from 40-42% to 25-35% at stresses of 20-30 MPa (Chuhan et al. 2002) which dominates in shallow part of the basin down to 2-4 km depth (80-100^{0}C), depending on the geothermal gradient (Chuhan et al. 2002; Mondol et al. 2007).

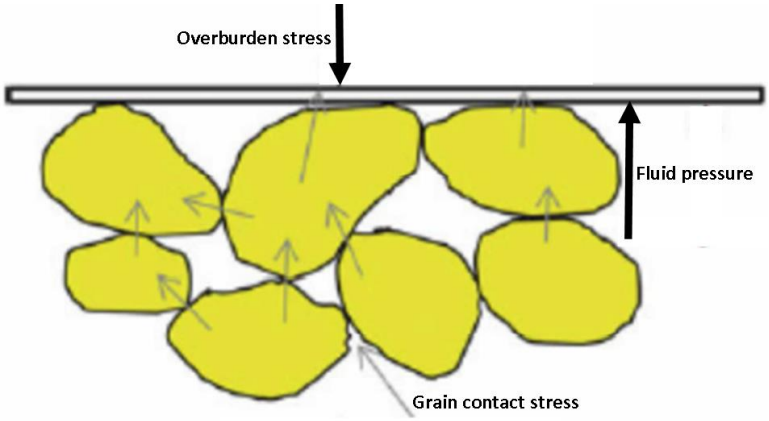

Figure 3.2: The effective stress from the overburden (σ'v) is carried by the mineral grain framework and pore pressure (modified after Bjørlykke and Jahren 2010).

The weight of the overburden sediments and fluids in the pore space produce a vertical stress and it can be calculated as follows:

$\sigma v = \rho b\, gh$ …….…… (3.1)

Where,

ρb = Average bulk density of overburden sediments.

g = Gravitational force.

h = Thickness of the overburden sediments.

The difference between the total vertical stress (σv) and the pore pressure (Pp) is called the effective stress (σ'v).

σ'v = σv–Pp …….…… (3.2)

This effective stress is the main controlling factor of mechanical compaction and if the pore pressure increases it reduces the vertical effective stress and will preserve porosity between the grains even in greater depth (Bjørlykke and Jahren 2010). Some other factors like grain size, sorting and the rate of fluid expulsion from the compacting sediments also affect mechanical compaction (Waples and Couples 1998; Bjørlykke et al. 2004). The compaction of sand varies depending upon the sorting and grain size. The coarse grained sand compact more compared to the fine grained due to grain crushing (Fig. 3.3) (Bjørlykke and Jahren 2010).

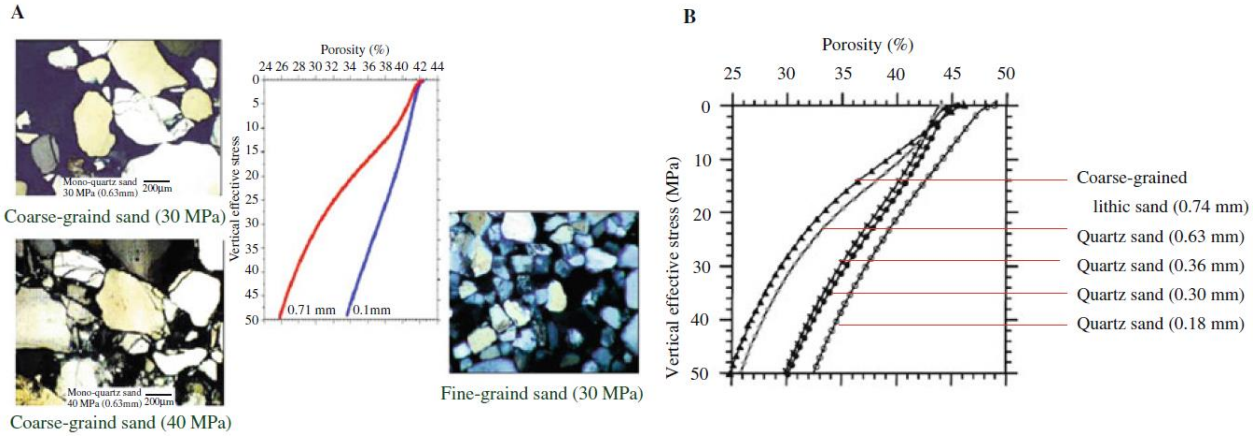

Figure 3.2: Experimental compaction of fine-grained and coarse-grained sand showing that well sorted fine-grained sand is less compressible as compared to the coarse-grained sand. (b) The porosity loss as a function of grain size due to more grain crushing (modified after Bjørlykke & Jahren 2010).

Carbonate cementation and leaching of K-feldspar are the two important processes for reservoir properties at shallow depth. At shallow depth, biogenic carbonate within the rock yields the carbonate cement due to the relatively high kinetic reaction rate of carbonate minerals, dissolve and re-precipitate as carbonate cement which becomes unstable below the redox boundary (Saigal and Bjørlykke 1987). The carbonate cement is mainly depending upon the biological production and rate of clastic sedimentation.

The pore filling Kaolinite precipitates by the leaching of K-feldspar and mica which affects the reservoir properties i.e Brent Group (Bjørlykke et al. 1992). Kaolinite is altered to illite in

the presence of K-feldspar at temperature 120-140˚C and affects the permeability of sandstones. The chemical reaction of this process is controlled by the K^+/H^+ ratio and can be written as:

$$2K\ (Na)\ AlSi_3O_8 + 2H^+ + 9H_2O = Al_2Si_20_5(OH)_4 + 4H_4SiO_4 + 2K^+(2Na^+)$$

Feldspar Kaolinite disolved silica disolved cations

$$2KAl_3Si_3O_{10}\ (OH)_2 + 2H^+ + 3H_2O = 3Al_2Si_20_5(OH)_4 + 2K^+$$

Muscovite Kaolinite (Bjørlykke & Jahren 2010)

3.2.2 Chemical compaction

Chemically compaction normally start from 2 to 2.5km depended on the temperature gradient and increase the strength of the rock and stop mechanical compaction. Temperature is the main factor in chemical compaction and other factors are primary mineral composition, pore-fluid composition and time-temperature history etc. (Bjørlykke 1998; Peltonen et al. 2008). The zone where mechanical compaction ceases and chemical compaction starts is called the transition zone (Fig. 3.3). The chemical compaction will continue during the uplift as long as the temperature is above 70-80℃ but the rate is slower because of the lowering of temperature due to upliftment (Bjørlykke and Jahren 2010) (Fig. 3.3).

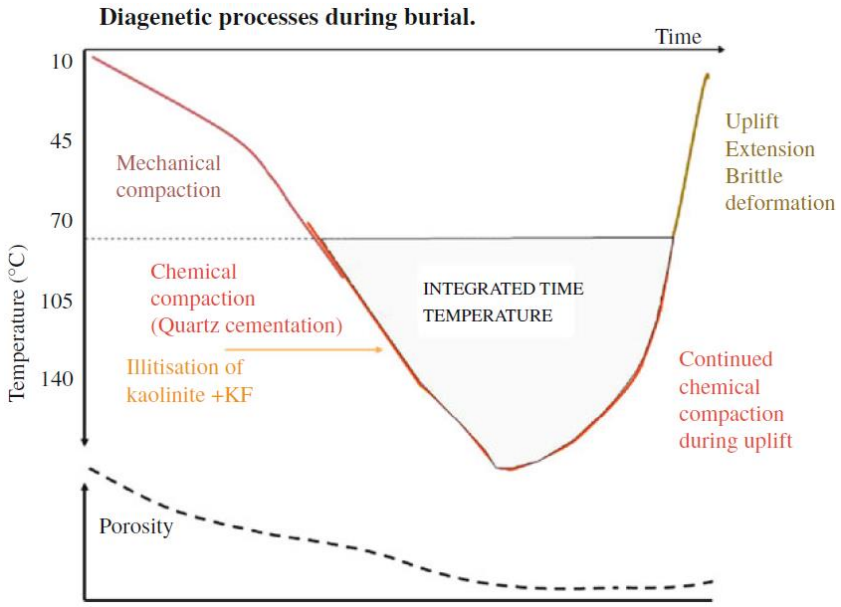

Figure 3.3: Diagenetic processes mainly quartz cementation as a function of temperature and time. Note that quartz cementation will continue also during uplift as long as the temperature exceeds 70-80℃ (Bjørlykke and Jahren 2010).

Albitization can also alter the composition of reservoir rocks during the intermediate depth (2.0–3.5 km, 50–120℃) (Bjørlykke and Jahren 2010). The reaction can be expressed as:

$$\underset{\text{K-feldspar}}{KAlSi_3O_8} + Na^+ \longrightarrow \underset{\text{Albite}}{NaAlSi_3O_8} + K^+$$

Saigal et al. (1988).

The transition in sandstones starts from 70-80℃ while in shales it depends upon the stability of the primary minerals and burial history (Bjørlykke 1998; Peltonen et al. 2008). The alteration from smectite to illite start from 60-70℃.

$$\text{Smectite} + \text{K-feldspar} = \text{Illite} + \text{Quartz}$$

With the increase in temperature and depth the quartz cementation continues until all porosity is lost and at temperature 200-300℃ sandstone converts into quartzite (Bjørlykke and Jahren 2010). If kaolinite and k-feldspar are present together in a reservoir and the temperature reaches 120-130℃, illitization starts (Storvoll and Brevik 2008). The transition of kaolinite to illite is most important reason of reducing reservoir properties (Bjørlykke et al. 1992). The illitization reaction can be written as:

$$\underset{\text{K-feldspar}}{2K(Na)AlSi_3O_8} + \underset{\text{Kaolinite}}{Al_2Si_2O_5(OH)_4} \longrightarrow \underset{\text{Illite}}{KAl_3Si_3O_{10}(OH)_2} + \underset{\text{Quartz}}{SiO_2} + 2H_2O$$

3.3 Quartz cementation

There have been different theories about the source of silica. These theories include a large flux of dissolved silica water into sandstones and internal pressure solution processes from quartz-quartz contacts. Dissolution often occurs at illite clay or mica and quartz grain contacts (Fisher et al. 2000). These contacts are called stylolites and due to the transportation of dissolved silica at stylolites to the grain surfaces by diffusion, quartz overgrowth is formed (Fig. 3.4).

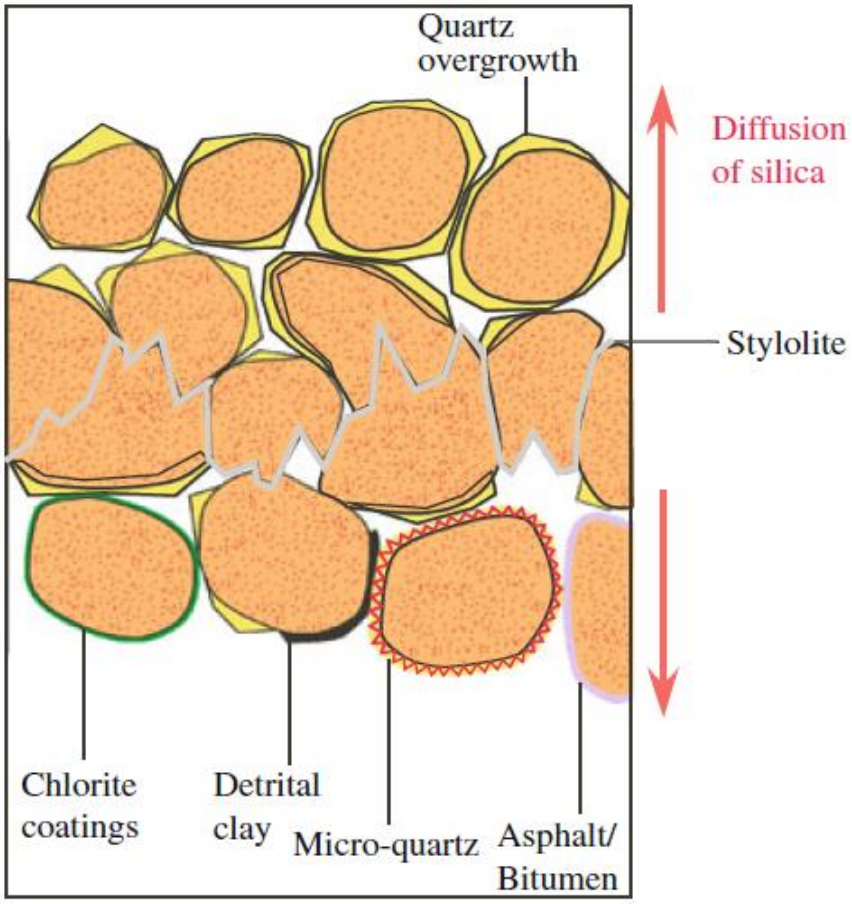

Figure 3.4: Schematic illustration of a stylolite. The dissolved silica is transported away from clay rich stylolite by diffusion (Bjørlykke and Jahren 2010).

According to Bjørlykke and Jahren (2010), sometimes the precipitation of micro-quartz acts as a coating which preserves porosity at greater depth by preventing the quartz cementation. This takes place when the pore water is supersaturated with respect to quartz through dissolution of Opal A or Opal CT around 65℃ forming porosity preserving micro quartz. The availability of the surface area is also an important factor for the quartz precipitation (Walderhaugs 1996).

3.4 Porosity preserving mechanisms

Several different mechanisms which preserve porosity at greater depth have been suggested. According to Bloch et al. (2002), high porosity in sandstones at a greater depth is due to:

- Early emplacement of hydrocarbons
- Shallow development of fluid overpressure
- Grain coats and grain rims
- Secondary porosity

3.4.1 Early emplacement of hydrocarbons

The Porosity preservation due to early emplacement of hydrocarbons in sandstones is still unclear in literature. The presence of hydrocarbons in sandstone reservoir can affect the porosity (Johnson et al. 1920) however, Aase and Walderhaug 2005; Ramm and Bjørlykke 1994; Walderhaug 1994 differ on this account.

3.4.2 Shallow development of fluid overpressure

The development of fluid overpressure in sandstones significantly reduces the effective stress, thus decrease mechanical compaction and preserve porosity. The overpressure can be developed if rate of pore volume reduction is fast relative to the rate of fluid release or if pore fluid expansion is fast relative to the rate of fluid release (Bloch et al. 2002).

3.4.3 Grain coats and grain rims

It is effective only in detrital-quartz-rich sandstones and is an important mechanism which preserve porosity at greater depth (Bloch et al. 2002). Sandstone grains can be coated with chlorite and illite but the most important is authigenic chlorite (Taylor et al. 2010). Grain-rims characterized by coats covering the entire grain surface are here termed allogenic grain-coats. The depositional environments of these clay-coats are Shelf and eolian (Wilson et al. 1992).

Chapter 4: Methods and Materials

4.1 Well information and data base

4.2 Well correlation

4.3 Petrophysical analysis

4.4 Mineralogical and Petrographical analysis

4.4.1 Optical microscopy

4.4.1.1 Thin section description

4.4.1.2 Minerals counting

4.4.2 Scanning electron microscopy (SEM)

4.4.3 XRD analysis

4.4.3.1 Bulk analysis

4.4.3.2 Clay separation

Chapter 4: Methods and Materials

4.1 Well Information and data base

A total of 8 exploration wells have been used in this study. Most of the wells are wildcat (W) and two are appraisal. The wells 7119/12-1, 7120/6-1, 7120/7-3 and 7121/5-1 are dry and the rest of others contain the hydrocarbon (mostly gas). All the wells used in this research have been given in the table 4.1.

Table 4.1: Wells summary sheet for petrophysical analysis (NPD 2013).

Basin	**Wells**	**Entry date**	**Completion date**	**Temp. gradient (^{0}C/km)**	**BHT (^{0}C)**	**Purpose**	**Content**
Tromsø/Hammerfest Transition	7119/12-1	14.06.1980	10.10.1980	29.8	96	W	Oil
	7120/7-1	31.07.1982	08.10.1982	34.52	102	W	Gas
	7120/7-3	18.03.1984	09.06.1984	30.38	97	W	Shows
Hammerfest	7120/8-1	28.06.1981	10.09.1981	34.86	95	W	Gas/Condensate
	7120/9-1	25.07.1982	26.09.1982	30	73	W	Gas
	7121/4-1	06.08.1984	27.10.1984	32.2	88	W	Oil/Gas
	7121/5-1	07.06.1985	28.09.1985	34.72	115	A	Oil/Gas
	7120/6-1	02.02.1985	02.05.1985	35.46	104	A	Oil/Gas

Different softwares like Petrel, Diffrac Eva and Interactive Petrophysics (IP) were used for the correlation and analysis of the well data.

4.2 Well correlation

The main objective of the well correlation was to correlate the Jurassic Sandstones Formations which have the reservoir capabilities. The correlation has been done by available information in literature, check shots and different wire line logs. The lithostratigraphic units in Stø and Nordmela Formations were recognized on the basis of high and low gamma ray, neutron porosity & density crossover. The main purpose of well correlation was

1. To understand the facies distribution
2. To understand the thickness of different zones
3. To understand the geological setting

4. Crossover of NPHI and ROHB
5. Calculation of Effective porosity

4.3 Petrophysical analysis

During the petrophysical analysis, the main focus was on porosity so different cross-plots were performed. For this purpose the logs are exported from Petrel and imported to Interactive Petrophysics (IP). Different logs were cross plotted against each other to extract more information and maintain the quality. The logs which were used in this analysis are neutron porosity, bulk density, gamma ray and Vp.

4.4 Mineralogical and Petrographical analysis

Petrographical analysis has been carried out by using Optical microscopy,Scanning electron microscopy (SEM) and X-Ray Diffraction (XRD) analysis.

4.4.1 Optical microscopy

4.4.1.1 Thin section description

All the thin sections have been studied under a Nikon Optiphot-Pol petrographic microscope in order to extract detailed information. The information about the lithology, grain contacts, cementation, grain coating, grain shape and sorting has been acquired from the thin sections.

4.4.1.2 Minerals counting

A Swift automatic counter was used for point counting 300 points on each thin section to find out the mineral content. Nikon Optiphot-Pol petrographic microscope was also use to present the results in this study. The minerals which were counted are as following:

1) Quartz 2) Feldspar 3) Rock Fragments 4) Matrix 5) Quartz cement 6) Carbonate cement 7) Authigenic clay 8) Total Porosity

4.4.2 Scanning electron microscopy (SEM)

To confirm the observations under optical microscopy JEO2 JSM-6460LV Scanning Electron Microscope (SEM) with a LINK INCA Energy 300 Energy Dispersive X-Ray (EDX) system was used. Both carbon coated thin sections and gold mounted stubs were used for SEM analysis.

Table4.1: Samples prepared for SEM analysis.

Thin section	Depth (m)	Well name
1	2532,4	7160/6-1
2	2529,6	
3	2534,31	
4	2558,51	
5	2494,3	
6	2423,45	7120/7-1
7	2432,10	
8	2250	7120/8-1
9	2253	
10	1922,1	7120/9-1
11	2393,65	7121/5-1
12	2441	
13	2446.9	
14	2463.7	
15	2499.1	
16	2500.45	
17	2895	7120/7-3
18	2703,5	7119/12-1
19	2752,76	
20	2360	7121/4-1

4.4.3 XRD analysis

The qualitative and semi-quantitative analysis has been extracted by XRD-analysis.

4.4.3.1 Bulk analysis

The bulk analysis has been carried out on selected 12 samples (Table 4.2) to get the mineralogical overview.

Table 4.2: XRD samples for both bulk and clay analysis.

XRD No.	Well	Depth (m)
1	7120/6-1	2532.4
2		2529.6
3		2534.31
4		2558.51
5		2494.3
6	7121/5-1	2393.65
7		2441
8		2446.9
9		2463.7
10		2499.1
11		2500.45
12	7120/9-1	1922.1

4.4.3.2 Clay separation

The clay fraction was separated from all the twelve samples (Table 4.2). For the making of clay samples following procedure were followed:

i) All the samples were crushed upto a size of 1-2mm in an agate motor.
ii) 8-10 grams amount of every sample has been put in beaker.
iii) Distilled water (300ml) added to each beaker and then stirred it for 1 minute.
iv) Samples were left for 24 hours.
v) Each sample has been stirred for 1 min and added 100 ml distilled water.
vi) Samples were left in suspension for three and half hours.
vii) Clay fraction transfers to new beaker and then filtered it in a vacuum suction.
viii) Approximately 20 ml solution run through the filter and then treated with 0.1 M Mgcl2 and washed it with distilled water.
ix) The filtered samples were put on silica glass slides.

Four different treatments were applied to all the samples. The samples were analyzed as air-dried, ethylene glycol vapor and heated upto 350°C and 550°C.

Chapter 5: Well correlation and Petrophysical analysis

5.1Results

5.1.1 Well correlation

5.1.2 Petrophysical analysis

Chapter 5: Well correlation and Petrophysical analysis

The aim of this chapter is to categorize the sandstone intervals in lithostratigraphic units of Jurassic age. Furthermore, the porosity distribution in these sandstone intervals has been calculated by the Petrophysical analysis.

5.1 Results

5.1.1 Well correlation

Figure 5.1 shows the lithostratigraphic study in eight wells (7119/12-1, 7120/7-1, 7120/7-3, 7120/8-1, 7120/9-1, 7121/4-1, 7121/5-1, 7120/6-1) on the basis of gamma ray log and wells have been flattened at a depth of 1800m (MD). The thicknesses of the formations vary in all wells but generally the Stø Formation becomes thicker towards the southwest (Fig. 5.1, 5.7). According to Bergland et al. 1986, the cyclical changes in the continental shale and shallow marine sediments are due to tectonic subsidence, sea level changes and local sediment input in the Late Triassic to Middle Jurassic. The deposition of the Stø Formation is the result of the relative rise in sea level in Middle Jurassic times.

The Stø Formation is mainly dominated by sandstone, thin layers of shale/sandstone are also present (Dalland et al. 1988). It is main reservoir rock in the study area and in figure 5.2 it is subdivided into two reservoir layers i.e. upper and lower Stø. The lower Stø has excellent reservoir properties and can be correlated easily in wells 7121/4-1 and 7121/5-1 on the basis of gamma ray, neutron porosity and bulk density logs. This portion is dominated by fine to medium grained clean sandstone reflecting the wave and tide agitation which resulted the uniform reservoir properties. The upper Stø comprises fine to medium grained, poorly sorted, biotubated sandstone with thinner mudstone and shales. This portion generally has low reservoir quality compared to the underlying portion. The characteristics of this portion are of middle to upper shore face environment.

The underlying Nordmela Formation consists of sandstone, interbedded siltstones, shales and minor coals (Dalland et al. 1988). It is also divided into two subdivisions (Fig. 5.2). The reservoir quality in the lower Nordmela is very poor and acts as a seal for the gas in Tubåen Formation in well 7121/4-1 (Linjordet and Olsen 1992). The low value of gamma ray reflects that the upper part of Nordmela is dominated with sands and it is also confirmed from the neutron porosity and density logs and has poor to moderate reservoir characteristics.

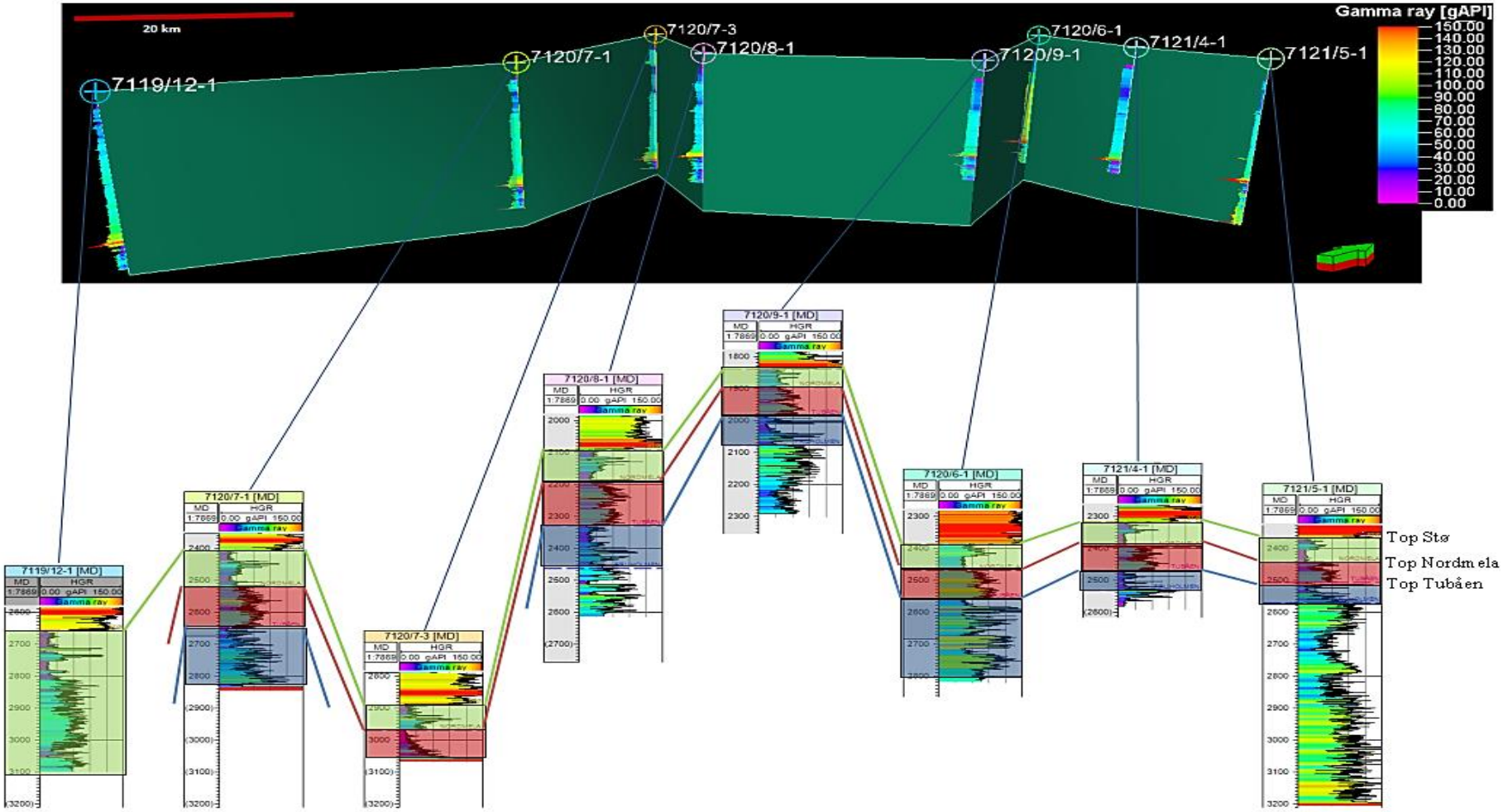

Figure 5.1: Stratigraphic correlation of the reservoir rocks (Stø, Nordmela and Tubåen Formations) of the study area, well fencing along with gamma ray log is showing the wells used for correlation.

The dominant lithology in the Tubåen Formation is sandstone with shales and minor coals (Dalland et al. 1988). The gamma ray response in the studied wells varies but overall the upper part is more sandy as compared to the lower part.

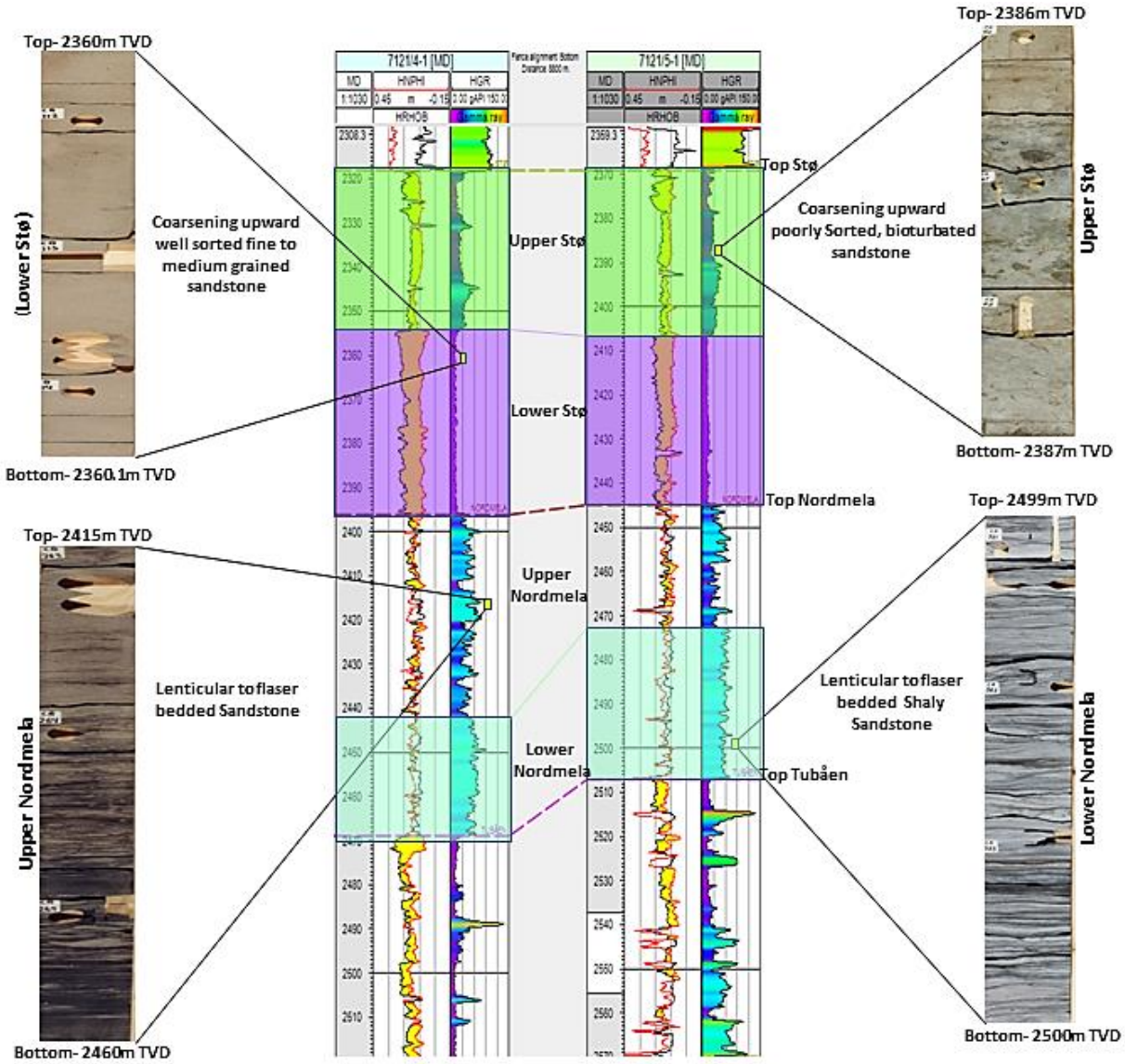

Figure5.2: Lithostratigraphic correlation with core photographs of Stø and Nordmela Formations from the wells 7121/5-1 and 7121/4-1 showing different sedimentary structure reflecting varying depositional environments (NPD 2013).

5.1.2 Petrophysical analysis

For a better understanding of the lithology and porosity distribution in all the study wells Petrophysical analysis has been carried out. Several cross plots and histograms were made to improve the understanding of Petrophysical properties.

Cross plots

To observe the porosity variation in Kapp Toscana Group several cross plots have been made for all the study wells. The generated histogram for the reservoir intervals in figure 5.3 shows the gamma ray population. The black line marks the critical point (60API) which separates sand and claystone. The porosity contribution from the claystone in wells 7120/6-1 and 7120/7-1 is higher compared to the other wells.

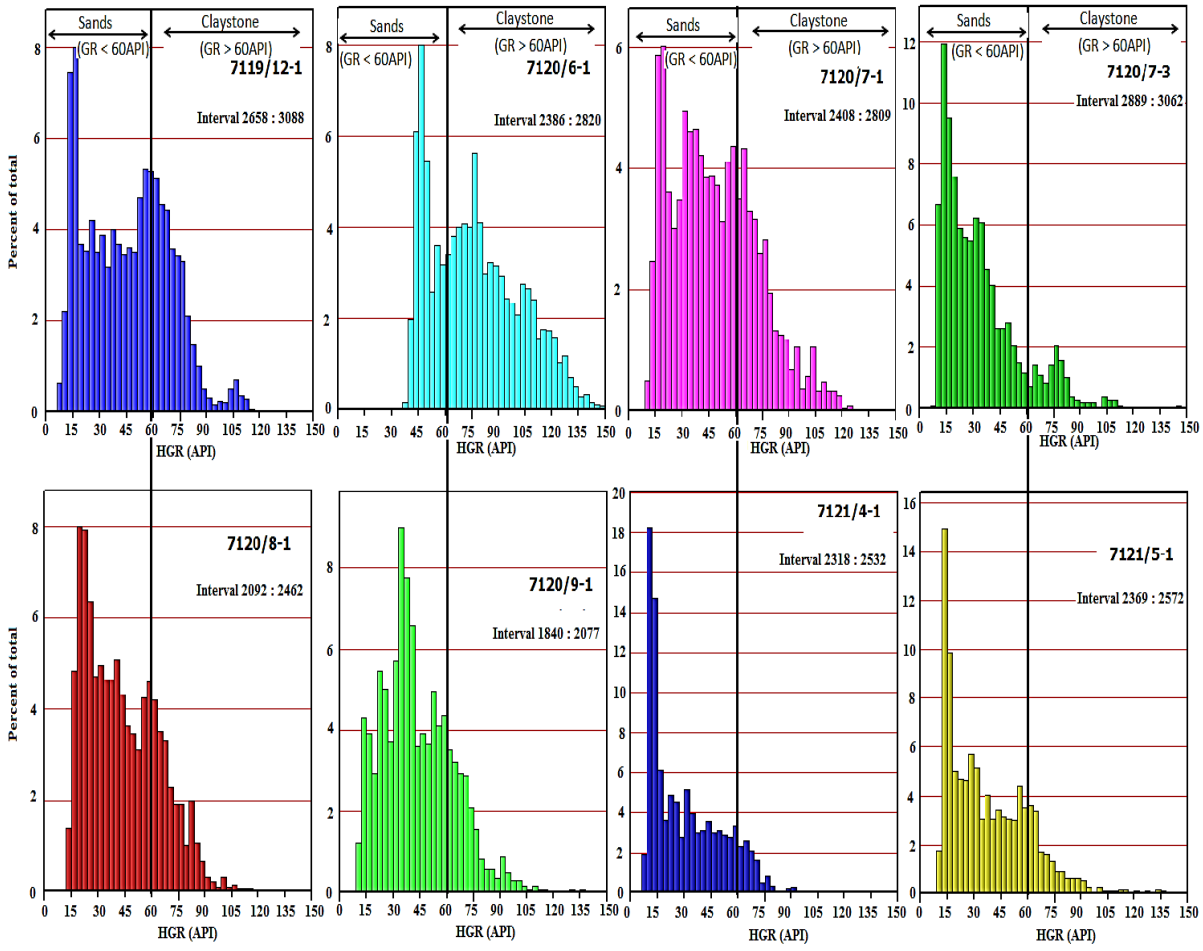

Figure 5.3: Distribution of Gamma ray in all study wells for the Kapp Toscana Group sandstones. Also showing sands (GR < 60API) and claystone (GR > 60API).

The porosity decreases with burial depth in all the wells (Fig. 5.4). The average porosity values of the reservoir part in wells 7120/9-1, 7120/8-1 and 7121/4-1 are 18%, 17% and 11.6% respectively. Furthermore, this percentage is decreasing more in the remaining wells because of the greater depth. The porosity comparison between the Stø and Tubåen Formation in any well depicts that later one is more porous. But because of the greater burial depth it is less promising for the hydrocarbon.

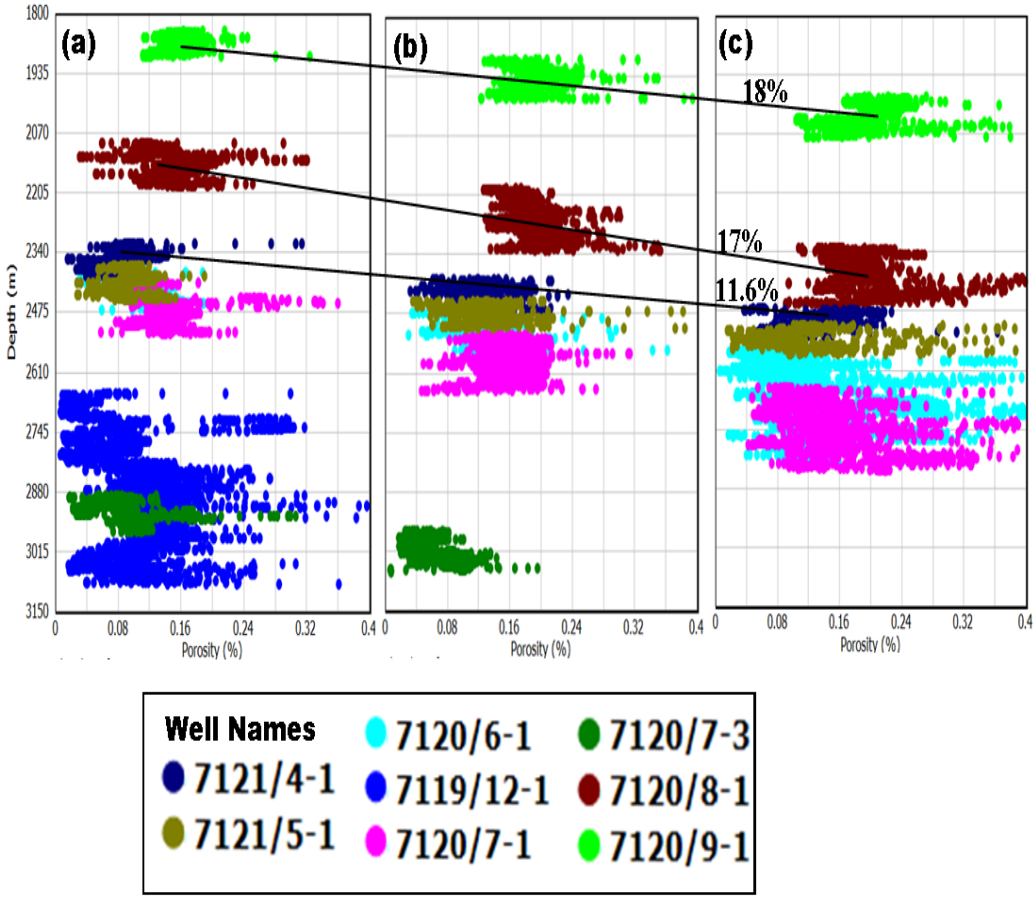

Figure 5.4: Porosity values versus measured depth (m) for the Jurassic sandstones (a) Stø Fm (b) Nordmela Fm (c) Tubåen Fm, where the black lines show the average porosity of these three. The color key refers to the well name.

The sediment's compaction can be divided into mechanical compaction (MC) and chemical compaction (CC). The factors which control this compaction are stress, time and temperature. Several rock properties like density, velocity and porosity change due to the effect of these two types of compactions. The velocity escalates in all the eight wells with burial depth while porosity depreciates. The mechanical compaction and chemical compaction zones are marked on the basis of Vp-depth trend (Fig. 5.5).

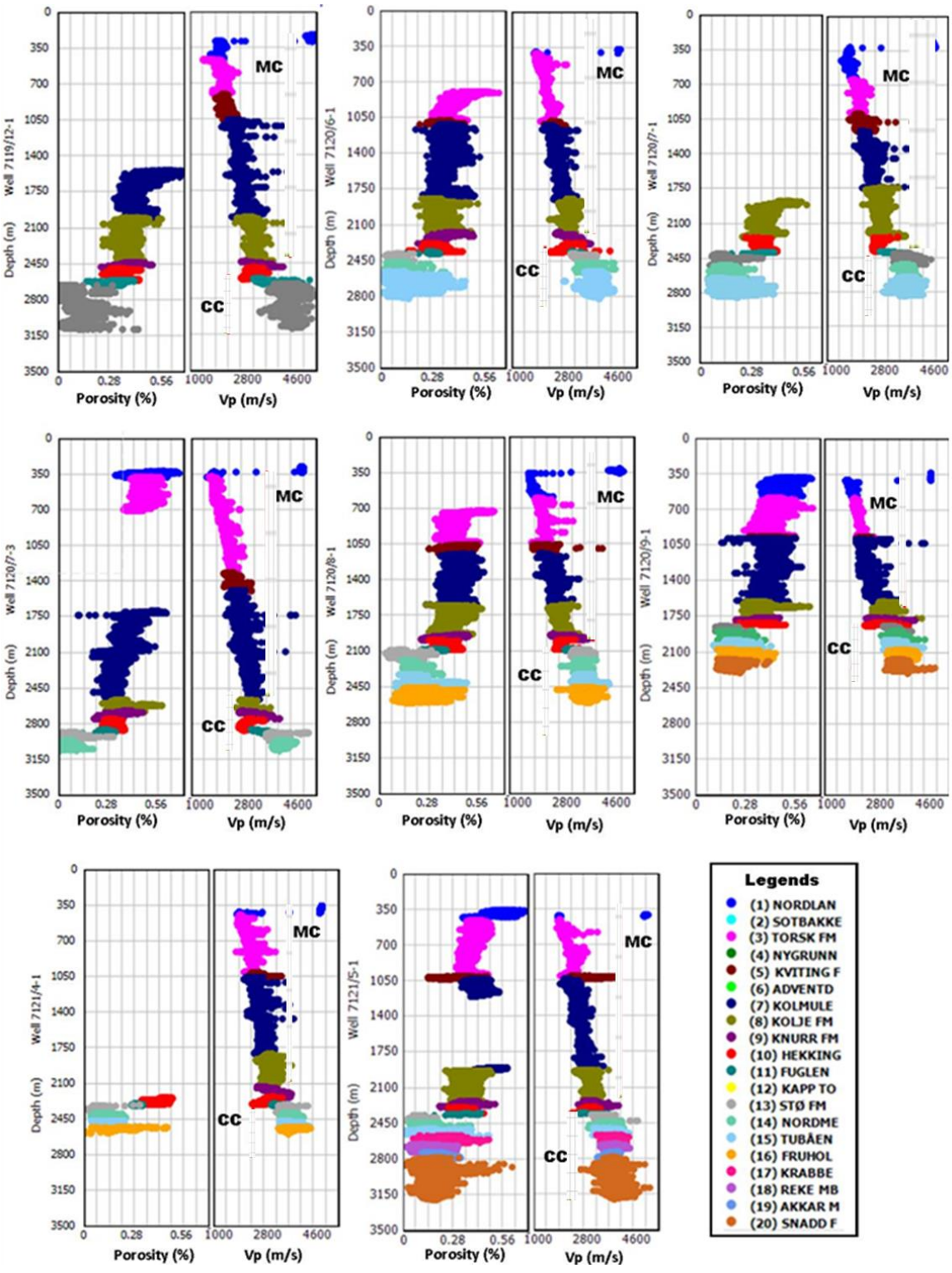

Figure 5.5: Observed compaction trends in all eight wells.

Bulk density is plotted against velocity (Fig. 5.6) to find out the transition from MC to CC. The change in compaction domain from MC to CC yields the increase in velocity and density values. Mechanical and chemical compaction zones can be seen in two clusters showing different colors for different formations. The first cluster with low Vp and density comprises

the mechanically compacted formations whereas the second one belongs to those formations which have been affected by chemical compaction.

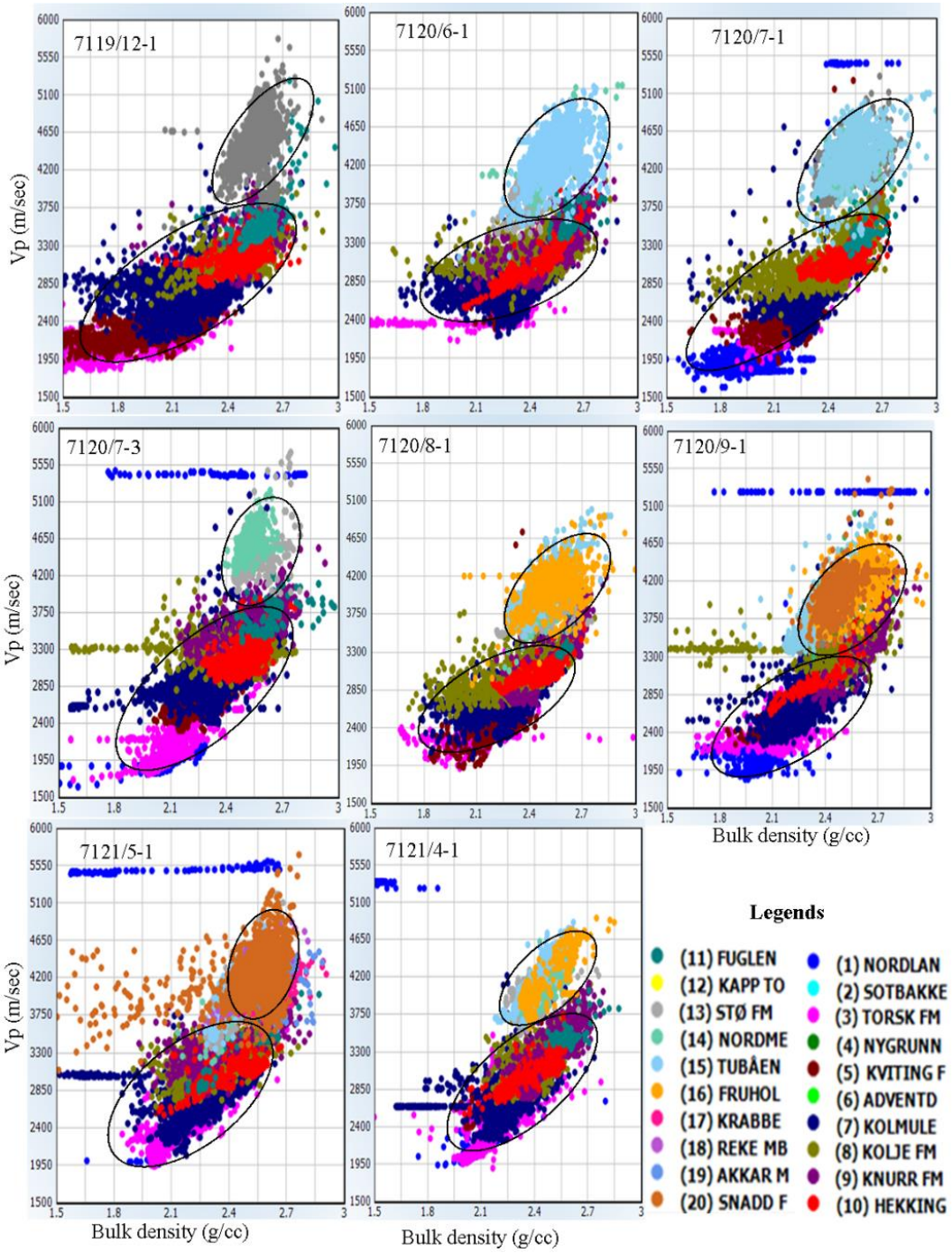

Figure 5.6: Cross plots between Vp (m/s) and bulk density (g/cc) in eight wells color coded with formations.

The area of interest (Jurassic sandstone) is in the CC zone and it has been changed the stiffness of rock by quartz cementation. The Vp values change affectedly due to this stiffness. The precipitation of quartz is discussed briefly in chapter 6.

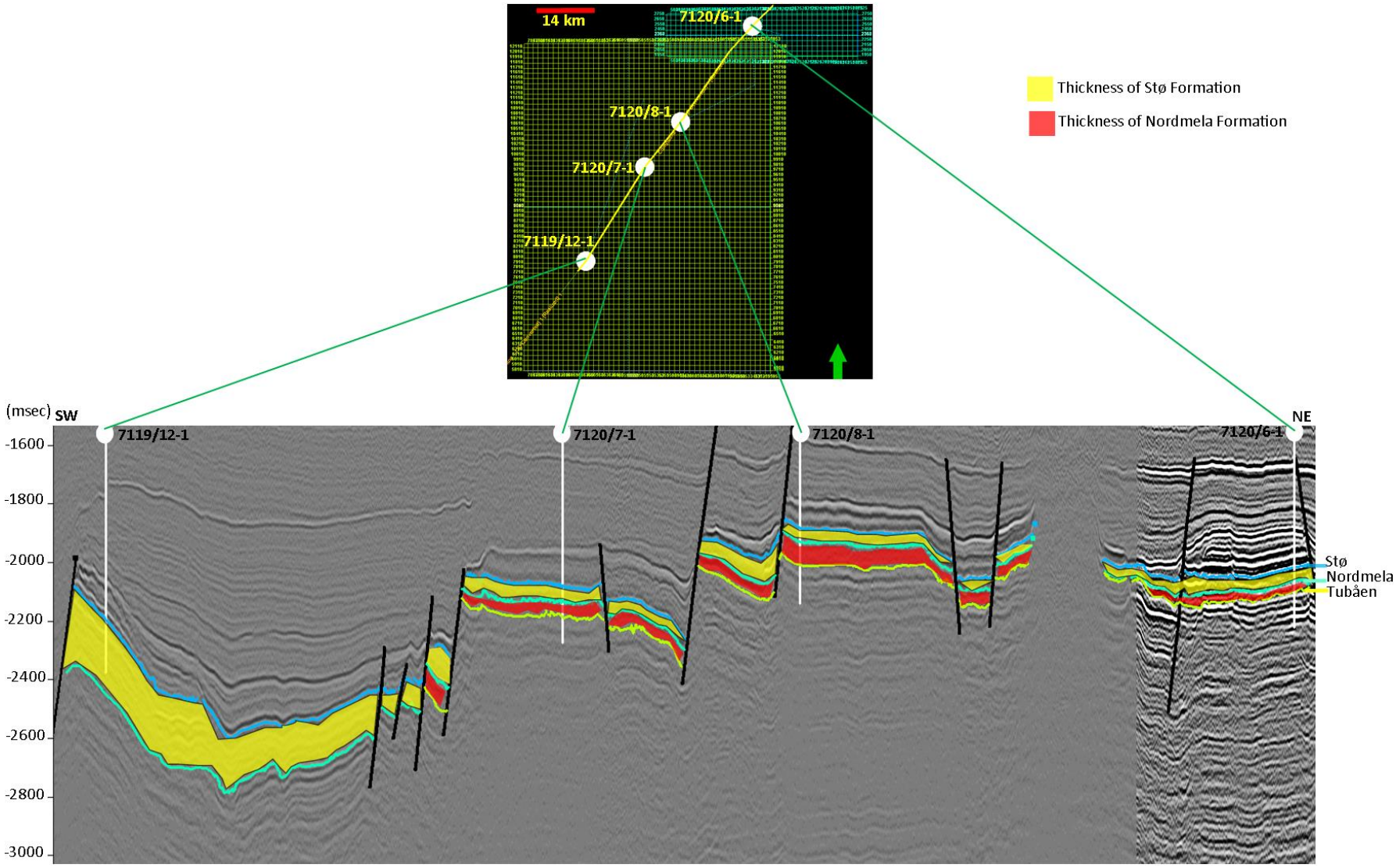

Figure 5.7: Well to seismic correlation showing the thickness variation of Stø and Nordmela Formations in different wells.

Chapter 6: Mineralogical and Petrographical analysis

Chapter 6: Mineralogical and Petrographical analysis

The preserved porosity and mineralogy of sandstone are examined by the mineralogical and petrographical analysis. Several techniques like thin section studies (with the help of optical microscopy and SEM analysis) and XRD analysis have been carried out to find the results.

6.1 Stø Formation

6.1.1 Thin section analysis

All the thin sections from different wells have been analyzed under the polarizing microscope and gathered the porosity and mineralogical information by point counting, sorting, calculated IGV and petrographical classification.

From Stø Formation, a total of six thin sections from four wells were studied. All the examined samples were well sorted, fine to medium grained sandstone (Table. 6.1). Most of the quartz grains are monocrystalline. Other observed minerals are kaolinite, illite, lithic fragments, polycrystalline quartz and muscovite. Organic matrix is also present in clay rich samples. Quartz is the dominant observed cement, but there is also some presence of calcite cement. The grain to grain contacts appear to be long, concavo-convex and sutured (Fig. 6.2). The quartz cementation varies from sample to sample (5-14%) depending upon the grain size (Fig. 6.3). The porosity range is (5-18%) and controlling factors are compaction and various cement types.

Table 6.1: Results from point counting.

Well	Formation	Depth (m)	Grains			Matrix		Cement		Sorting	Porosity		IGV (%)	Grain Size (mm)
			Quartz	Felds	Lithic Frag	Clay	Muscovite	Quartz	Carbonate		Prim	Sec		
7120/7-1	Stø	2423,45	64,8	0	1,2	5,7	1,2	13,5	1,5	Well	11,4	0,6	33,3	0,12
		2432,10	53,7	1,2	1,2	11,8	0,6	5	20,6	Moderate	5,6	0	43,6	0,09
7120/7-3	Stø	2895	66,3	0,9	2,1	3,6	2,4	11,4	2,7	Well	9,6	0,9	29,7	0,26
7119/12-1	Stø	2703,5	69	0,3	0,3	6,9	0,9	12,3	0	Well	9,3	0,9	29,4	0,13
		2752,76	71,4	0,3	2,7	4,2	2,1	10,5	1,2	Well	7,5	0	25,5	0,2
7121/4-1	Stø	2360	65	0,6	1,2	5	0	8,7	1,2	Well	17,5	0,6	32,4	0,18

Figure 6.1 is showing the point count results and is subdivided into detrital grains, matrix, quartz cement, calcite cement and porosity. Well 7119/12-1 has the highest percentage of detrital grain reflecting low cement and matrix. On the other hand a sample from well 7120/7-1 and depth 2432, 10 m has the highest amount of calcite cement and matrix with least porosity.

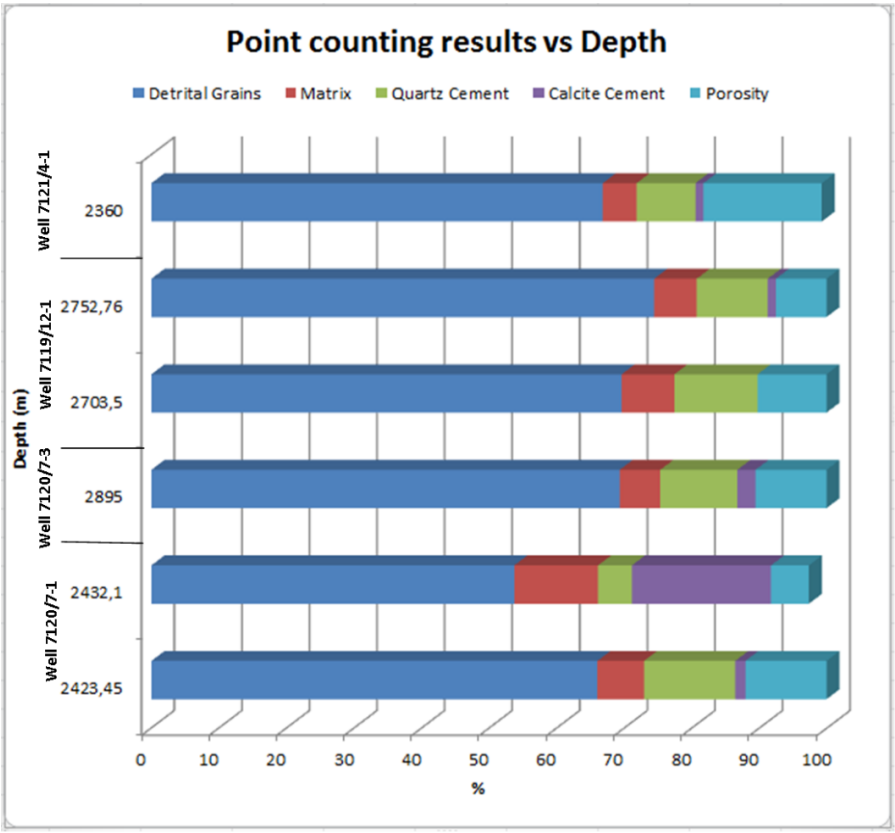

Figure 6.1: Point counting results Vs depth from different wells.

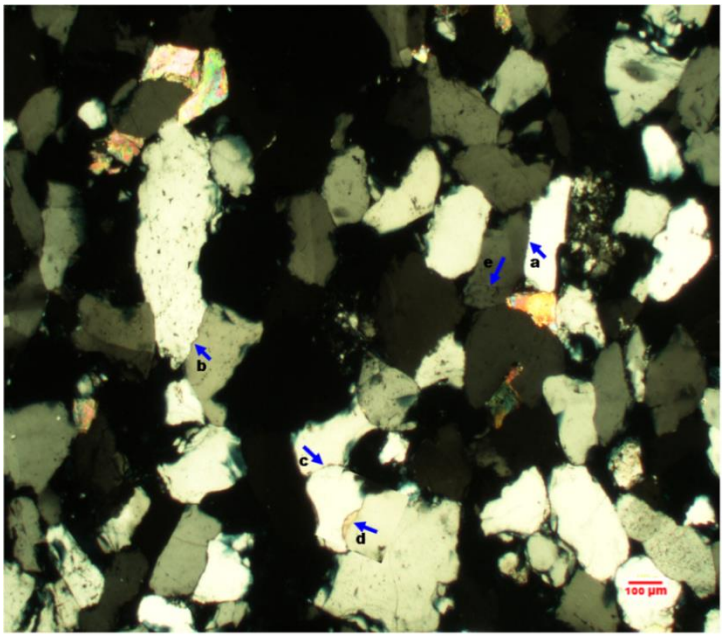

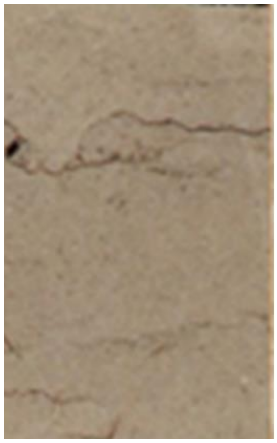

Figure 6.2a: Core photograph showing the stylolites in Stø Formation (NPD 2013).

Figure 6.2: Thin section from well 7121/4-1, depth 2360m. The contacts between the quartz grain are (a) long (b) suture and (c) concavo-convex. The early digenetic effect (d) destroyed by compaction and late diagenetic effect (e) which filled the porosity in Stø Formation.

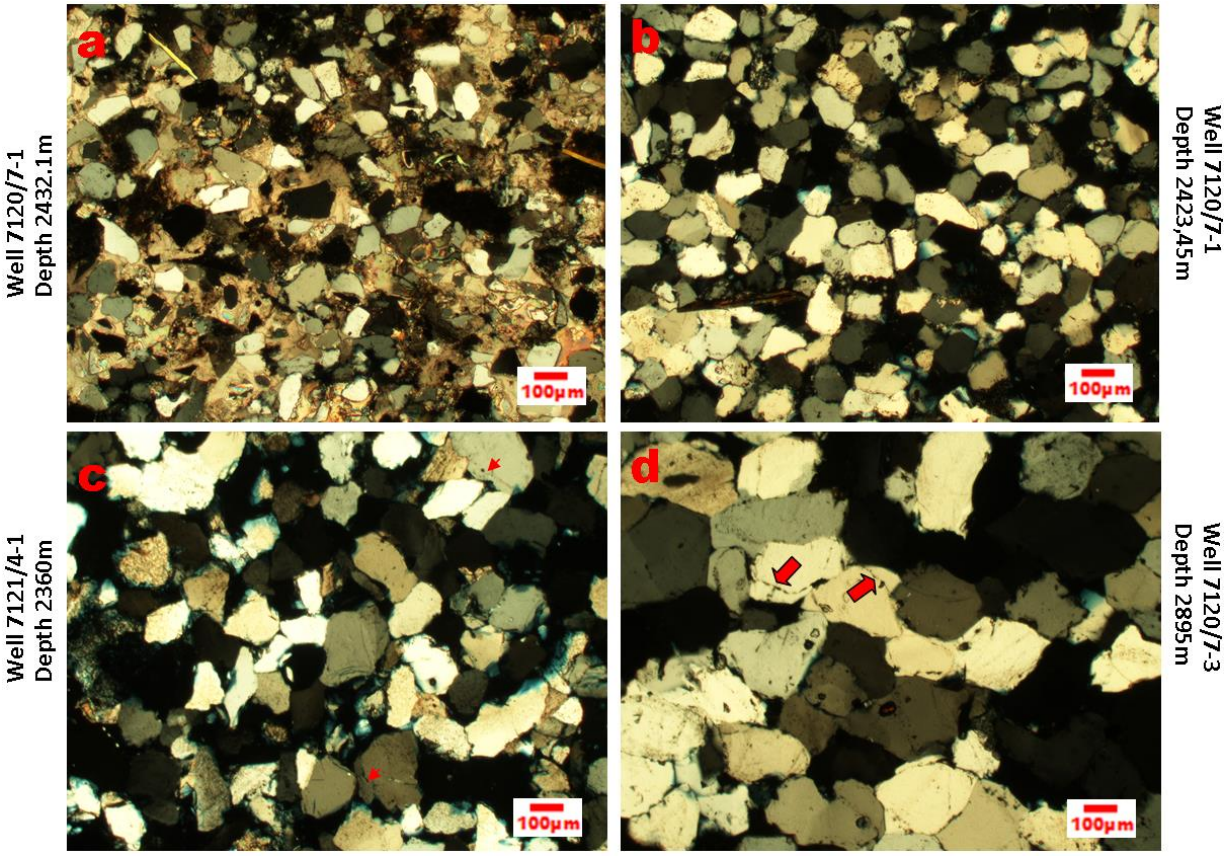

Figure 6.3: Cementation decreasing from a to d. The thickness of quartz cement is less (↙) in shallow well and high (↗) in deep well.

6.1.1.1 Petrographical Classification

All the detrital grains observed during point counting have been divided into three components; quartz, feldspar and lithic fragments and plotted in a petrographic classification diagram (6.4a). All the samples from Stø Formation have less than 15% matrix and thus belongs to arenite because whole six samples fall in the quartz arenite area (6.4a). Quartz arenites having more than 95% quartz are considered as mineralogically mature sandstones (Adams et al. 1986). The results in table 6.1 show that Stø Formation is texturally and mineralogically mature.

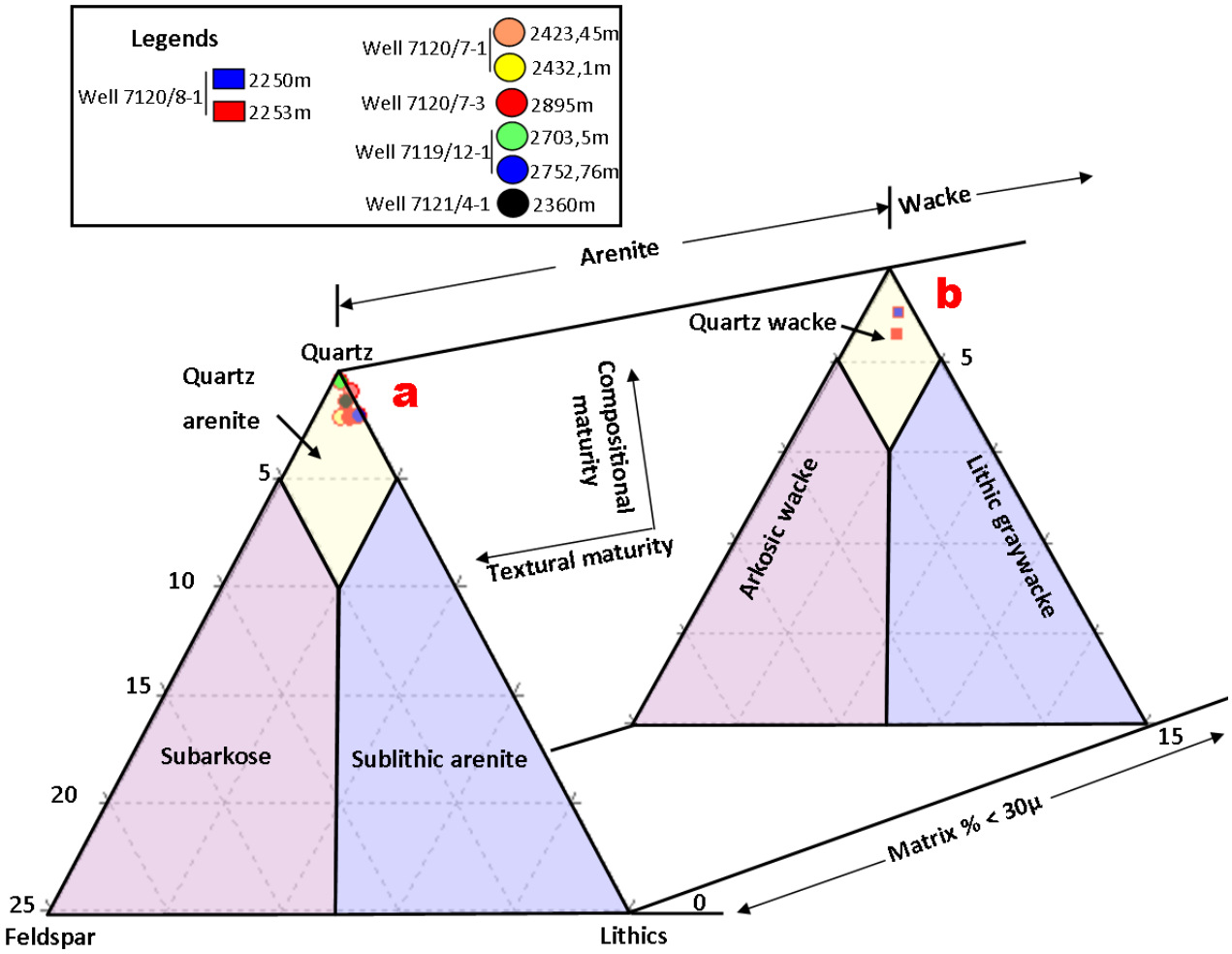

Figure 6.4: Petrographical classification of sandstone (Dott 1964). All the samples are classified and plotted according to their depth and wells.

6.1.1.2 Total porosity:

The term total porosity is used for the both primary and secondary porosities. The overview of the total porosity is shown in figure 6.5. The porosity in all the six samples varies from 5.6% to 18.1% (Table 6.2). The calculated mean porosity in two wells shows that the sandstone found in well 7119/12-1 is slightly more porous compared to well 7120/7-1.

Table 6.2: Calculated mean porosity of Stø Formation in different wells.

Mean Porosity (%)					
Stø Formation					
Well 7120/7-1		Well 7120/7-3	Well 7119/12-1		Well 7121/4-1
8,8			8,85		
2423,45	2432,10	2895	2703,5	2752,76	2360
12	5,6	10,5	10,2	7,5	18,1

The porosity is high in samples from depth 2423.45 m and 2703.5 m, where 5.6% and 7.5% are the porosity values from depth 2432.10 m and 2752.76 m respectively. Well 7121/4-1 has the highest porosity i.e. 18.1%. Only one sample from well 7120/7-3 is showing 10.5% porosity value.

The main reason of the porosity reduction at greater depth is the quartz cementation. To examine the relationship between the porosity and quartz cementation, the histogram between porosity and quartz cementation is displayed in figure 6.6.

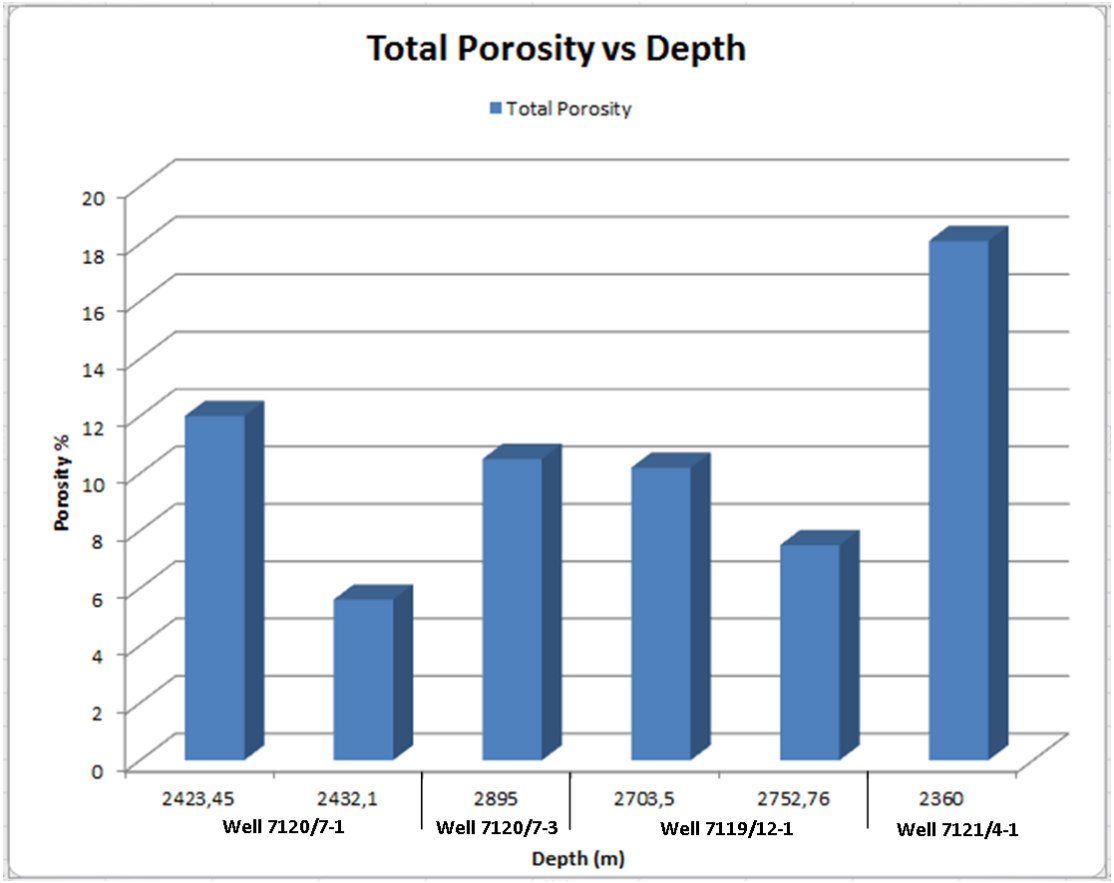

Figure 6.5: Percentage of total porosity vs depth from different wells.

The well 7120/7-1 has the highest cementation (quartz and calcite) and lowest average porosity depending upon the depth as compared to the other wells. All the wells have the coupled relationship; low porosity; high quartz cementation and vice versa. High porosity and low quartz cementation in well 7121/4-1 shows the opposite behavior than that of well 7120/7-3.

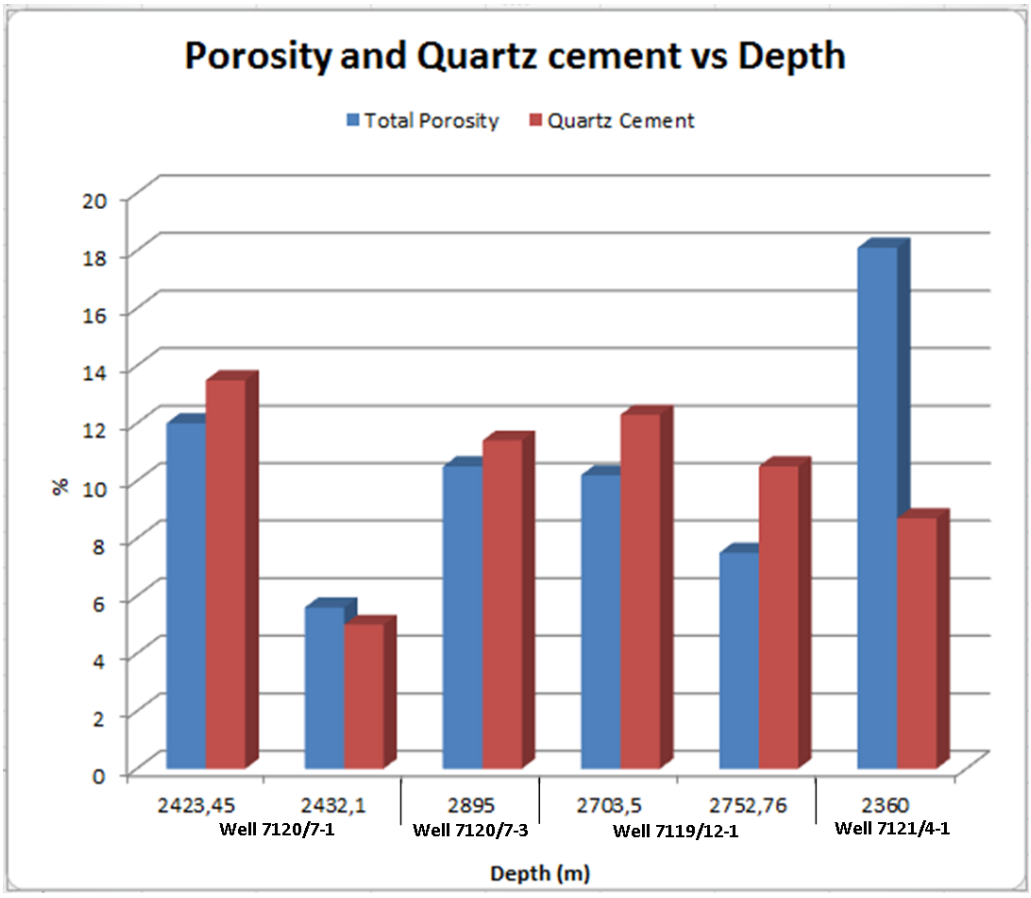

Figure 6.6: Percentage of porosity and quartz cement vs depth from different wells.

6.1.1.3 Clays

In all the examined samples, clays are mostly present in the pores and reduce the porosity but in some cases those exist as grain coating. The clays percentage varies in all the wells from 3.6% to 11.8%. The percentage of total porosity and clays are displayed together to check any coupled relationship (Fig. 6.7).

The average amount of clays observed (8.75%) in well 7120/7-1 is higher than that of well 7119/12-1 (5.55%). Both the wells 7120/7-3 and 7121/4-1 have the less clays amount with a value of 3.6% and 5% respectively (Table 6.3).

Table 6.3: Calculated mean from clays percentages in different wells.

Average Clays (%)					
Stø Formation					
Well 7120/7-1		Well 7120/7-3	Well 7119/12-1		Well 7121/4-1
8,75			5,55		
2423,45	2432,10	2895	2703,5	2752,76	2360
5,7	11,8	3,6	6,9	4,2	5

Most of the clay is pore filling in all the samples, so it has an impact on the porosity which is clear in figure 6.7. The samples with high clay content reflecting low porosity and vice versa.

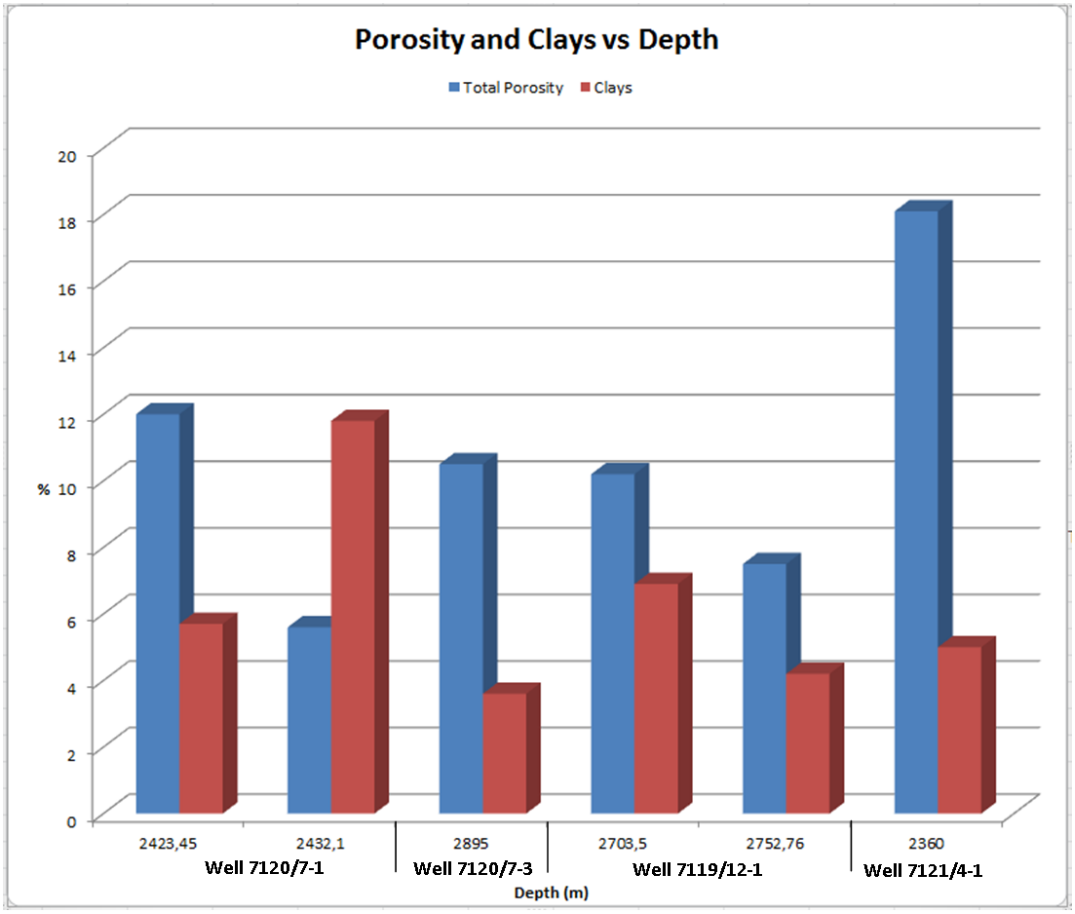

Figure 6.7: Percentage of porosity and clays vs depth from different wells.

6.1.1.4 Carbonate cement

During the early diagenesis carbonate cement is one of the major porosity reduction factors in sandstones. The results of carbonate cement during point counting are plotted together with the total porosity to see any relationship in samples (Fig. 6.8).

Table 6.4: Calculated average calcite cement in each well.

Carbonate cement (%)					
Stø Formation					
Well 7120/7-1		Well 7120/7-3	Well 7119/12-1		Well 7121/4-1
11,05			0,6		
2423,45	2432,10	2895	2703,5	2752,76	2360
1,5	20,6	2,7	0	1,2	1,2

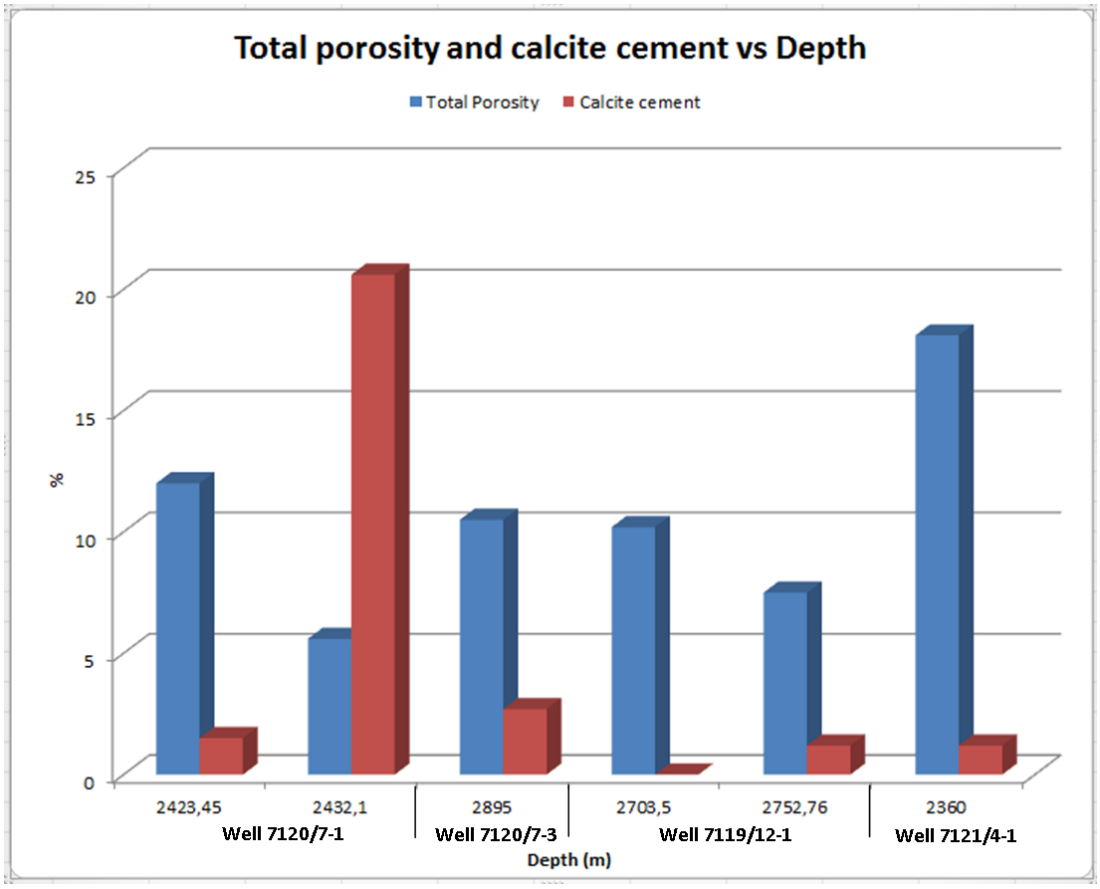

Figure 6.8: Histogram showing the comparison of total porosity and calcite cement.

6.1.1.5 Intergranular volume (IGV)

The porosity is lost by the mechanical and chemical compaction. On the basis of point counting results the intergranular volume was calculated by this formula.

Intergranular Volume (IGV) = cement + depositional matrix + intergranular porosity

The highest average IGV value is in well 7120/7-1, making up 41.5% (well 7120/7-3, 30.6%), with well 7121/4-1 contributing with 33%. 30.6% IGV belongs to well 7120/7-3 (Table 6.5).

Table 6.5: Calculated average IGV of each well.

Average IGV (%)					
Stø Formation					
Well 7120/7-1		Well 7120/7-3	Well 7119/12-1		Well 7121/4-1
38,45			27,45		
2423,45	2432,10	2895	2703,5	2752,76	2360
33,3	43,6	29,7	29,4	25,5	32,4

Figure 6.9 shows the average IGV values from all samples arranged according to depths from different wells. High amount of calcite cement and matrix are the main reasons for the greater IGV in a sample from depth 2432.10 m. The sample from depth 2752.76 m has the minimum IGV i.e. 25.5%. The reason for low IGV value is that the sample is more mechanically compacted.

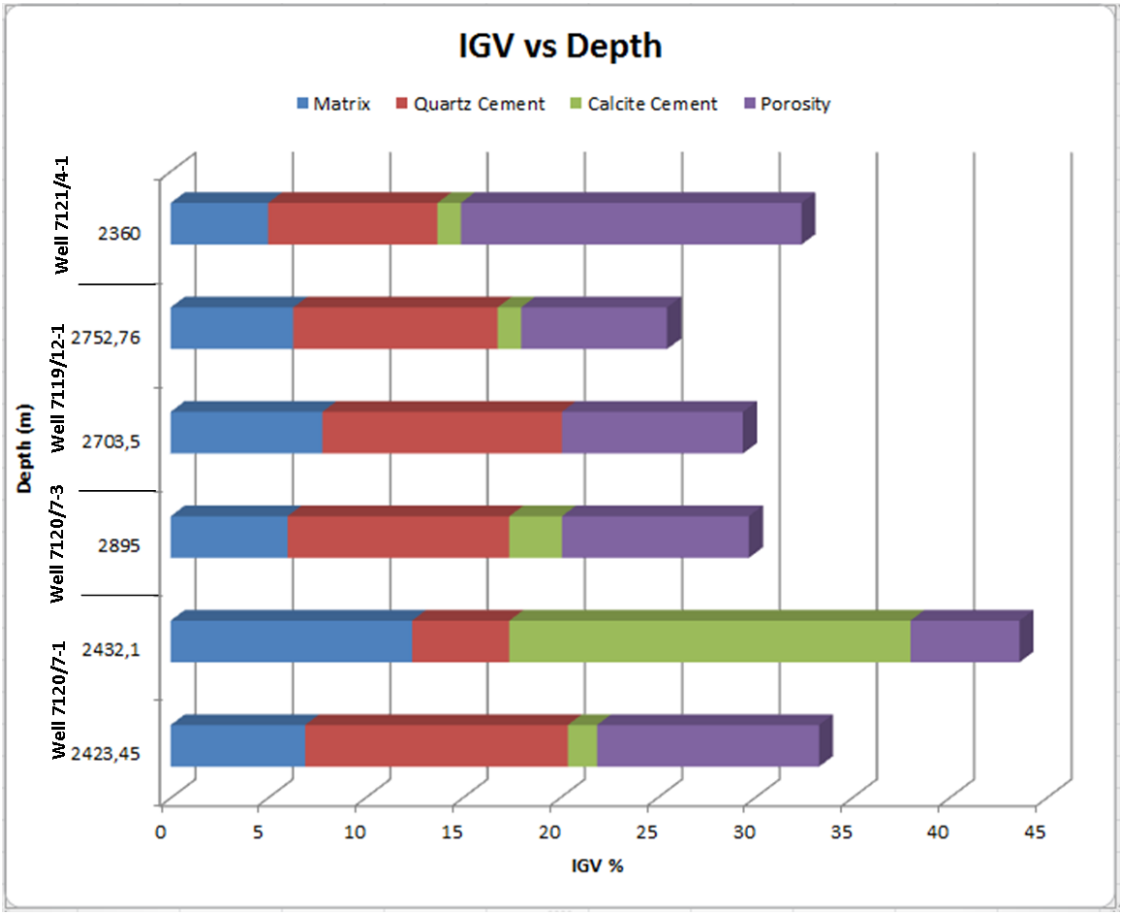

Figure 6.9: Calculated IGV vs depth from different wells.

6.1.1.6 Textural characteristics

The sorting has been calculated by applying the diversion on measured grain sizes and plotted against each other (Fig. 6.10). All the samples are well sorted with varying grain sizes. The grain size, degree of sorting and grain shape was plotted against the calculated IGV (Fig. 6.11A, B and C).

The most prominent trend between the IGV% and grain size (Fig. 6.11 B) is showing that the decrease in IGV% with increase in grain size and vice versa.

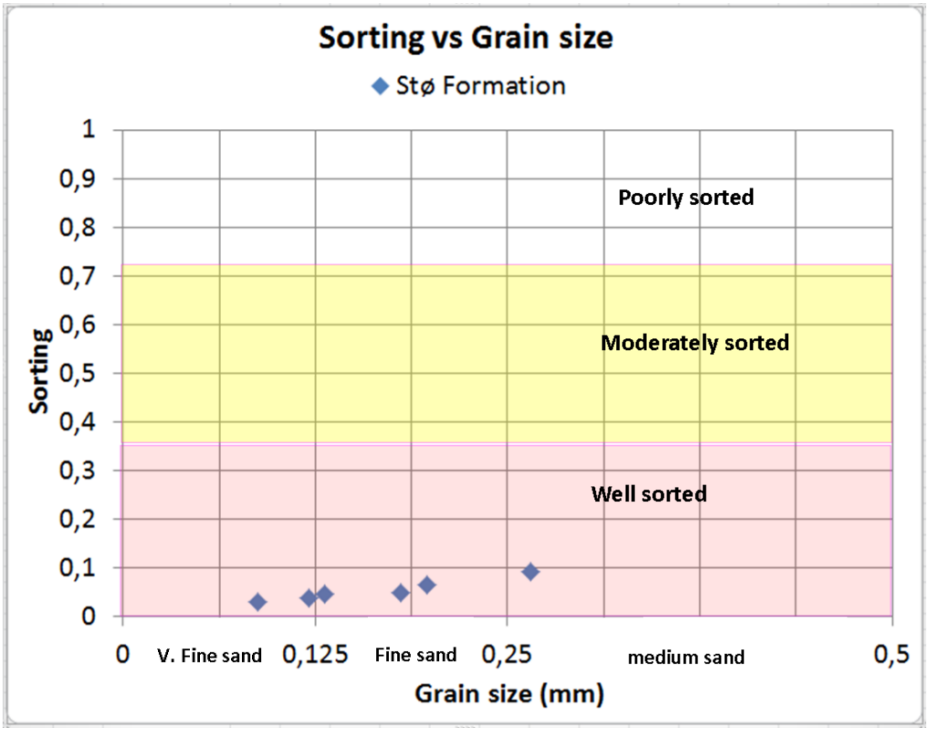

Figure 6.10: The relationship between the degree of sorting and grain size.

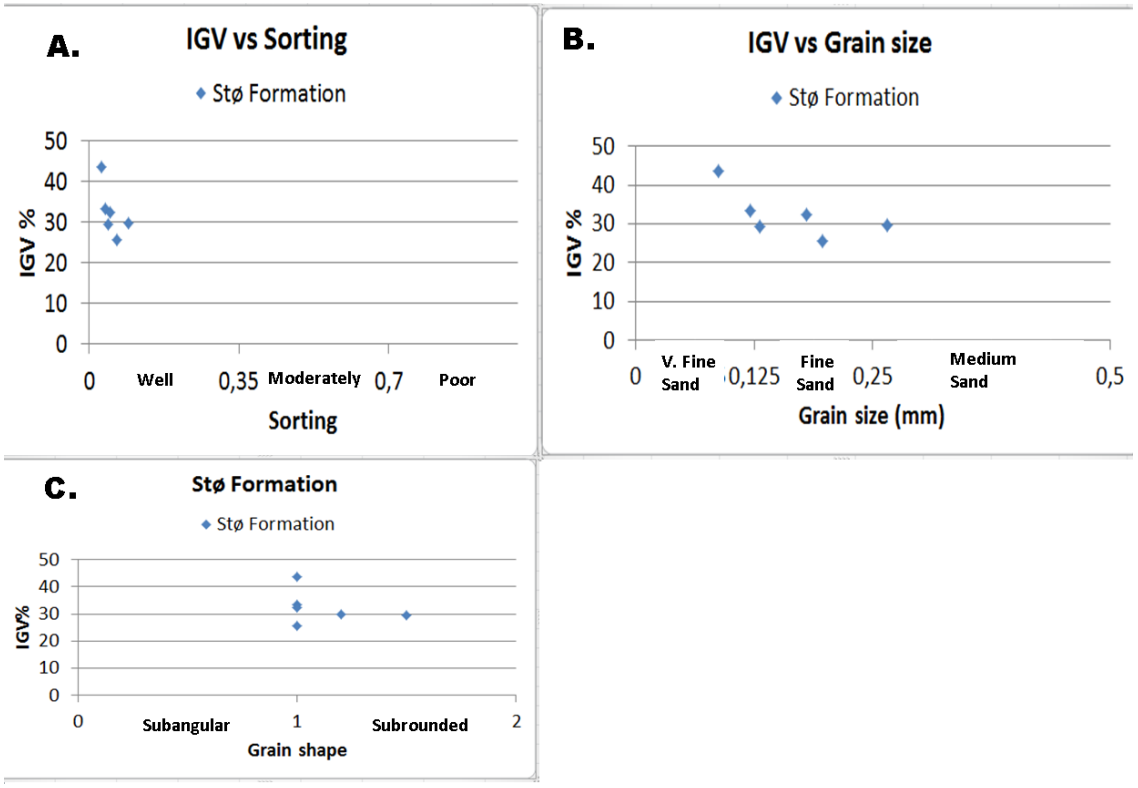

Figure 6.11: The relationship between the percentage of IGV and A) sorting, B) grain size and C) grain shape.

6.1.1.6.1 Textural Maturity

The maturity of the Stø Formation has been assessed by the measured and visualized results and their comparison with the table 6.6. According to stages of textural maturity by Folk (1951); the insignificant amount of detrital clay, well sorting and subangular to subrounded grain shape make Stø Formation texturally mature.

Table 6.6: Stages of textural maturity. Revised from Folk (1951).

I. Immature stage	II. Submature stage	III. Mature stage	IV. Supermature stage
Sediments have considerable clay and fine mica with poorly sorted and angular grains.	Sediments have little or no clay with poorly sorted and angular grains.	Sediments have no clay. The grains are well sorted, but their shape is still subangular.	Sediments have no clay with well sorted and rounded grains.

6.1.2 Scanning electron microscopy (SEM)

The scanning electron microscopy (SEM) analysis has been employed on the samples for the further investigation of cementation, authigenic clays and coating on grains.

6.1.2.1 Grain coats

Stub mounted samples have been investigated to find out the coating. There is no significant amount of coating in all the examined samples with some exceptions. The presence of micro-quartz coating in well 7120/7-1 is shown in figure 6.12. The area which is uncovered with grain coating is highly cemented. Clay coatings are also very rare.

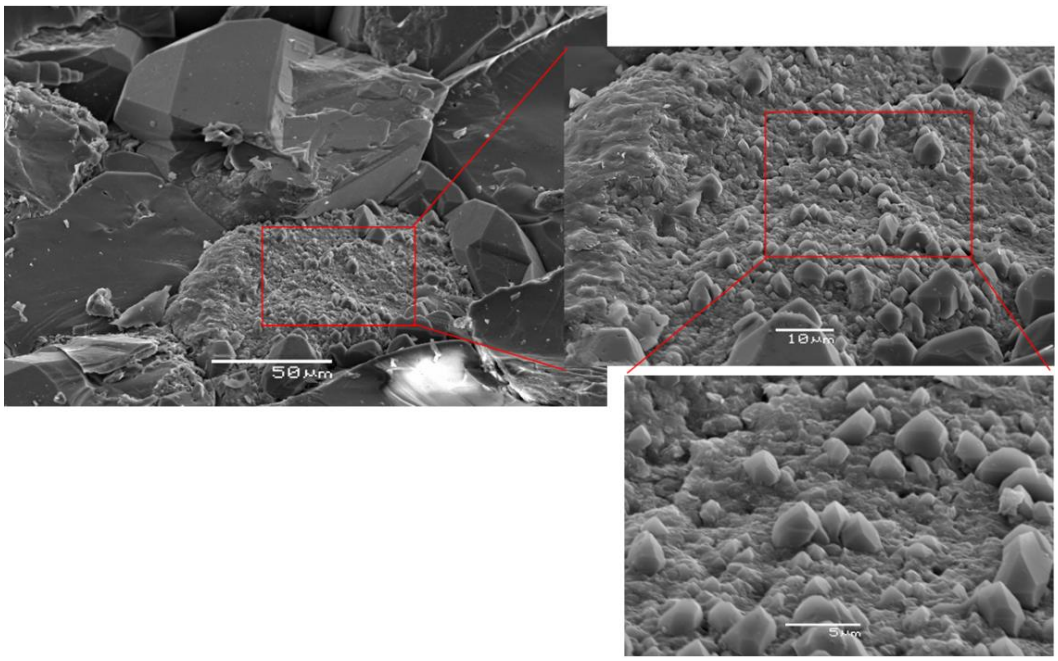

Figure 6.12: Showing microquartz (mQz) coating in well 7120/7-1 depth 2423.45m.

The illite coating (Fig. 6.13) is not covering the whole grain (morphology looks like kaolinite); it is present only at one side of the grain.

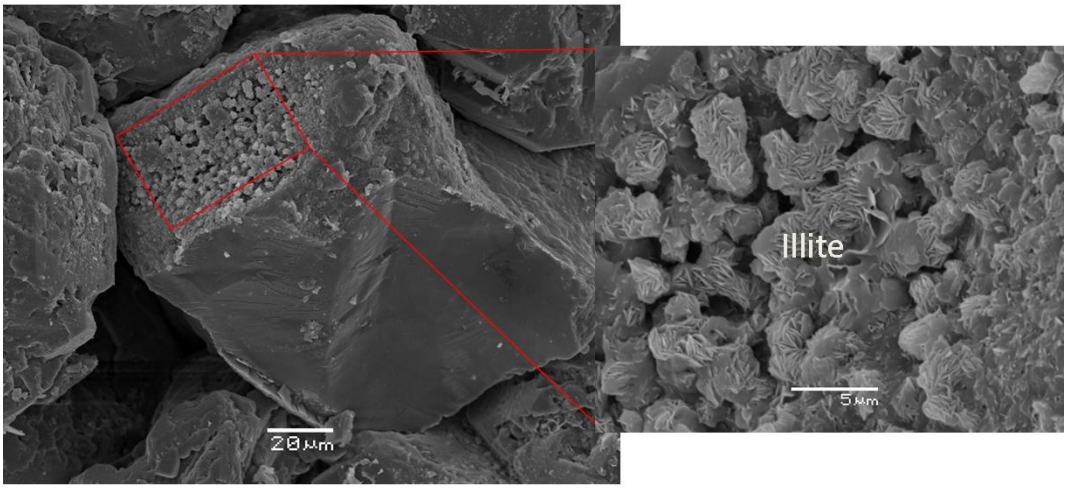

Figure 6.13: Illite coating from well 7121/4-1 (depth 2360m)

6.1.2.2 Authigenic clays and porosity

The observed clay minerals are kaolinite and illite in all the samples. Most of the clays have been found in the pores. The morphological features of both clays reflect their authigenic origin. The vermicular booklet shape (Fig.6.14, 6.15 and 6.16) is a feature of kaolinite, while illite shows a needle like structure (Fig. 6.16 and Fig 6.17).

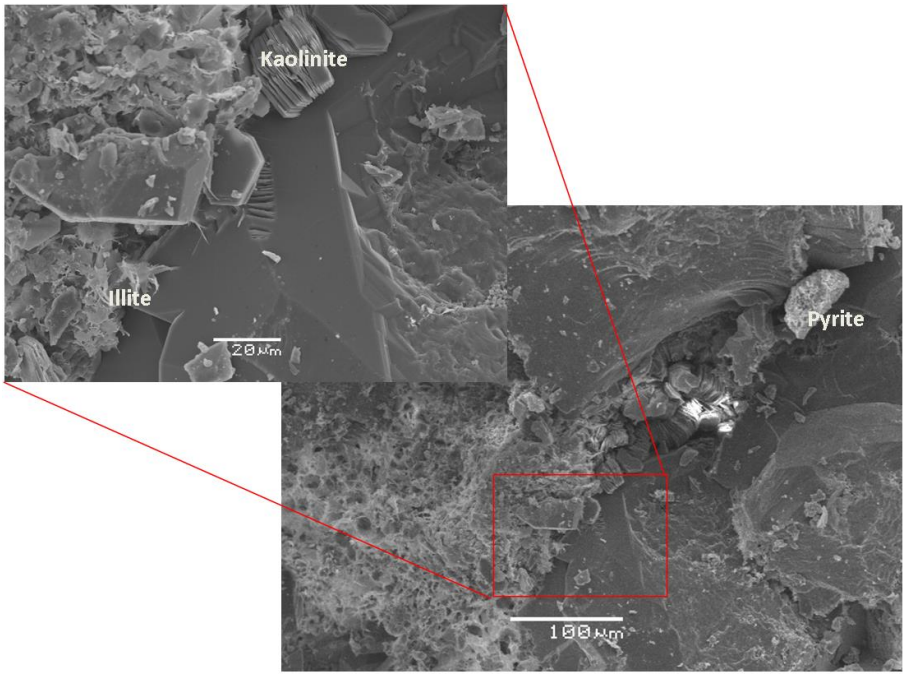

Figure 6.14: Figure from well 7120/7-3 (depth 2895m) showing pore filling kaolinite and illite with crystals of quartz overgrowth and pyrite.

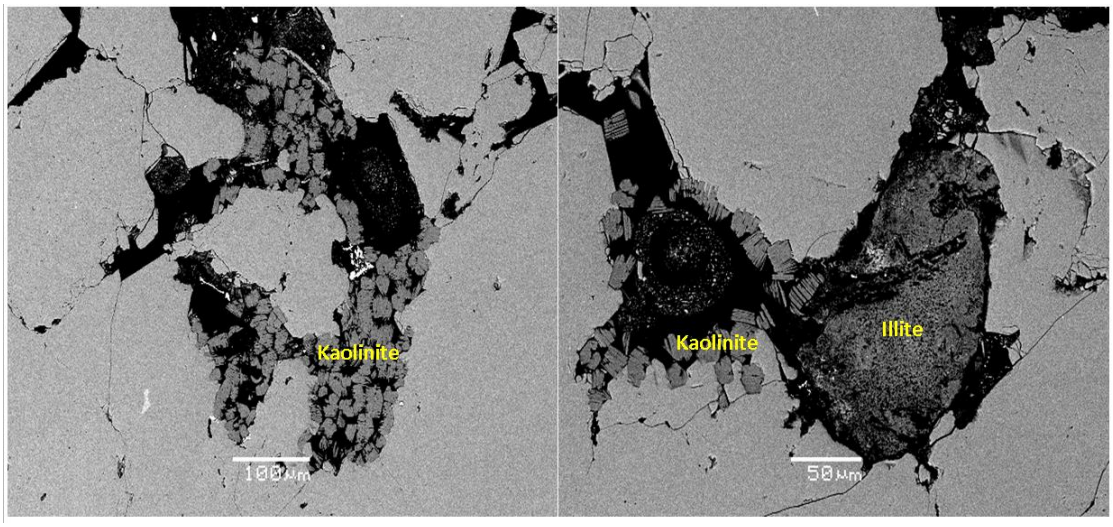

Figure 6.15: A backscattered electron image from well 7120/7-3 (depth 2895m) showing the presence of pore filling kaolinite and illite.

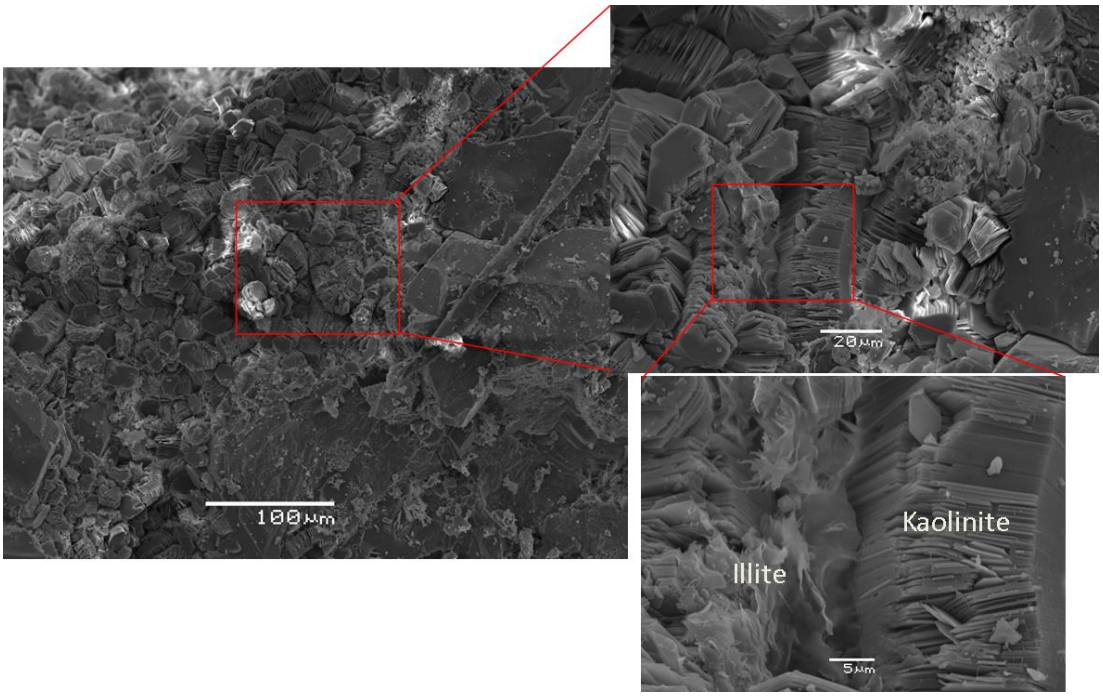

Figure 6.16: SEM picture from well 7120/7-3 (depth 2895m) showing the characteristic morphology of pore filling kaolinite and illite**.**

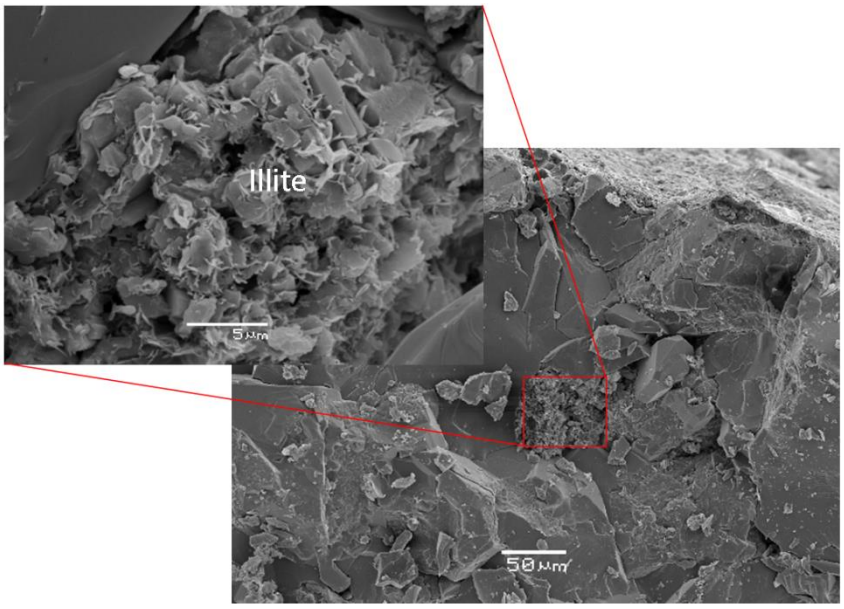

Figure 6.17: Figure showing illite in well 7120/7-1 from depth 2895m.

6.1.2.3 Quartz overgrowth and porosity

For the confirmation of point counting results, SEM analysis has been carried out which shows that the results of quartz cementation under the microscope are closely matched with the SEM observations. The Stø Formation is strongly affected by the quartz overgrowth. The high amount of quartz overgrowth (Fig. 6.18) supports this statement.

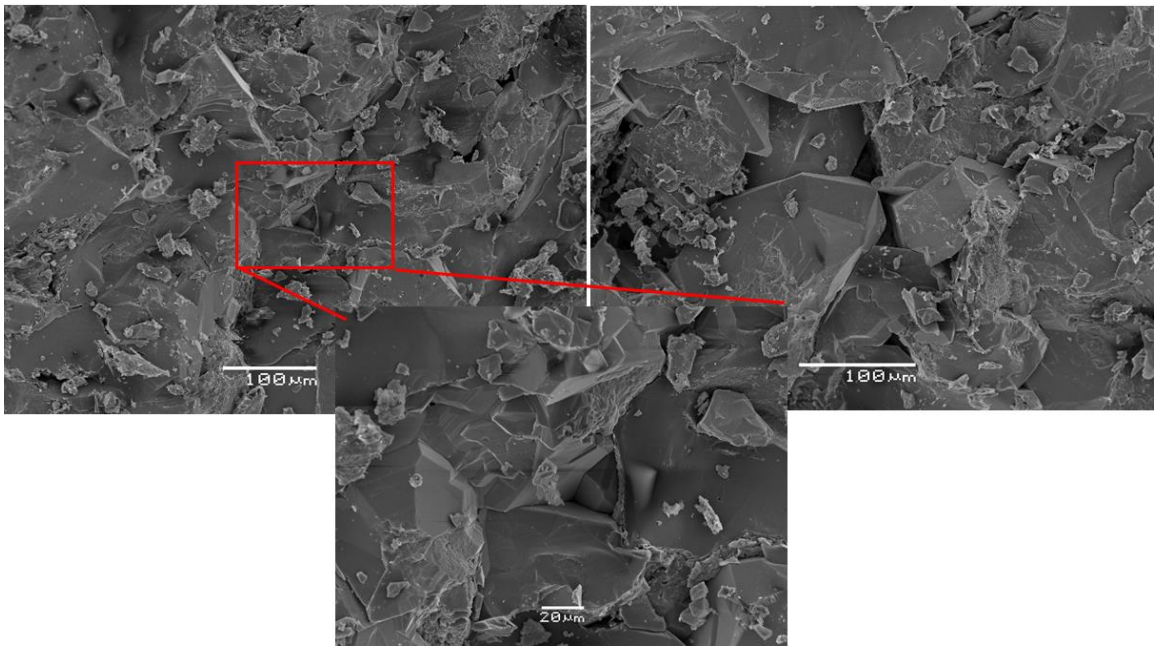

Figure 6.18: A relatively high quartz overgrowth in well 7119/12-1 (depth 2703.5m). Enlarged part is showing the growing crystal of quartz.

The porosity is decreased and quartz cementation is increased with increase in burial depth. In accordance with this the highest quartz cementation is found in deepest well (7119/12-1), a general overview is extracted with the comparison of two figures (Fig. 6.19 and Fig. 6.20) which supports this statement.

The quartz overgrowth can be separated from the detrital grains by the cathode luminescence (CL) and detrital grains will illuminate strongly compared to the cement. In Figure 6.19 the CL image depicts that the quartz cementation is much higher than the expectation from the secondary electron image. In this sample the effect of chemical compaction is higher than the mechanical compaction. Similar behavior was also observed when another sample from well 7119/12-1 (depth 2703.5m) exposed to cathode luminescence (CL) (Fig. 6.20). Both of these examples may indicate that the Stø Formation has been compacted more by quartz cement rather than effective stress.

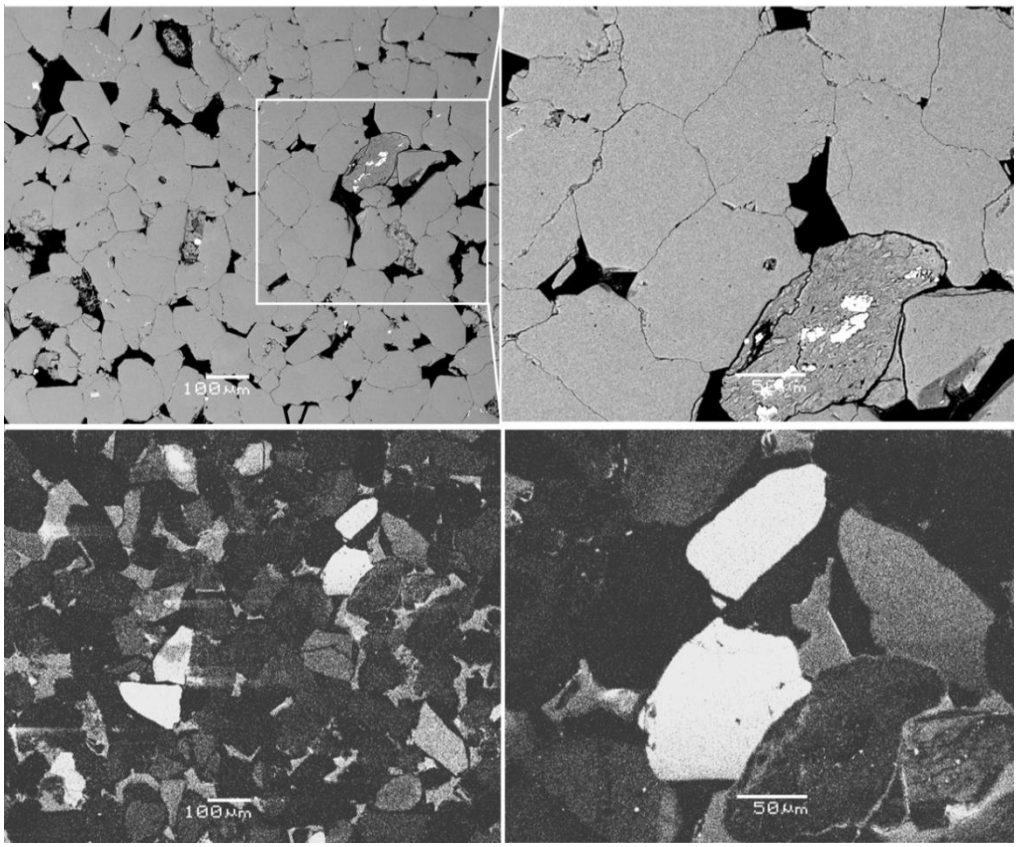

Figure 6.19: Top row back scattered electron images and CL images of same sections below showing the amount of quartz cement. (Picture was taken from well 7120/7-1 with depth 2895m)

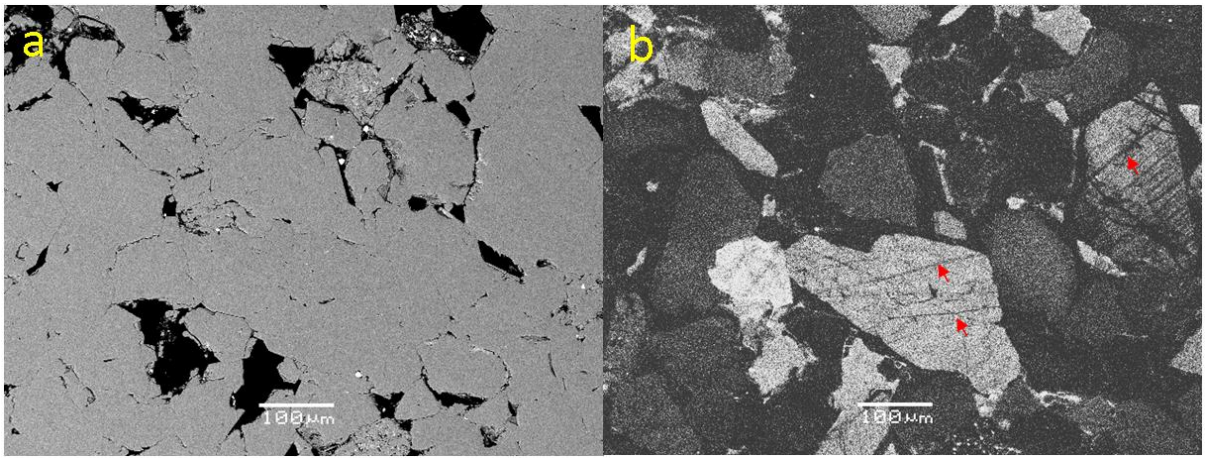

Figure 6.20: a) Overview of the porosity destruction along with its CL image (b) showing the fractures on the grains (red arrows) which are filled with silica cement. (Image from well 7119/12-1 with depth 2703.5m)

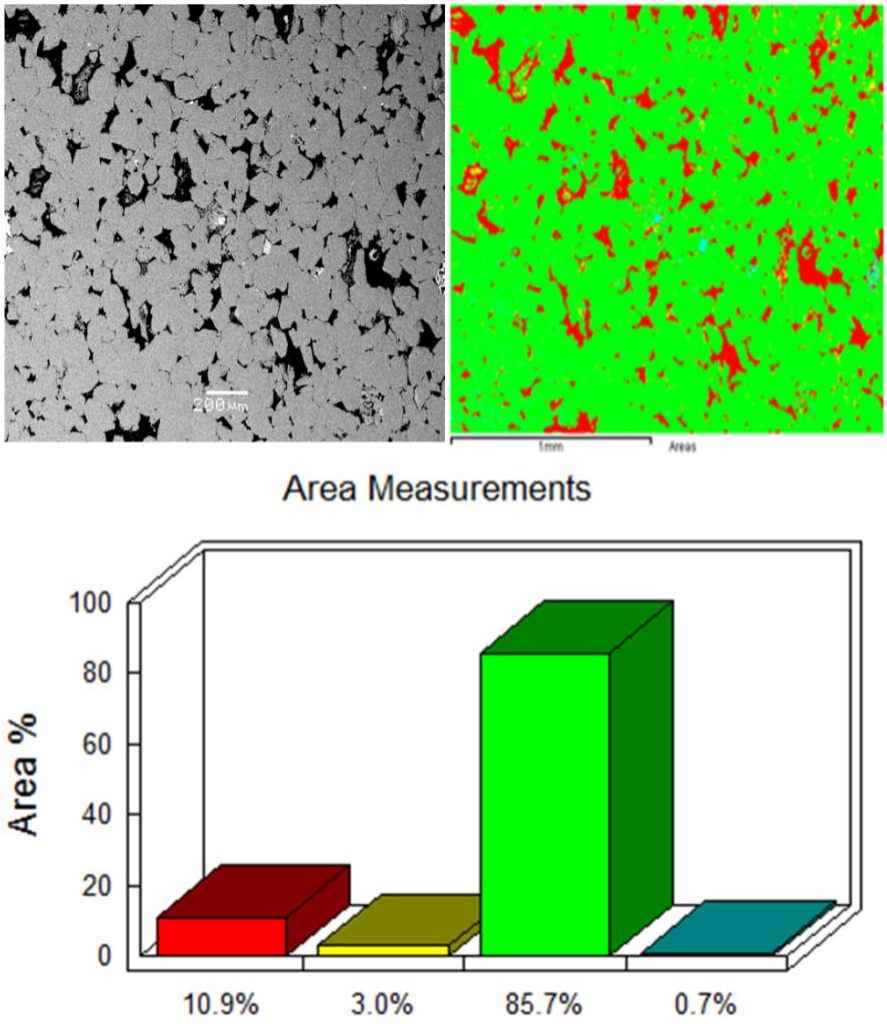

Figure 6.21: Measurement of are from SEM of well 7120/7-1 (depth 2423.45m). Red, yellow, green and teal colors belong to porosity, clays, quartz and other minerals respectively.

6.1.2.4 Other minerals

Some amount of minerals other than the frequently found minerals (quartz, feldspar, illite and kaolinite) have been observed. A carbon coated thin section image (Fig. 6.22) shows the presence of muscovite, zircon and titanium oxides in the Stø Formation.

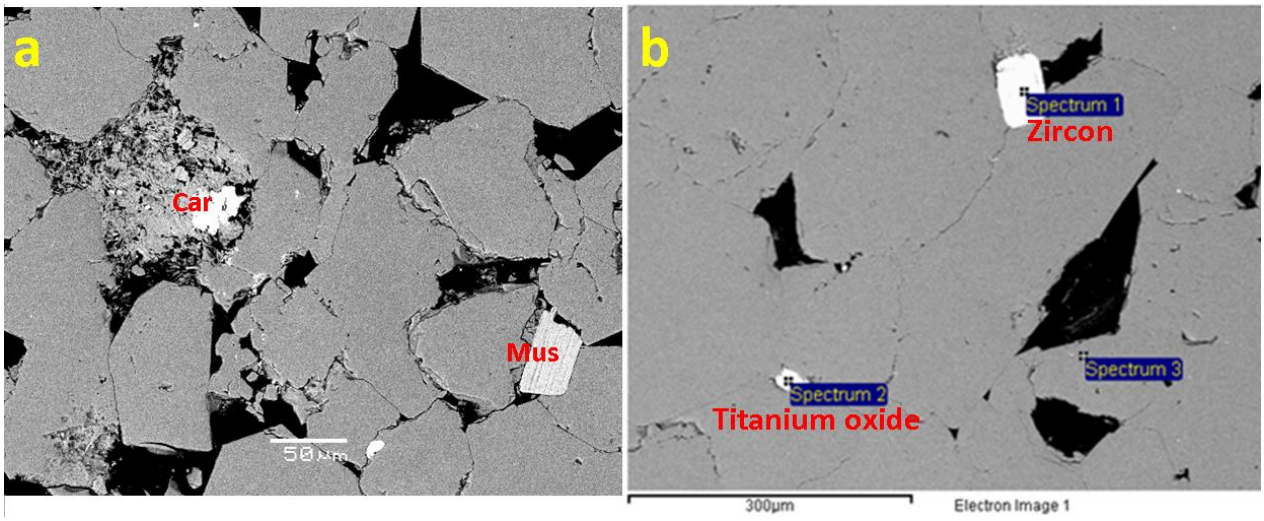

Figure 6.22: A SEM picture of carbon coated thin section showing some observed minerals. a) Well 7120/7-1 (depth 2423.45m), b) Well 7119/12-1 (depth 2703.50m). Mus = Muscovite, Car = carbonate

6.2 Nordmela Formation

6.2.1 Thin section analysis

A total of twelve thin sections from different wells and depths were studied. The Formation contains large amount of clay matrix both illite and kaolinite but the overall impression is as a grain supporting framework. Most of the clay is present in the pores but there are also some examples of detrital clays.

The most abundant minerals are quartz, feldspar, kaolinite, illite, albite and muscovite (Fig. 6.25). The degree of sorting is poor in most of the samples. The sand grains have an average of very fine size but subangular to angular in shape. Only dispersed open pore spaces with no visible pore to pore connections made it a formation of low permeability. The existence of stylolites is also supporting its low reservoir properties (Fig. 6.24).

Table 6.7: Point counting results of Nordmela Formation.

Well	Formation	Depth (m)	Grains			Matrix		Cement		Sorting	Porosity	IGV (%)	Grain Size (mm)
			Quartz	Felds	Lithic Frag	Clay	Muscovite	Quartz	Carbonate				
7120/8-1	Nordmela	2250	52,4	0,8	1,6	22,1	0,8	3,2	10,6	Poor	8,1	44,8	0,038
		2253	61,4	1,8	2,7	17,4	4,8	6,1	0	Moderate to poor	5,5	33,8	0,062

The unusuall large pores mark the secondary porosity and it is due to the presence of high amount of unstable minerals in Nordmela Formation (Fig. 6.23).

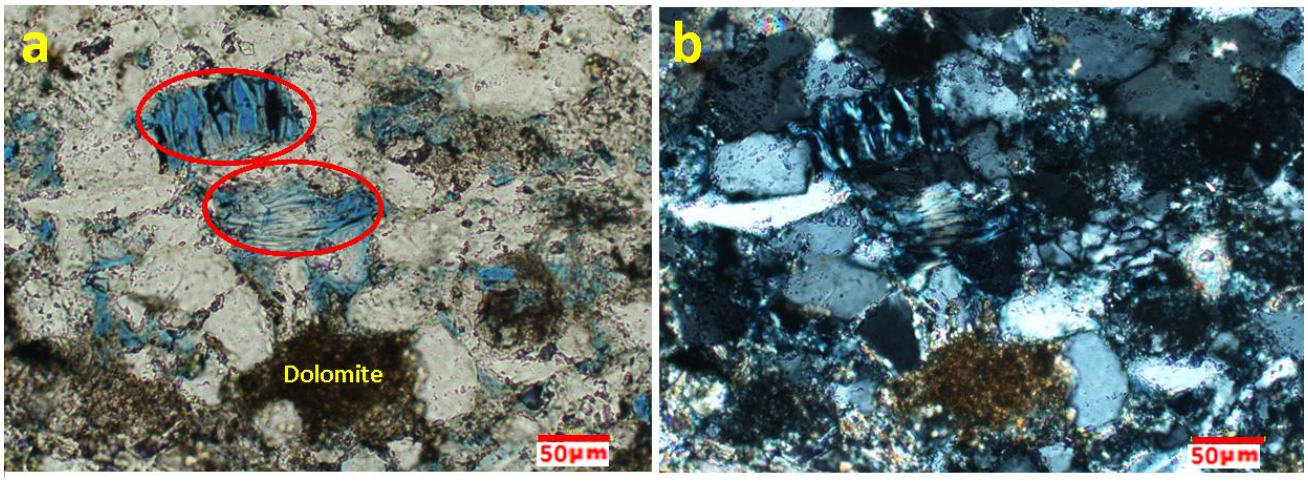

Figure 6.23: a) A sample from well 7120/8-1 (depth 2253m) showing the development of secondary porosity (red circle). b) Same view in cross nickel.

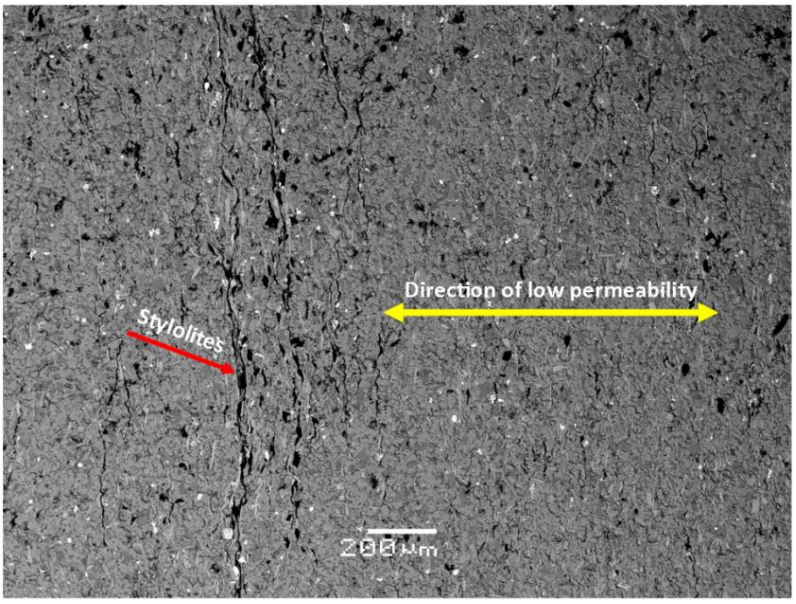

Figure 6.24: SEM picture of well 7121/5-1 (2441 m), showing the low porosity and permeability in the presence of stylolites.

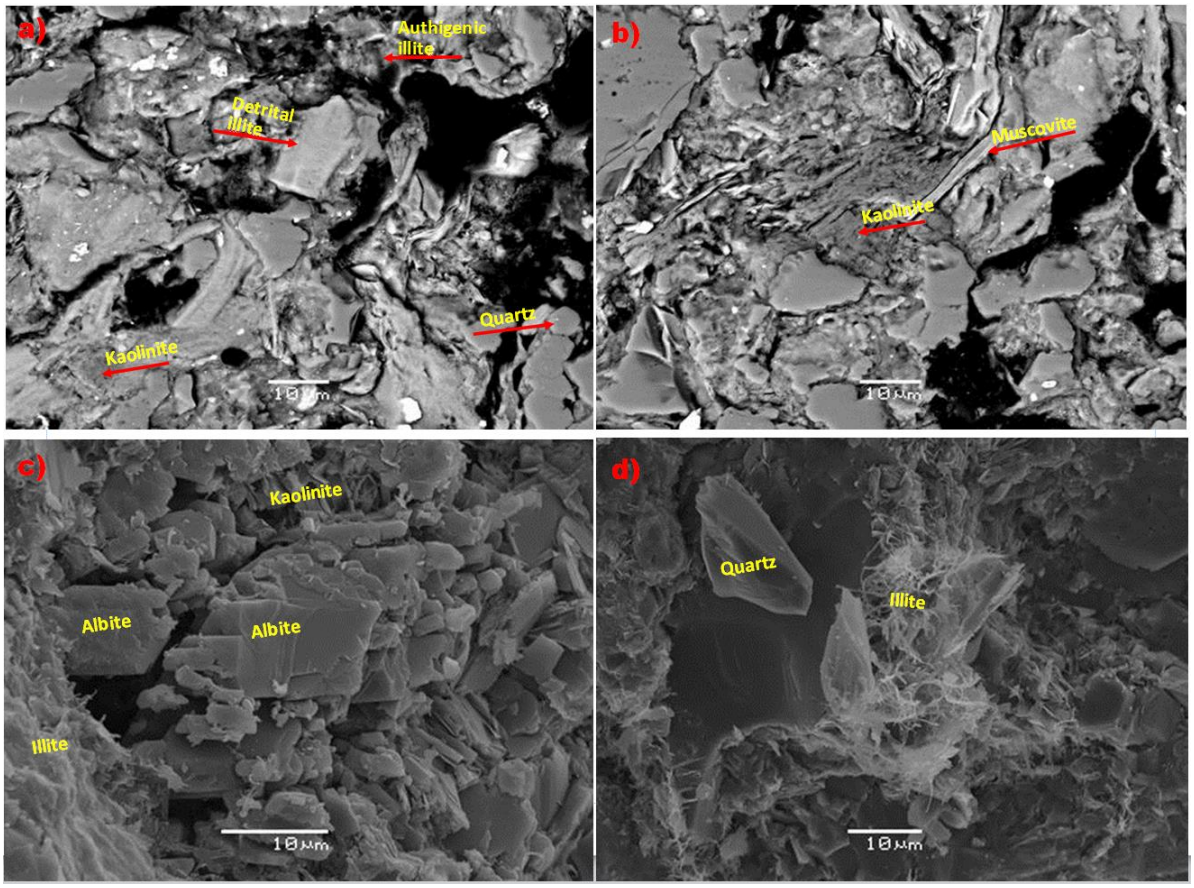

Figure 6.25: Thin sections a, b) from well 7120/9-1 (1922.10 m), stub samples c, d) from well 7120/6-1 showing different minerals and their distribution in the Nordmela Formation.

6.2.2 X-Ray Diffraction (XRD) analysis

Several samples from the Nordmela Formation were very fine graind; so XRD analysis has been carried out for the better mineralogical understanding. The peak height of each mineral has been identified and semi-quantified. It should be kept in mind that XRD% does not reflect the true volume percentage of a particular mineral in an analyzed sample.

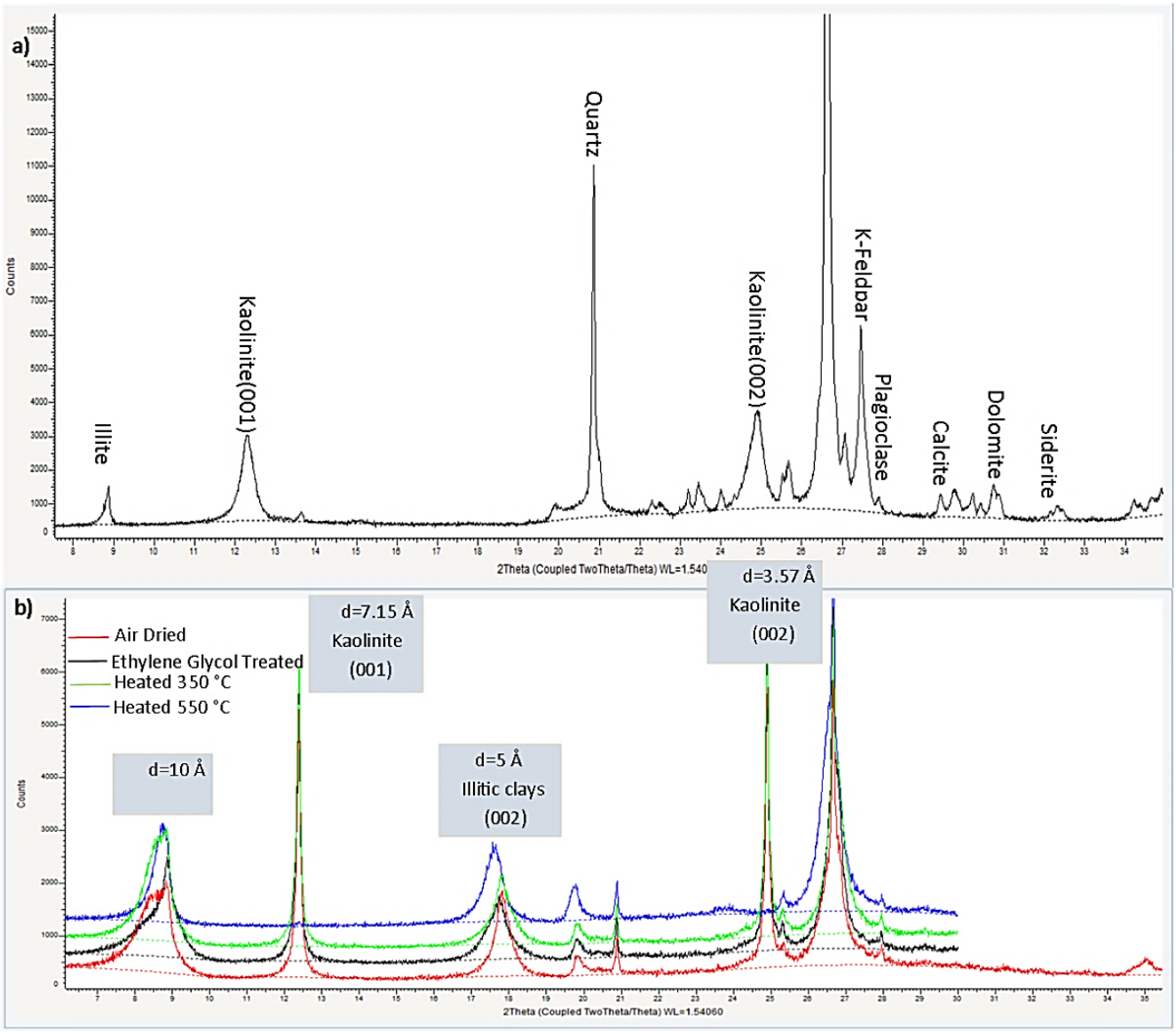

Figure 6.26: a) Figure showing the peaks for specific minerals, b) Sample showing four diffractograms (airdried, ethylene glycol treated and heated (350°C and 550°C) from well 7120/6-1.

6.2.2.1 Bulk analysis

Bulk XRD was employed on the samples from wells 7120/6-1, 7121/5-1 and 7120/9-1. The results from this analysis are shown in Figure 6.27 and presented in table 6.8.

Well 7121/5-1

Bulk XRD analysis of the selected six samples has been studied. Quartz is the most dominant mineral with an average of 56 XRD%, where the average contribution from Kaolinite and illite is 18.5 XRD% and 14 XRD% respectively. Dolomite and k-feldspar are present only in

one sample with 15 XRD% and 3 XRD% values. In some samples siderite and pyrite are present with the highest content of 3 XRD%. The contribution of mean plagioclase in the total feldspar is 9 XRD%.

Table 6.8: X-ray diffraction percentages of all the minerals from XRD analysis.

Well	Depth (m)	Illite XRD%	Quartz XRD%	Kaolinite XRD%	K-feldspar XRD%	Plagioclase XRD%	Dolomite XRD%	Siderite XRD%	Pyrite XRD%
7120/6-1	2532.4	9	66	10	0	11	0	4	0
	2529.6	12	64	7	4	10	0	3	0
	2534.31	16	45	20	4	11	0	4	0
	2558.51	19	48	25	0	5	0	3	0
	2494.3	14	54	13	4	11	0	3	2
7121/5-1	2393.65	2	73	3	3	2	15	0	3
	2441	13	51	25	0	6	0	3	3
	2446.9	11	53	20	0	11	0	3	2
	2463.7	31	33	29	0	4	0	3	0
	2499.1	12	66	17	0	2	0	2	0
	2500.45	16	62	17	0	2	0	2	0
7120/9-1	1922.1	20	52	15	5	4	0	2	2

Well 7120/6-1

Five samples of different depths have been analyzed from this well. Again quartz is the dominant mineral with an average content of 55 XRD%. Both kaolinite and illite have the same average quantities i.e. 15 XRD%, where K-feldspar make up 2.4 XRD% and plagioclase 9.6 XRD%. Siderite is one of the least mineral in this well with an average of 3.4 XRD%.

Well 7120/9-1

To identify the mineralogy of the Nordmela formation only one available sample is analyzed. Highest values are of quartz (52 XRD %), followed by Illite (20 XRD %) and kaolinite (15 XRD %). The 5 XRD% and 4 XRD% are the extractions from k-feldspar and plagioclase yield a total 9 XRD% feldspar content. The least values are 2 XRD% which belong to both siderite and pyrite.

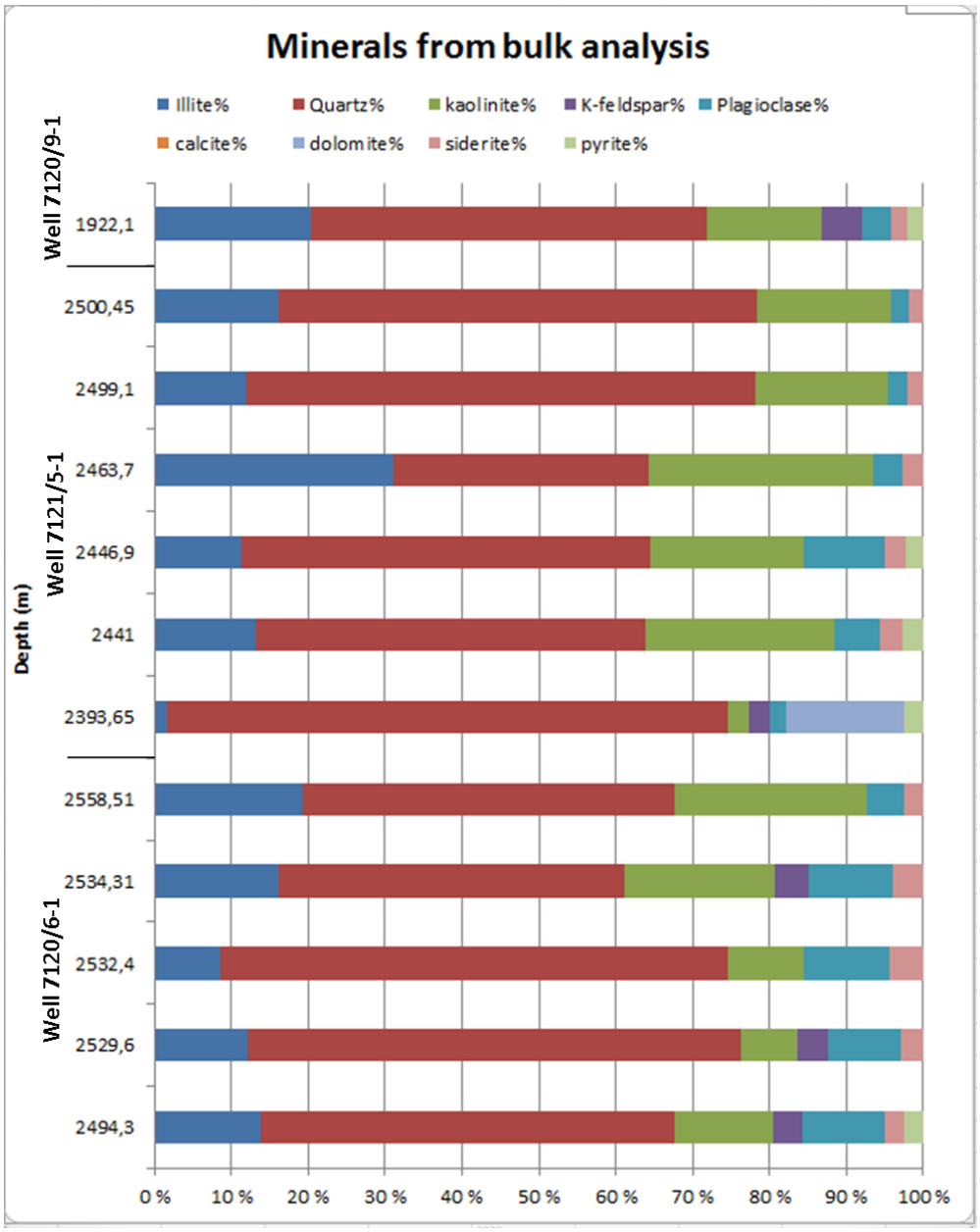

Figure 6.27: Identified minerals from bulk analysis.

Comparison

For the prediction of reservoir quality a comparison between two wells (7121/5-1 and 7120/6-1) is shown in figure 6.28. There is an assumption that whole quartz is detrital because XRD analysis cannot calculate the quartz cementation. The amount of cement (carbonate and pyrite) and matrix is higher in well 7121/5-1 (Fig. 6.28a) with respect to well 7120/6-1 (Fig. 6.28b). In a nut shell later one has better reservoir properties.

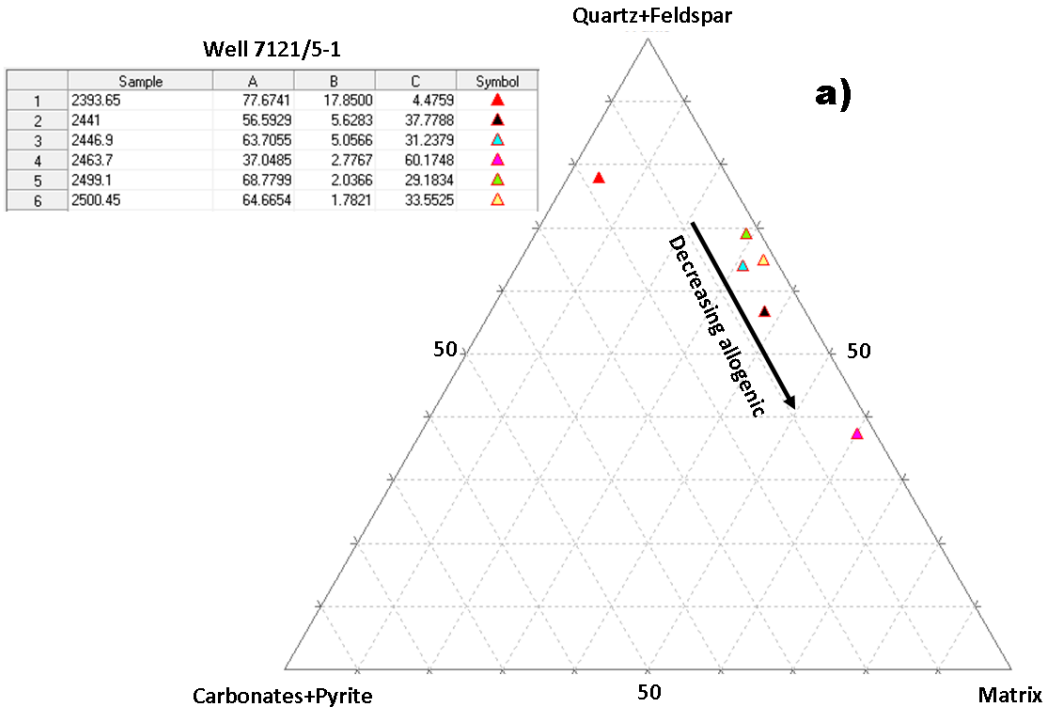

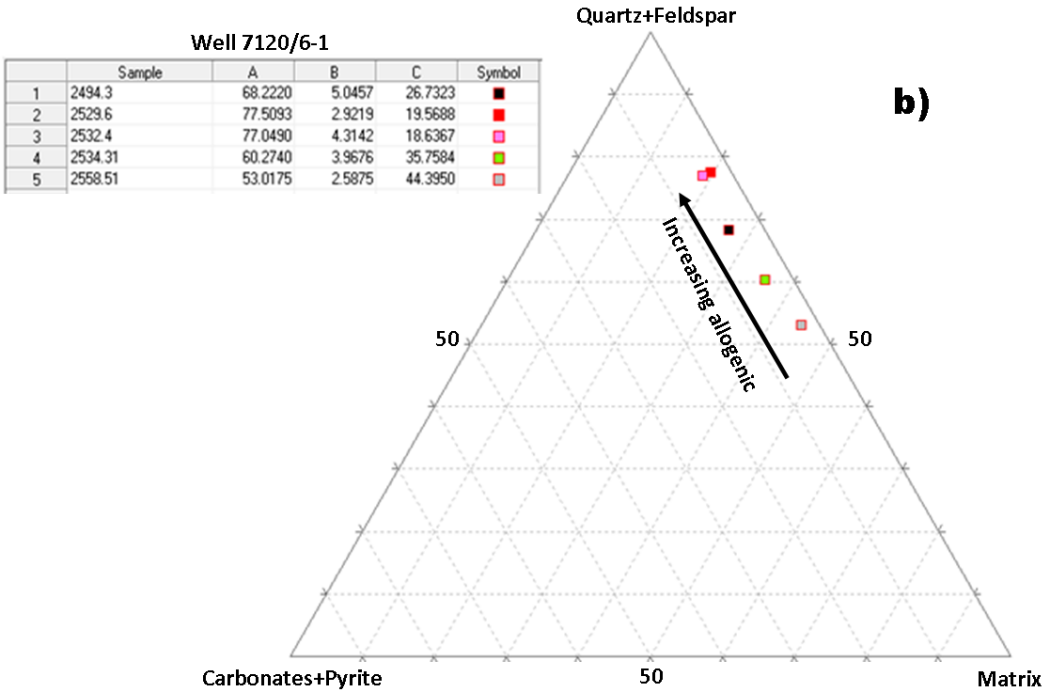

Figure 6.28: Prediction of reservoir quality on the basis of bulk analysis.

General trends

i) Clay minerals

The distribution of clay minerals is shown in figure 6.27. Generally kaolinite is the most abundant clay mineral. Its ratio with illite is divided into four phases i.e. 1, 2, 3 and 4 (Fig.

6.29a). The lowest part of the section is indicating the upward decreasing trend (phase 1). The phase 2 has almost still stand trend in all the samples. The well 7121/5-1 starts with a relatively high ratio and distinguished from the phase 4 which has low ratio.

ii) Carbonates and pyrite

In figure 6.27, the amount of carbonates (dolomite and siderite) and pyrite is shown and they are discussed together as they have an authigenic origin. Their contribution in the Nordmela Formation is relatively low. Overall their abundance is high in well 7121/5-1 as compared to other two wells (Fig. 6.28b).

iii) Quartz and feldspar

The distribution of feldspar and quartz minerals is presented in figure 6.27. The feldspar content is very low as compared to quartz in all the wells. The contribution of plagioclase is greater in the total feldspar with the range of 2 to 11 XRD%. On the other hand k-feldspar is absent in some samples and its quantity remains almost the same in the remaining ones.

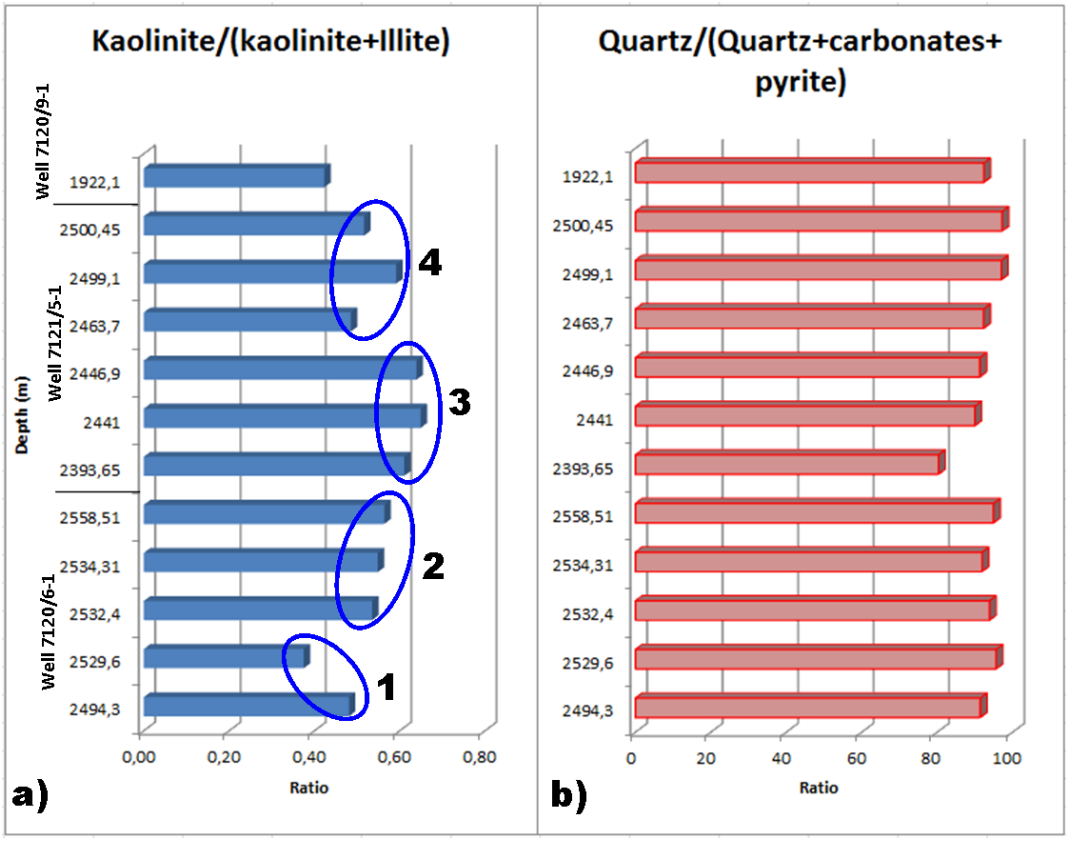

Figure 6.29: a) Kaolinite/(kaolinite+illite) ratio in the Nordmela Formation. b) Quartz/(Quartz+carbonates+pyrite) as a measure of authigenic vs. allogenic minerals in the same Formation.

6.2.2.2 Clay separation

The qualitative analysis is based upon the interpretations of the diffractograms from EG-saturated, air-dried, heated 350° C and 550° C. All the samples from the Nordmela Formation on which Clay separation is applied are shown in table 6.9.

Table 6.9: Observed XRD% of clay minerals in Nordmela Formation.

Well	Depth	Formation	Illite XRD%	Kaolinite XRD%
7120/6-1	2494.3	Nordmela	27	73
	2529.6	Nordmela	32	68
	2532.4	Nordmela	24	76
	2534.31	Nordmela	21	79
	2558.51	Nordmela	16	84
7121/5-1	2393.65	Nordmela	62	38
	2441	Nordmela	17	83
	2446.9	Nordmela	19	81
	2463.7	Nordmela	16	84
	2499.1	Nordmela	8	92
	2500.45	Nordmela	8	92
7120/9-1	1922.10	Nordmela	24	76

Only two clay minerals are observed in all the samples. An abnormally low kaolinite and high illite XRD% value in well 7121/5-1 from 2393.65 m depth differ from the other observations. Kaolinite is the most abundant mineral (68 XRD% to 92 XRD%), where the range of illite is from 8 XRD% to 32 XRD% in all the samples excluding one.

In figure 6.30, the kaolinite/(kaolinite + illite) ratio indicates the four zones. The first zone is at the shallower depth of well 7120/6-1 indicating low ratio. Upto first zone (level 2532.4) the ratio is increased and marking second zone. The well 7121/5-1 is started with an exceptionally low value (level 2393.65) and then upward increasing ratio trend marked the third zone. The remaining well (7120/9-1) is showing a 0.76 value.

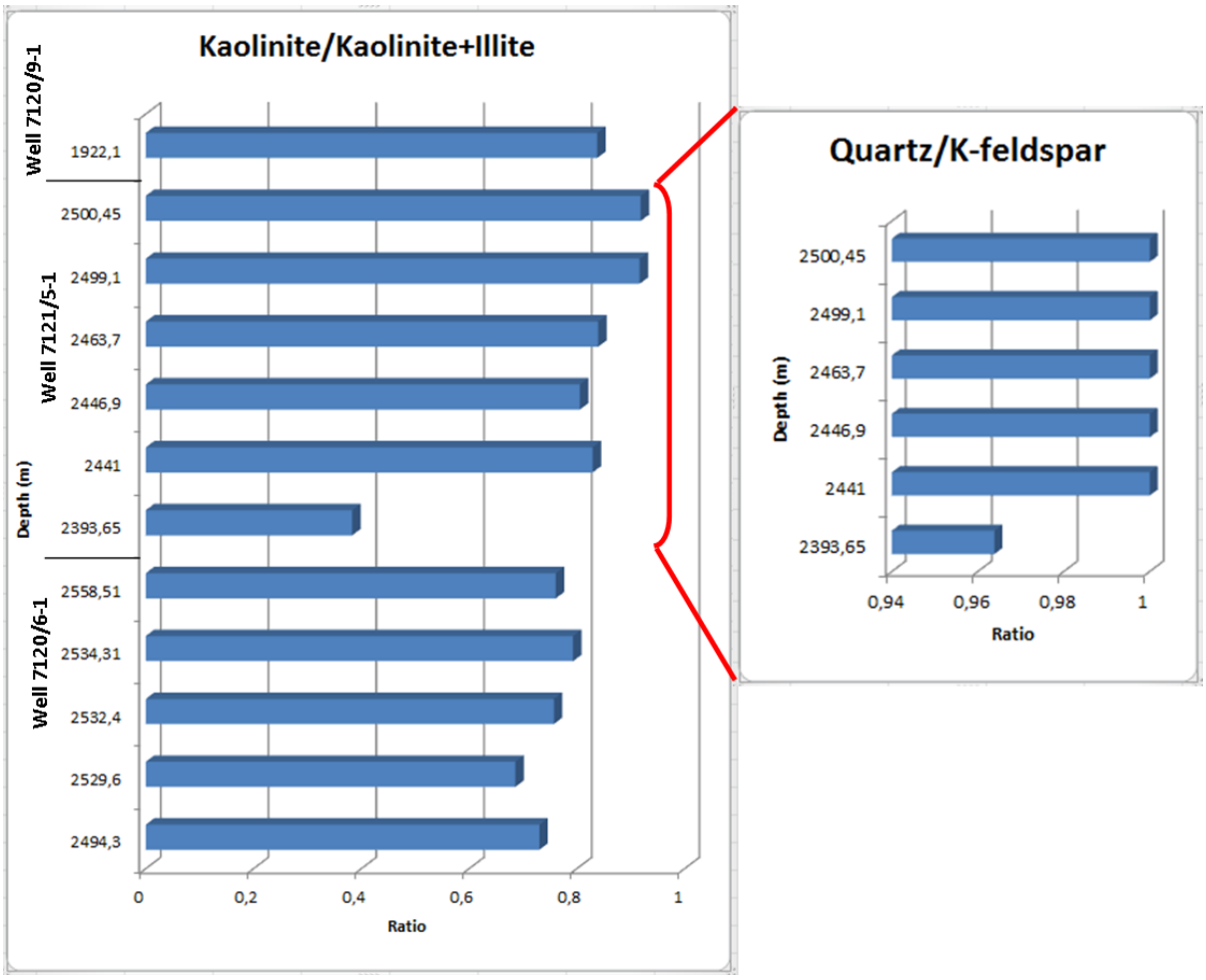

Figure 6.30: The kaolinite/(kaolinite + illite) ration from clay separation in all the samples.

Chapter 7: Discussion

7.1 Mineralogy

7.2 Sedimentology

7.3 Detrital sandstone petrography

7.4 Estimation of uplift

7.5 Mechanical compaction

7.6 Sorting and grain size

7.7 Grain shape

7.8 Carbonate cement

7.9 Quartz cementation

7.10 Authigenic clays

7.11 Reservoir quality vs depth

7.12 Porosity preserving mechanisms

7.13 Observed reservoir quality

Chapter 7: Discussion

7.1 Mineralogy

The Stø Formation is generally well sorted, medium to fine grained sub-rounded sandstone (Fig. 6.10, 6.11c). Most of the detrital grains are of monocrystalline quartz. Quartz is the major cement but there are also minor amounts of ankerite, dolomite, calcite and pyrite.

Samples from the Nordmela Formation were poorly sorted and generally finer in grain size than those of Stø Formation. Majority of detrital grains are mono-crystalline quartz with some silica, carbonates and pyrite cement. Silty shales contents are higher in some deep samples (Table 6.8).

7.2 Sedimentology

Sandstone of Stø Formation is texturally and mineralogically mature (table 6.6 and Fig. 6.4a) and most prominent reservoir rock in the Barents Sea area. After consulting the well log data and core photographs, the Stø Formation has been divided into two layers that are categorized as upper Stø and lower Stø (Fig. 5.2). The lower Stø is well sorted fine to medium grained clean sandstone which can be easily correlated in wells 7121/4-1 and 7121/5-1. This layer has the better reservoir properties. The relatively uniform reservoir properties reflect the dominance of sand deposits and wave actions.

The upper Stø comprises poorly sorted and highly bioturbated sandstone. Thin shale layers in this part reduce the vertical permeability. This unit has a poorer reservoir quality than that of underlying unit. The low energy and cyclic transgression/ regression could be the predicted depositional environments of this unit.

The well log data and core photographs (Fig. 5.2) also divided Nordmela Formation into two portions (lower Nordmela and upper Nordmela). The lower Nordmela has lenticular to flaser bedded shaly sandstone, reflecting the tidal flat to flood plain environment, high marine influx and poor reservoir quality. In upper Nordmela sandy content increases and degree of reservoir quality becomes poor to moderate. The average clay contents increase towards the eastern side well 7121/5-1 (Table 6.8).

7.3 Detrital sandstone petrography

All the detrital grains (quartz, feldspar and lithic fragments) have been plotted in petrophysic classification which reveals that all the sandstone samples of the Stø Formation are pure quartz-arenites (Fig. 6.4a). The presence of fractures in the detrital quartz grains are the indication of severe mechanical crushing. There is minor amount of detrital feldspar (table 6.1), and crystals of siderite and pyrite. Detrital rock fragments comprises of polycrystalline quartz, chert and calcite. Minute sub-rounded muscovite is found between the grains. Rutile, zircon, tourmaline, garnet are some of the observed detrital heavy minerals in samples.

The point counting results from well 7120/8-1 depicts that the Nordmela Formation has a considerable amount of matrix (>15%) and represent quartz wackes (figure 6.4b). Nordmela Formation is underlying the Stø Formation but contains less fracture. The small grain size could be the possible reason (Chuhan et al. 2003) that the fracturing in grains increases with increase in grain size.

7.4 Estimation of Uplift

The degree of quartz cementation is high relative to burial depth (2-2.8km) which suggests that the area has been buried deeper relative to present day depth. The present day bore hole temperature reflects the normal geothermal gradient in the area. Based on amount of quartz cementation, study of uplift has been carried out and a comparison between the Etive Formation of northern North Sea (Marcussen et al. 2009) and the Stø Formation of South West Barents Sea has been constructed (Fig. 7.1). Both the Etive and Stø Formations are quite similar in properties and their diagenetic comparison can give an idea about the actual depth of the area of interest. However, this estimation may vary with the previous published uplift estimations in the greater Barents Sea due to quality and less available data.

Quartz cementation plotted v. present depth (Fig 7.1a) yields a weak depth trend and the plot does not give a good comparison with the trend line from the Etive Formation. After restoring the quartz cement measurements to the inferred burial depth, a reasonable fit with the Etive Formation can be established (Fig. 7.1b). When 800m is added to the current burial depth, most of the points fall on the trend line of Marcussen et al. 2009 (Fig. 7.1b). The observed average 800m uplift in the study area is quite similar to the observation made by Ohm et al. 2008, in the SW Barents Sea (Appendix 2).

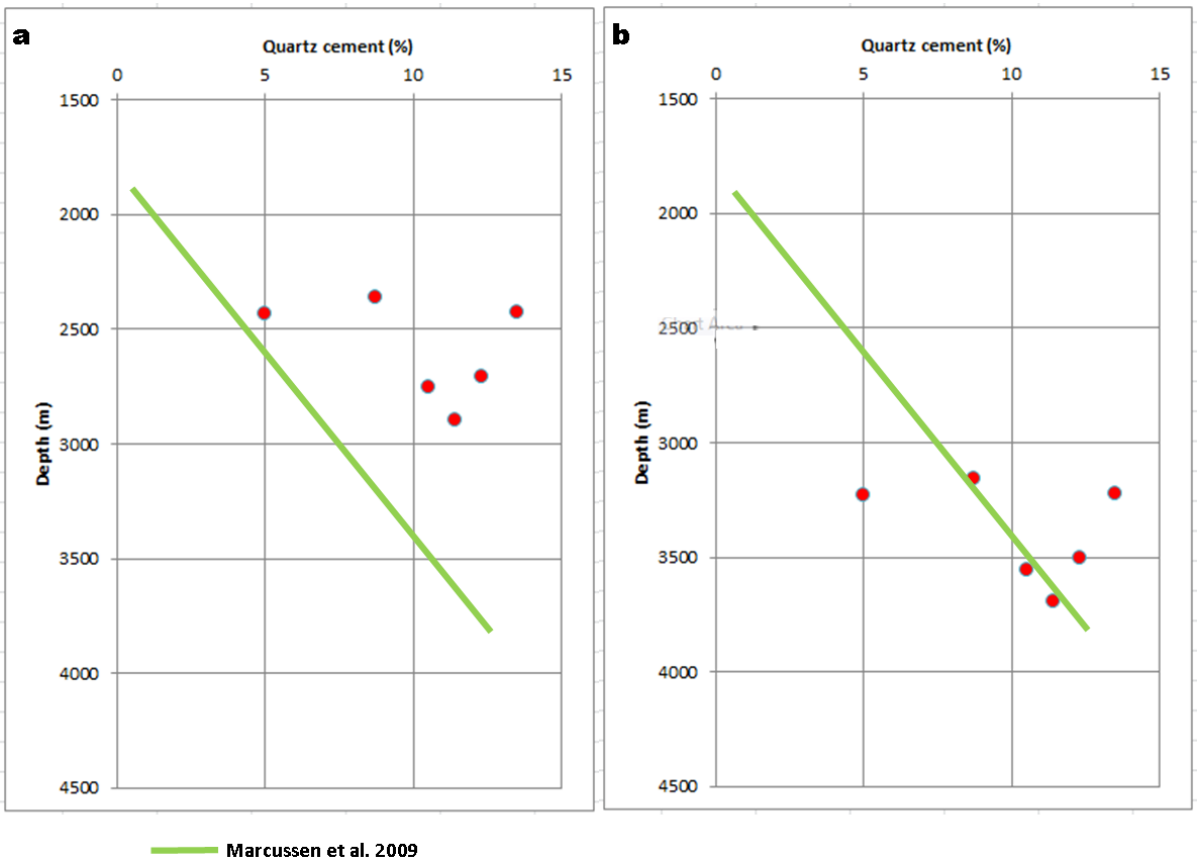

Figure 7.1: Uplift estimation of the study area. A trend line (green line) for the Etive Formation, northern North Sea (Marcussen et al. 2009) is inserted for comparison.

7.5 Mechanical compaction

Mechanical compaction is the major porosity reduction factor before the chemical compaction. The grain contacts (long, concavo-convex and suture), grain fracturing and pressure solution reveal high degree of mechanical compaction (Fig. 6.2). Porosity reduction in the Stø Formation is mainly due to the grain crushing while in the Nordmela Formation grain reorientation and sliding causes the porosity loss. Chuhan et al. (2002) experimentally proved similar porosity loss phenomena in fine and coarse grain sands.

The calculated IGV from point counting ranges from 25.5% to 43.6% (Table 6.1). The low IGV is the result of maximum mechanical compaction, whereas high IGV in two samples (well 7120/7-1, depth 2432.1m and well 7120/8-1, depth 2250m) depicts that the porosity has been preserved during early deposition. Early carbonate cementation has the ability to preserve the IGV (Bjørlykke and Jahren 2010); in accordance with the calcite cement found in those samples. IGV is also affected by grain size, grain shape and sorting (Fig. 6.11).

7.6 Sorting and Grain size

The calculated IGV and sorting crossplot (Fig. 6.11A) does not give any prominent trend, but a slight increase in IGV in more sorted samples is observed. The IGV against the grain size gives a relatively better trend (Fig. 6.11B). Increase in IGV with decrease in grain size and vice versa. Less intergranular contact in coarse grained samples and subsequently grain-crushing is the reason of low IGV value (Chuhan et al. 2002; Fawad et al. 2011).

7.7 Grain shape

Angular grains underwent more mechanical compaction and have lower IGV as compared to rounded grains because of low contact area. All the samples from the Stø Formation are almost sub-rounded, so grain shape has not significant effect on IGV (Fig. 6.11C).

Influence on reservoir properties

Overall high IGV values are found in most of the wells (Fig. 6.9) indicating that the mechanical compaction has not been very significant in the Stø Formation. Fine gains, subrounded to rounded shape and well degree of sorting provided the platform for the high IGV preservation. The addition of early carbonate cement and later quartz cement play a catalystic role to cease the mechanical compaction (increase the strength of the rock).

7.8 Carbonate cement

In some samples carbonate cement has been observed (table 6.1). The amount of carbonate cement (calcite) in two samples (well 7120/7-1, depth 2432.1m) and (well 7120/8-1, depth 2250m) is significantly high and resulting the high IGV. The reason of this could be the high biogenic carbonate at that particular depth (possibly related to a maximum flooding surface) which consequently cemented the sandstone at an early stage of compaction.

7.9 Quartz cementation

The velocity/depth distribution for the 8 wells shows that the velocity/depth gradient changes with depth. The log velocities are increasing nearly linearly from the Nordland Group to Stø Formation (Fig. 7.2). However, carefull observation reflects that the velocity/depth gradient starts to increase more from about the bottom of the Kolmule Formation in wells 7119/12-1, 7121/5-1, 7120/6-1, 7120/7-3 and 7120/9-1. The Kolje Formation is the starting point of higher velocity/depth gradient in wells 7120/7-1, 7120/8-1 and 7121/4-1. Both of these Formations may be interpreted as the start of the chemical compaction.

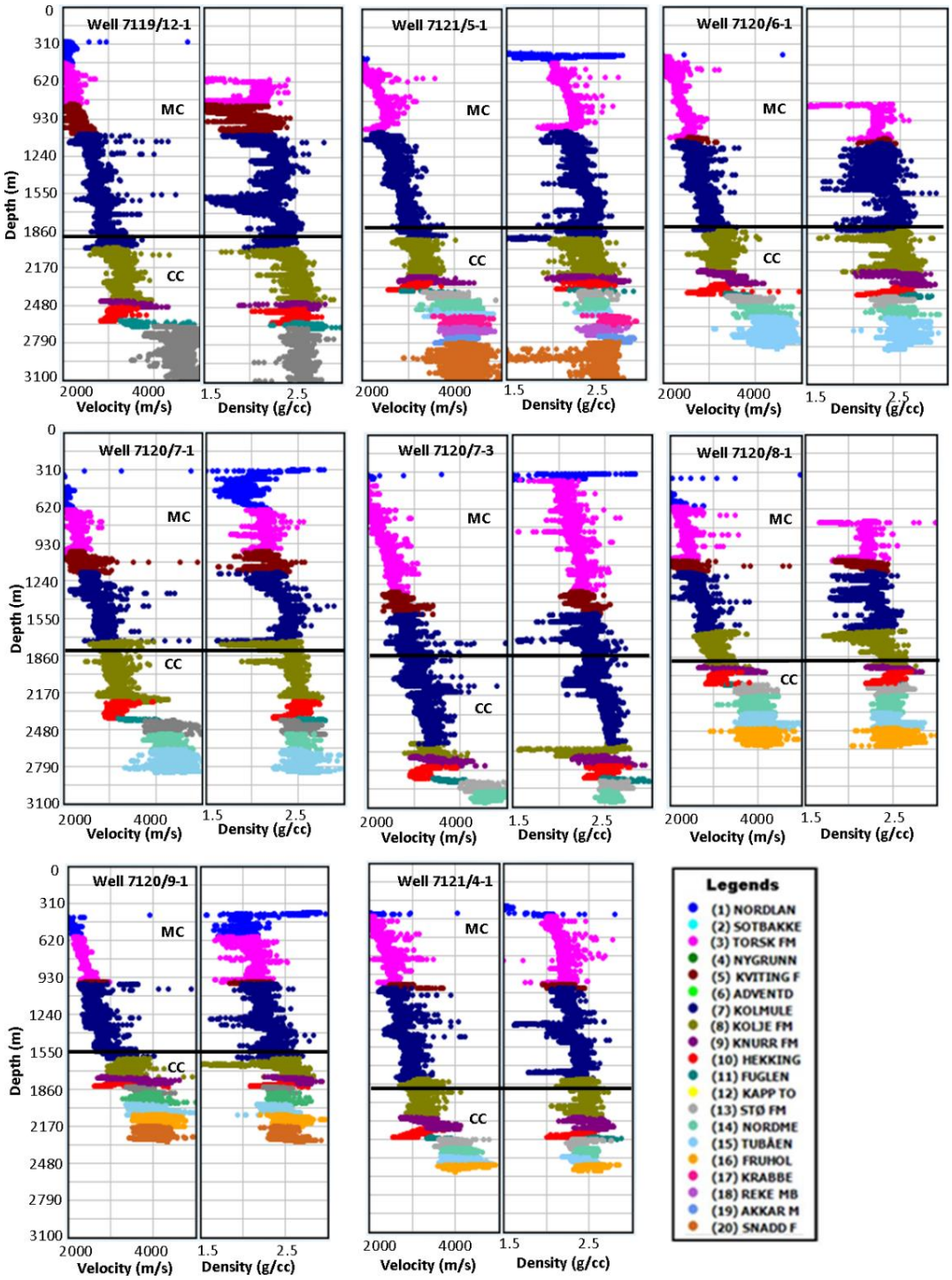

Figure 7.2: Compaction trends in the study area.

These Formations consist of claystone and shale; so the transition zone is not very clear. Figure 7.3 shows the relationship of the amount of quartz cement observed in the Stø Formation and velocity which reveals that the cementation is nearly zero at 3500 m/s velocity. This threshold velocity (3500 m/s) assumed as the starting point of quartz cementation in other Formations also and marked the transition zone. On the basis of this assumption and

well log data the transition from mechanical compaction to chemical compaction seems to occur at the depth of 1500-2000m in the study area (Fig. 7.2).

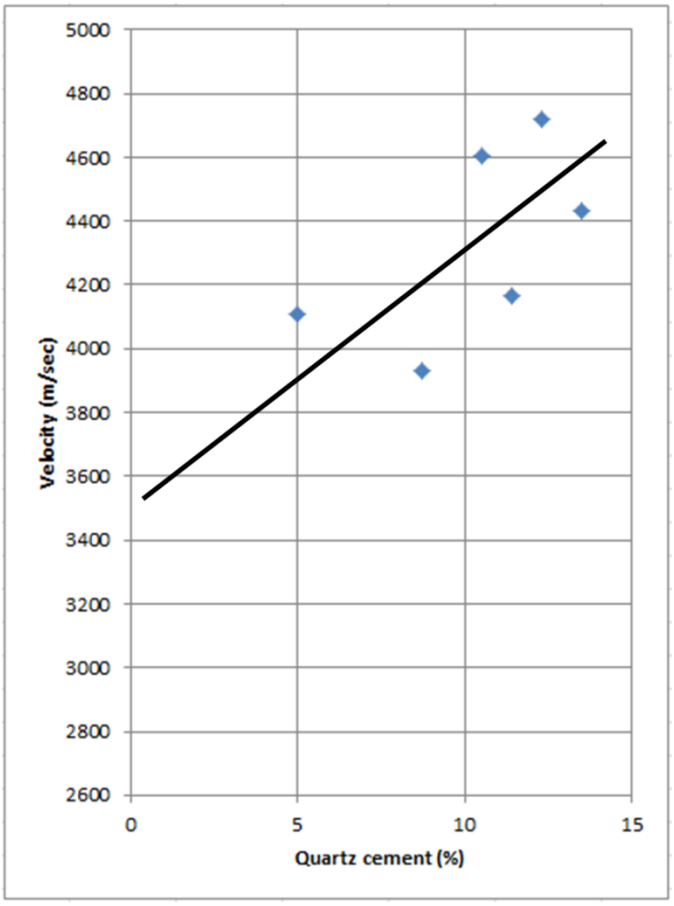

Figure 7.3: Relationship between velocity and quartz cement.

The reservoir rocks (Stø, Nordmela and Tubåen Formations) are well below to this transition zone with the addition of 800m uplift estimation on the basis of quartz cementation (Fig. 7.2, 7.1). The average geothermal gradient is 30^0C/Km (Table 4.1). The temperature required for quartz cementation (70-100^0C) has been achieved in this area; so high degree of cementation should be expected (Fig. 5.5, Fig. 5.6). The observed unusual angular shapes in the Stø Formation i.e. suture contacts probably representing micro-stylolites (Fig. 6.2) are the indicative feature of partial dissolution of detrital grains. Comparatively, the amount of quartz cementation is higher in deep wells (Fig. 6.3d) than in shallow wells (Fig. 6.3c). This is due to the dependence of pressure solution and degree of silicification on the time-temperature integral (TTI). The quartz cementation is high in well 7120/7-1 while the other wells have slightly less than this (Fig. 6.3). The possible reason could be the grain size which is very fine in well 7120/7-1 (Table 6.1), so the available area for the quartz overgrowth is higher.

The visual thin section study of the Nordmela indicates comparatively low silica cementation as compared to the Stø Formation, while it has high burial depth. The reason of low cement is the less available area to quartz overgrowth due to high mechanical compaction and matrix content.

Stylolites are one of the main diagenetic features in the study area (6.2a). Majority of the stylolites developed where thin laminae of clay occuring between detrital grains specially in the wells 7120/7-3 and 7119/12-1. According to Walderhaug and Bjørkum (2003), the silica cementation is more intense near the stylolites which reflect that the migration path of silica was not too far.

Influence on reservoir properties

The degree of quartz cementation was high compared to present day geothermal gradient which strongly affected the reservoir quality. No significant coating was observed in samples which could retard silica cementation. Different sources of silica (stylolites and illitization) enhanced the cementation.

7.10 Authigenic clays

Kaolinite and illite are the two observed authigenic minerals in the Stø Formation. Both kaolinite and illite content varied from sample to sample during the point counting and SEM analysis. But generally the fraction of kaolinite is relatively higher than to illite. During early diagenesis dissolution of feldspar and mica by meteoric water influx yield the kaolinite.

High permeable clean sandstone of the Stø Formation deposited in a shallow marine environment is prone to meteoric influx producing kaolinite from feldspar leaching. Low permeable Nordmela Formation consists of alternating sand/mud layers belongs to the tidal flat to flood plain environment and is therefore subjected to less meteoric water flushing. High amount of clay in XRD analysis is due to the presence of detrital clay. XRD data (Table 6.8) revealed that the clay content is high in deep Nordmela samples of well 7120/6-1 and 7121/5-1. The deep samples belong to flood plain environment so the amount of detrital clay is higher in it.

The kaolinite which formed during the early diagenesis becomes unstable in the presence of k-feldspar and altered into illite during deep burial. The alteration of kaolinite to illite usually occurs at temperatures 130-140°C in the North Sea (Bjørlykke 1998). The study area experienced the average uplift of 800m and the present borehole temperature with respect to

measured depth suggests that geothermal gradient in the study area is high (30^0C/Km); so required amount of temperature has been achieved for the formation of illite. The high clay content in well 7120/7-1 (2432.1m) is due to regional transgressive pulses (NPD 2013). The illite content in some samples from well 7121/5-1 is high due to the presence of k-feldspar at that particular depth (Fig. 6.30).

Influence on Reservoir properties

Reservoir properties particularly porosity and permeability change in relation to authigenic kaolinite and illite. Studies from the samples suggest that pore filling kaolinite in all the samples significantly reduced the porosity in the sandstones. The permeability is less sensitive to the morphology of kaolinite because fluids can easily flow pass. Furthermore, illitization of kaoline considerably reduced the permeability due to its fibrous structure which blocked the flow.

7.11 Reservoir quality vs Depth

Generally reservoir quality has been decreased with increase in burial depth. The shallowest well 7121/4-1 has the highest porosity and lowest silica cementation (Fig. 6.6).

While the shallower sample of well 7119/12-1 has higher silica cementation and lower porosity than the deeper sample. This low cementation is considered to be a result of low stylolite occurrence at that depth resulting in a supply controlled quartz cement amount that is lower than the usual precipitation rate controlled quartz cement amount (Walderhaug and Bjørkum 2003).

7.12 Porosity preserving mechanisms

The high degree of quartz cementation and pore-filling clays in all the samples has reduced the pore spaces and considered as the major porosity reducing factor (Table 6.1, Table 6.7). Coating (illite, microquartz) could slow down the cementation and preserve porosity in deep burial sandstones. The coating is not frequent and previous literature does not give any evidence of micro-quartz coating in this area. One of the samples from the Stø Formation of well 7120/7-1 has microcrystalline quartz of unknown origin (Fig. 6.12).

Illite coating is also very sparse and not covering the whole grains or thick enough to retard the quartz overgrowth. Figure 6.13 displays an example from well 7121/4-1 where illite is only on one side of the detrital quartz grain. The illite coating should form earlier than quartz

cementation to preserve the porosity. Illite can precipitate from smectite at temperature ranges from $60C^{o}$-$100C^{o}$ (Hoffman and Hower 1979) and reflects flaky to honey comb morphological features (Pollastro 1985). The SEM analysis displays such kind of coating structure (Fig. 6.13) which is a clue of alteration of smectite to illite.

Influence on Reservoir properties

Petrographic study point outs high amount of quartz cementation along with minor coating. The coverage area of coating was also less. So, coating has been of negligible significance to the reservoir properties in the Stø Formation.

7.13 Observed Reservoir Quality of the study area

The reservoir quality of the both Stø and Nordmela Formations in all the study wells varies. Cementation is the major reason of porosity loss in the Stø Formation, while mechanical compaction and cementation are the major factors of porosity loss in the Nordmela Formation (Table 6.1, 6.7). The porosity in some samples is still good enough (Table 6.1, 6.7, Appendix 1) which reflects that cementation and mechanical compaction are not so extensive. Thin sections from the Nordmela have altering sand and mud/clay layers, while the thin sections from the Stø have sand with low muddy content.

The observed quartz overgrowth is not so extensive which can fill the whole pore spaces and porosity is still left. However, cementation has covered whole pores in some places and alternating layers of sand/clay in the Nordmela Formation, leading to low permeability. The presence of calcite cemented layers can also act as a potential barrier for fluid flow. From all the observations during this study the reservoir quality of the Stø Formation is quite good with the porosity ranges from 10.5% to 18.1%; estimations are from homogeneous sands (Table 6.2). Some samples from sandy portion of the Nordmela Formation show a reasonable porosity but reservoir quality in the study area may not be good due to the hetrolithic nature of the formation.

Conclusion

- The sandstones of Stø Formation are mineralogically and texturally mature, while the Nordmela Formation is mineralogically mature like Stø but texturally less than this.
- Cementation is the major reason of porosity loss in Stø Formation, while both mechanical compaction and cementation are the major porosity reducing factors in Nordmela Formation.
- Early carbonate cement is the cause of observed high IGV, where variation in IGV values depicts different extents of mechanical compaction.
- The area has been subjected to an average of 800m uplift. The degree of quartz cementation in the deepest well is not comparable to the shallowest well and differences in uplift between the two wells is not possible.
- The coating on grains is low and do not have significant effect on the porosity preservation.
- Dissolution of detrital grains at stylolites is the main reason of silica cementation in the study area.
- The quartz cementation in the study area is controlled by the grain size and the presence of stylolites.
- Most of the clay (kaolinite, illite) is present in the pores and controlling the porosity and permeability in the sandstones, the calcite cement in some samples is also acting as a potential barrier.
- The reservoir quality of the Stø Formation is quite good with the porosity ranges from 10.5% to 18.1%; while some samples from sandy portion of the Nordmela Formation show a reasonable porosity but the reservoir quality may not be good due to frequently altered sand/clay layers.

References

Aase, n. E. And o. Walderhaug (2005). The effect of hydrocarbons on quartz cementation: diagenesis in the upper jurassic sandstones of the miller field, north sea, revisited. 11: 215–223.

Adams, a.e., mackenzie, w.s. And guilford, c. 1986. Atlas of sedimentary rocks in thinsection.: ferdinand enke stuttgart federal republic of germany. Pages: 103.

Berglund l. T., augustson j., færseth r., gjelberg j. And ramberg-moe h. (1986). The evolution of the hammerfest basin. Norwegian petroleum society, p. 319-338.

Bjørlykke, k., and p. Aagaard, 1992, clay minerals in north sea sandstones, in d. W. Houseknecht, and e. D. Pittman, eds., origin, diagenesis, and petrophysics of clay minerals in sandstones, v. Special publication no. 47, sepm (society for sedimentary geology).

Bjørlykke, k. 1994. Fluid-flow processes and diagenesis in sedimentary basins. Geological

Society special publications 78, 127-140.

Bjorlykke k. (1998). Clay mineral diagenesis in sedimentary basins - a key to the prediction

Of rock properties. Examples from the north sea basin. Clay minerals 33(1), p. 15-34.

Bjørlykke, k. And j. Jahren, (2010). Sandstones and sandstone reservoirs. Petroleum geoscience: from sedimentary environments to rock physics, springer berlin heidelberg: 113-140.

Bloch, s., h. Ler robert, et al. (2002). "anomalously high porosity and permeability in deeply buried sandstone reservoirs; origin and predictability." aapg bulletin 86: 301-328.

Breivik, a. J., gudlaugssin, s. T., & faleide, j. I. (1995) ottar basin, sw barents sea : a major upper paleozoic rift basin containing large volume of deeply buried salt. Basin research 7, 299-312.

Chuhan f.a., kjeldstad a., bjørlykke k. And høeg k. (2002). Porosity loss in sand by grain

Crushing. Experimental evidence and relevance to reservoir quality. Marine and petroleum

Geology, v. 19, p. 39–53.

Chuhan, f. A., a. Kjeldstad, et al. (2003). "experimental compression of loose sands: relevance to porosity reduction during burial in sedimentary basins." canadian geotechnical journal 40(5): 995-1011.

Dalland a., worsley d. And ofstad k. (1988). A lithostratigraphic scheme for the mesozoic

And cenozoic succession offshore mid and northern norway. Norwegian petroleum

Directorate bulletin, v.4, p. 65.

Dengo, c. A., & røssland, k. G., 1992, extensional tectonic history of the western barents sea. In: r. M. Larsen, h. Brekke, b. T. Larsen & e. Talleraas (eds.), structural and tectonic modeling and its applications to petroleum geology. Norwegian petroleum society, special publication v.1, p. 91-107.

Dore a. G. (1995). Barents sea geology, petroleum resources and commercial potential.

Arctic, v. 48(3), p. 207-221.

Dore a. G. And jensen l. N. (1996). The impact of late cenozoic uplift and erosion on

Hydrocarbon exploration: offshore norway and some other uplifted basins. Global and

Planetary change, v. 12(1–4), p. 415-436.

Dott, r.h., 1964: wacke, greywacke and matrix- what approach to immature sandstone

Classification? Journal of sedimentary petrology 34, no. 3, 625-632.

Faleide j. I., gudlaugsson s. T. And jacquart g. (1984). Evolution of the western barent sea.

Marine and petroleum geology, v. 1.

Faleide j. F., bjørlykke k. And gabrielsen r. H. (2010). Geology of the norwegian

Continental shelf in bjorlykke k. (2010), petroleum geoscience: from sedimentary

Environments to rock physics, berlin, heidelberg, springer-verlag berlin heidelberg, p. 467

–499.

Fawad, m., mondol, n.h., jahren, j. And bjørlykke, k. 2011. Mechanical compaction and

Ultrasonic velocity of sands with different texture and mineralogical composition.

Geophysical prospecting, no-no.

Fisher, q., r. Knipe, et al. (2000). "the relationship between faulting, fractures, transport of silica and quartz cementation in north sea oil fields." blackwell science, oxford.

Folk, r.l. 1951. Stages of textural maturity in sedimentary rocks. Journal of sedimentary

Petrology 21, 127-130.

Gabrielsen, r. H., faerseth, r. B., jensen, l. N., kalheim, j. E., & riis, f, 1990, structural elements of the norwegian continental shelf. Part 1: the barents sea region: norwegian petroleum directorate, bulletin no. 6, p. 1-33.

Glørstad-clark. E.. J. I. Faleide. Et al. (2010). "triassic seismic sequence stratigraphy and paleogeography of the western barents sea area." marine and petroleum geology 27(7): 1448-1475.

Gudlaugsson, s. T., faleide, j. I., johansen, s. E., & breivik, a. J, 1998, late paleozoic structural development of the south-western barents sea: marine and petroleum geology, v. 15, p. 73-102.

Henriksen, e. 2011. Uplift and erosion of the greater barents sea: impact on prospectivity and petroleum systems. Memoirs of the geological society of london, 35, 271.

Hoffman, j. And hower, j. 1979. Clay mineral assemblages as low grade metamorphic

Geothermometers; application to the thrust faulted disturbed belt of montana, u.s.a.

Special publication society of economic paleontologists and mineralogists 26, 55-79.

Jakobsson, m., l. A. Mayer, b. Coakley, j. A. Dowdeswell, s. Forbes, b. Fridman, h. Hodnesdal, r. Noormets, r. Pedersen, m. Rebesco, h.-w. Schenke, y. Zarayskaya a, d. Accettella, a. Armstrong, r. M. Anderson, p. Bienhoff, a. Camerlenghi, i. Church, m. Edwards, j. V. Gardner, j. K. Hall, b. Hell, o. B. Hestvik, y. Kristoffersen, c. Marcussen, r. Mohammad, d. Mosher, s. V. Nghiem, m. T. Pedrosa, p. G. Travaglini, and p. Weatherall, 2012, the international bathymetric chart of the arctic ocean (ibcao) version 3.0, geophysical research letters.

Johnson, r. H. (1920). "the cementation process in sandstones." aapg bulletin 4: 33-35.

Linjordet, a. And olsen r. G. (1992). The jurassic snohvit gas field, hammerfest basin, offshore northern norway. Aapg bulletin m 54, p. 349-370.

Md Rahman. J, thesis 2012: compaction, rock properties evaluation, rock physics diagnostics, avo modeling and seismic inversion in the snøhvit field, sw barents sea, university of oslo, norway.

Mondol n. H., bjørlykke k., jahren j. And hoeg k. (2007). Experimental mechanical

Compaction of clay mineral aggregates - changes in physical properties of mudstones during

Burial. Marine and petroleum geology, v. 24, p. 289-311.

Norwegian Petroleum Directorate (NPD) Factpages and Factmaps (www.npd.no). Latest visited 30th of May.

Nyland b., jensen l. N., skagen j., skarpnes o. And vorren t. (1992). Tertiary uplift and

Erosion in the barents sea: magnitude, timing and consequences, in larsen r. M., brekke h.,

Larsen b. T. And talleraas e., eds., structural and tectonic modeling and its application to

Petroleum geology. Amsterdam, elsevier, p. 153-162.

Ohm s. E., karlsen d. A. And austin t. J. F. (2008). Geochemically driven exploration

Models in uplifted areas: examples from the norwegian barents sea. Aapg bulletin, v. 92,

P. 1191-1223.

Paxton, s. T., j. O. Szabo, et al. (2002)."construction of an intergranular volume compaction curve for evaluating and predicting compaction and porosity loss in rigid-grain sandstone reservoirs." aapg bulletin 86(12): 2047-2067.

Peltonen c., marcussen o., bjørlykke k. And jahren j. (2008). Mineralogical control on

Mudstone compaction: a study of late cretaceous to early tertiary mudstones of the voring

And more basins, norwegian sea. Petroleum geoscience 14(2), p. 127-138.

Pollastro, r.m. 1985. Mineralogical and morphological evidence for the formation of illite at

The expense of illite/smectite. Clays and clay minerals 33, 265-274.

Ramm, m. And k. Bjørlykke (1994). "porosity/depth trends in reservoir sandstones; assessing the quantitative effects of varying pore-pressure, temperature history and mineralogy, norwegian shelf data." clay minerals 29(4): 475-490.

Riches, p., i. Traub-sobott, w. Zimmerie, and u. Zinkernagel, 1986, diagenetic peculiarities of potential lower jurassic reservoir sandstones, troms 1 area, off northern norway, and their tectonic significance: clay minerals, v. 21, p. 565-584.

Roufosse, m. C., 1987, the formation and evolution of sedimentary basins in the western barents sea. In: j. Brooks & k. Glennie (eds.), petroleum geology of north west europe , graham & trotman, london, p. 1149-1161.

Saigal, g. C., and k. Bjørlykke, 1987, carbonate cement in clastic reservoir rocks from offshore norway -relationship between isotopic composition, textural development and burial depth, in j. D. Marshall, ed., the diagenesis of sedimentary sequences: spec. Publ., v. 36, geol. Soc. London.

Saigal, g. C., s. Morad, k. Bjørlykke, p. K. Egeberg, and p. Aagaard, 1988, diagenetic albitization of detrital k-feldspars in jurassic, lower cretaceous and tertiary clastic reservoirs from offshore norway, i. Textures and origin: journal of sedimentary petrology, v. 58, p. 1003-1013.

Storvoll v. And brevik i. (2008). Identifying time, temperature and mineralogical effects on

Chemical compaction in shales by rock physics relations. The leading edge, p. 750-756.

Taylor, t. R., m. R. Giles, et al. (2010). "sandstone diagenesis and reservoir quality prediction: models, myths, and reality." aapg bulletin 94(8): 1093-1132.

Walderhaug, o. (1994). "precipitation rates for quartz cement in sandstones determined by fluid-inclusion microthermometry and temperature-history modeling." journal of sedimentary research 64(2a): 324-333.

Walderhaug, o. (1996). "kinetic modeling of quartz cementation and porosity loss in deeply buried sandstone reservoirs." aapg bulletin 80: 731-745.

Walderhaug, o. & bjørkum, p.a., 2003: the effect of stylolite spacing on quartz cementation

In the lower jurassic stø formation, southern barents sea. Journal of sedimentary

Research 73, 146-156.

Waples d. W. And couples g. D. (1998). Some thoughts on porosity reduction - rock

Mechanics, overpressure and fluid flow. In: s.j. Düppenbecker & j.e. Iliffe (eds.), basin

Modelling: practice and progress. Geol. Soc., london, spec. Pub. 141, p. 73-81.

Wennberg o. P., malm o., needham t., edwards e., ottesen s., karlsen f., rennan l. And

Knipe r. (2008). On the occurrence and formation of open fracture in the jurassic reservoir

Sandstones of the snøhvit field, sw barents sea. Petroleum geoscience, v. 14, p. 139-150.

Wilson, m. D., 1992, inherited grain-rimming clays in sandstones from eolian and shelf environments: their origin and control on reservoir properties, in d. W. Houseknecht, and e. D. Pittman, eds., origin, diagenesis and petrophysics of clay minerals in sandstones, p. 209-227s.

Worden, r. H. And s. Morad (2009). Quartz cementation in oil field sandstones: a review of the key controversies. Quartz cementation in sandstones, blackwell publishing ltd.: 1-20.

Øvrebø, o., & talleraas, e., 1976, the structural geology of the troms area. In: exploraiton geology and geophysics. Offshore north sea conference, norwegian petroleum society, article g/tv-6.

Øvrebø, o., & talleraas, e., 1977, the structural geology of the troms area barents sea: geojournal, v. 1, p. 47-54.

Appendix 1

Well	Formation	Depth (m)	Porosity
7120/6-1	Nordmela	2494,3	6,3
	Nordmela	2529,6	10
	Nordmela	2532,4	5,6
7120/9-1	Nordmela	1922,10	0,6

Appendix 2

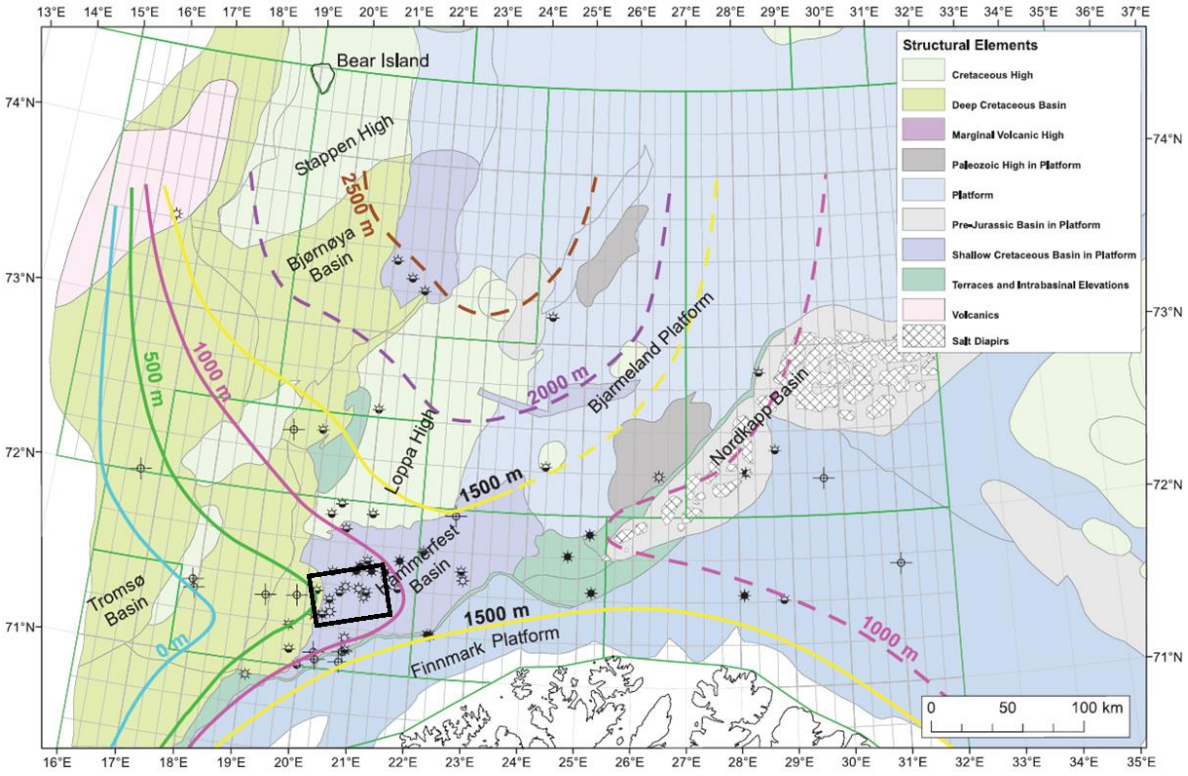

Uplift map of greater Barents Sea based on vitrinite data (Ohm et al. 2008). Study area is marked with black triangle.